Infrared Factorisation for Parton Showers Beyond One Emission

Zur Erlangung des akademischen Grades eines

Doktors der Naturwissenschaften

von der KIT-Fakultät für Physik
des Karlsruher Instituts für Technologie (KIT)

genehmigte

Dissertation

von

MSci. Emma Simpson Dore

aus Edinburgh

Referent: PD Dr. Stefan Gieseke

Korreferent: Prof. Dr. Dieter Zeppenfeld

Tag der mündlichen Prüfung: 13. November 2020

Eidesstattliche Versicherung gemäß § 13 Absatz 2 Ziffer 3 der Promotionsordnung des Karlsruher Instituts für Technologie (KIT) für die KIT-Fakultät für Physik:

1. Bei der eingereichten Dissertation zu dem Thema

   Infrared Factorisation for Parton Showers Beyond One Emission

   handelt es sich um meine eigenständig erbrachte Leistung.

2. Ich habe nur die angegebenen Quellen und Hilfsmittel benutzt und mich keiner unzulässigen Hilfe Dritter bedient. Insbesondere habe ich wörtlich oder sinngemäß aus anderen Werken übernommene Inhalte als solche kenntlich gemacht.

3. Die Arbeit oder Teile davon habe ich bislang nicht an einer Hochschule des In- oder Auslands als Bestandteil einer Prüfungs- oder Qualifikationsleistung vorgelegt.

4. Die Richtigkeit der vorstehenden Erklärungen bestätige ich.

5. Die Bedeutung der eidesstattlichen Versicherung und die strafrechtlichen Folgen einer unrichtigen oder unvollständigen eidesstattlichen Versicherung sind mir bekannt.

Ich versichere an Eides statt, dass ich nach bestem Wissen die reine Wahrheit erklärt und nichts verschwiegen habe.

Karlsruhe, den 15. December 2020

....
(Emma Simpson Dore)

Abstract

Soft and collinear approximations are the fundamental concepts used to construct parton showers. Infrared singularities are also important for the calculation of cross sections beyond leading order. Current parton showers implement the iteration of one emission, but for comparison to higher order cross sections a framework for two or more emissions is needed. The work in this thesis focuses on developing such a framework, to factorise soft and collinear emissions from multi-parton amplitudes for two or more emissions. Firstly, the kinematic mapping for the one-emission case is investigated and modified to introduce a global recoil via a Lorentz transformation. Then, the concepts are extended to a generalised case and a partitioning formalism is developed to separate different collinear sectors. This allows the mapping for multiple emissions to be developed and the corresponding phase space factorisation to be established. An example is made of the new mapping applied to the two-emission case and important cross checks are carried out. Finally, the mapping is implemented, for the one-emission case, in the Herwig 7 dipole shower and compared to the existing mapping and other variants. This shows the potential for improvement in the kinematics of the parton shower.

Zusammenfassung

Weiche und kollineare Annäherungen sind die grundlegenden Konzepte, woraus Partonschauer-simulationen gebaut werden. Infrarotsingularitäten müssen sorgfältig behandelt werden, um Querschnitte von nächst-führender Ordnung zu berechnen. Aktuelle Partonschauersimulationen implementieren die Iteration einer Emission, aber um sie mit Querschnitten höherer Ordnung zu vergleichen, ist ein Rahmen für zwei oder mehr Emissionen erforderlich. Die Arbeit in dieser Dissertation konzentriert sich auf die Entwicklung eines solchen Rahmens zur Faktorisierung weicher und kollinearer Emissionen aus Mehrteilchenamplituden für zwei oder mehr Emissionen. Der erste Teil der Arbeit besteht darin, die kinematische Abbildung für den Einemissionsfall zu untersuchen und diese zu modifizieren, um einen globalen Rückstoß über eine Lorentztransformation einzuführen. Dann werden die Konzepte auf einen verallgemeinerten Fall erweitert und ein Partitionierungsformalismus entwickelt, um verschiedene kollineare Sektoren zu trennen. Dadurch kann auch die Abbildung für mehrere Emissionen entwickelt und die entsprechende Faktorisierung des Phasenraums festgelegt werden. Als nächstes wird ein Beispiel für die neue Abbildung gemacht, angewendet auf den Fall mit zwei Emissionen, und wichtige Gegenprüfungen werden durchgeführt. Schließlich wird die Abbildung für den Einemissionsfall in den Herwig 7-Dipolschauer implementiert und mit der vorhandenen Abbildung und anderen Varianten verglichen. Dies zeigt das Potenzial für eine Verbesserung der Kinematik des Partonschauers.

Contents

Introduction

Particle physics experiments, such as the Large Hadron Collider (LHC), seek to understand the building blocks of matter and how fundamental particles interact with each other. Over many years physicists have developed a model that aims to describe all concepts of the physical world, the Standard Model (SM). The SM contains all fundamental particles and forces except gravity, and combines the theories of electrodynamics and the weak and strong forces. However, the SM is not complete; there are many examples of experimental observations that are inconsistent with the SM. Some examples include: dark matter and dark energy, massive neutrinos and the strong CP problem. Theorists have proposed several ways to extend the SM such as supersymmetry, string theory and composite Higgs models, although none of these have yet been shown to be consistent with data. Therefore, the search for new physics continues and is the motivation for future high-energy particle-physics experiments such as the Future Circular Collider (FCC) [1] and the Electron-Ion Collider (EIC) [2].

The component of the SM of interest in this thesis is quantum chromodynamics (QCD), that describes the parton model to explain the behaviour of protons and neutrons as composite hadrons composed of quarks. The quarks are held together by the short-range strong force, which is mediated by gluons. Due to confinement, which can be explained by the scaling of the strong force at large distances, it is not possible to observe free quarks. Structure functions describe the behaviour of partons at small distances and evolution equations describe how these functions change with the energy scale. Another key concept is factorisation, that allows the separation of physics at different scales, *e.g.* perturbative and non-perturbative physics. It will be shown that using factorisation enables physicists to produce predictions for multi-scale processes.

Work that is currently carried out at the LHC and other particle physics experiments is searching for a solution to the problem of the incomplete SM. The discovery of new physics requires an accurate comparison of data and theory. At the LHC this is most commonly done by comparing event data to event simulations, especially for exclusive final states which are not calculable analytically. The simulated events are generated by Monte Carlo Event Generators (MCEG), such as Pythia [3], Herwig [4, 5] and Sherpa [6, 7]. These are powerful tools capable of simulating particle collisions and their subsequent decays.

A standard MCEG contains many components, each with a specific task and different physics to implement. The hard process is the highest energy component and can be calculated

analytically. The hard matrix element is usually built into event generators, although there are also specific matrix element programs that can be interfaced. The hard process connects to the parton shower, that controls the emissions from the highest energies $\mathcal{O}(\text{TeV})$ to $\mathcal{O}(1\,\text{GeV})$, at which point perturbation theory no longer holds. Hadronisation models then take over and form hadrons from the final state partons. These hadrons are involved in decay processes to produce the whole range of particles which can be detected by experiments. Development of these simulations is aimed at increasing their accuracy and predictive power, which will result in improved sensitivity to new physics when compared to data. Methods to increase the accuracy of the predictions include; higher order calculations and matching to the parton shower, better description of soft physics and background processes and a better description of small regions of phase space for the prediction of highly exclusive observables.

Hard processes are usually calculated at leading or next-to-leading order, then the parton shower adds emissions to the initial and final states, to connect the energy scales. These emissions contain poles in the soft and collinear limits. Being able to describe the behaviour both at and away from these limits is important for the determination of the showering process. The expressions for the singular limits can also be used for subtraction schemes, which enable the calculation of higher-order cross sections. When higher order corrections are included in the matrix element they need to be combined with the parton shower which needs to have a comparable level of accuracy.

Currently, parton showers are based on single-emission kinematics and splitting functions that are then iterated by the shower algorithm to produce multiple emissions. To increase the precision of the shower the next order of emissions needs to be included, which requires implementation of the two-emission splitting functions. Including two emissions in a parton-shower framework requires structural changes within the shower, including the kinematic mapping. As existing shower mappings result in errors of logarithmic accuracy beyond the leading terms, which have been highlighted in recent years, it is desirable to redesign the mapping. Hence, in this thesis the aim is to investigate the factorisation of soft and collinear emissions beyond the one-emission case and to develop an appropriate kinematic mapping within a framework that can describe the two-emission case. This framework is designed so that it can be easily and systematically extended to describe more than two emissions.

In Chapter 2 the concepts of QCD are introduced, with a focus on infrared singularities, as these are particularly relevant to this thesis. The scaling conventions for soft and collinear limits are given, as well as examples of soft and collinear factorisation that are important for constructing parton showers. At the end of this chapter, the relevant notation for this thesis is given, including the Feynman rules and colour algebra.

As an introduction to event simulation in Chapter 3, Monte Carlo (MC) methods are explained and shown in the context of MCEG. The components of event generators are outlined, from the high energy scales of the hard matrix element via parton showers to non-perturbative hadronisation models and soft physics models. To illustrate the application of MC methods in the parton shower, an example of a shower algorithm is shown. In Chapter 4, more complete and detailed background information for parton showers is given. This includes DGLAP evolution, next-to-leading order (NLO) subtraction and examples of the Catani-Seymour dipole formalism. To give context to the motivation of this thesis, the current status and issues with parton showers are discussed, as well as insights into areas for improvement.

The aim of Chapter 5 is to investigate the kinematic mapping used for collinear factorisation, as it is implemented in the parton shower, to see where improvements can be made. The single-emission case is first outlined, then detailed calculations are shown to expose the scaling of all terms that can contribute in both the soft and collinear limits. Steps are taken to improve the kinematic mapping by introducing a global recoil distribution via a Lorentz transformation.

As a cross-check of the methods used for two different mappings, the collinear limit is taken and the result is compared to the known splitting functions.

Having examined the single-emission case, Chapter 6 extends the concepts to an arbitrary number of emissions. This requires careful enumeration of possible diagrams and the development of a partitioning formalism to separate overlapping collinear sectors. In Chapter 7, a mapping for k-emissions is established and tested for the two-emission case. Again, the collinear limit is checked to give the known splitting function. The other infrared limits are also compared as an illustration of the connections between limits and how subtraction counter terms can be constructed.

To see the effect of the mapping development in the context of an event generator, the multiple emission mapping is implemented in the Herwig parton shower, as discussed in Chapter 8. This first implementation uses the single emission form of the mapping, that is then iterated by the shower algorithm so that this can be directly compared to the existing dipole shower. The existing framework for the splitting functions and phase space from the Herwig dipole shower are used. Two other mappings are implemented for comparison, that differ from the standard mappings by not assigning a transverse momentum component to the emitter. The analysis shows some small differences between the mappings. Future work will adjust the phase space and splitting function implementation to give more conclusive results.

Quantum Chromodynamics and Infrared Singularities

The singularities of interest in this thesis arise in both the electromagnetic and strong fields. The factorisation concepts discussed apply to both cases with the inclusion of colour charge for quarks and gluons. The colour charge and correlations between colour charges are the main motivation for development of the methods and formalisms for infrared (IR) radiation in QCD amplitudes. To discuss the behaviour of quarks and gluons, it is first important to introduce QCD, the theory that describes strong interactions.

This chapter starts by introducing the key concepts of QCD in Sec. 2.1 and discusses the process of calculating QCD amplitudes in Sec. 2.1.1. The central issue considered in this thesis is IR singularities, *i.e.* soft and collinear singularities that can occur in QCD amplitudes, and how to treat them. Sec. 2.2 outlines how these singularities arise and under which circumstances they cancel. Finally the notation used for the calculations in subsequent chapters is established in Sec. 2.3. This includes the Feynman rules in Sec. 2.3.1, colour operators in Sec. 2.3.2 and cutting rules in Sec. 2.3.3.

2.1. Quantum Chromodynamics (QCD)

Experimental evidence in the last century led to several conclusions about atomic substructure, including the discovery that quarks are the building blocks of hadrons and that gluons are the mediators of the strong force that holds quarks together. Hadrons are defined as particles containing two or more quarks. They therefore interact with the strong force via hadronic interactions. States with two quarks are known as mesons and those with three quarks as baryons. The first three quarks postulated were the 'u' (up), 'd' (down) and 's' (strange) quarks and to satisfy the flavour SU(3) symmetry observed, carry the electric charges $\pm 1/3$ and $\pm 2/3$ of the electron charge and spin of $1/2$ [8]. The parton model was developed as a result of observed nucleon substructure which then was combined with the quark model to give the quark parton model (QPM).

However, the QPM was not complete as for bayrons containing three of the same quark the wave function was totally symmetric which violates the Pauli-principle. This required a new degree of freedom to be introduced, colour, with three values referred to as red, blue and green. The resulting wave function is completely antisymmetric and is a colour singlet when

it is assumed that the colour charge has SU(3) symmetry. Only colour singlet states are observed, in agreement with the SU(3) symmetry, including the known mesons and baryons. Therefore, the colour charge can only be measured when momentum transfer takes place.

The combination of flavour and colour symmetries and evidence of the strong interaction, determined from experimental observations, led to the development of the non-abelian Yang-Mills gauge theory of QCD. This theory can be used to describe the interactions of quarks and gluons via Feynman rules, (given in Sec. 2.3.1), derived from the QCD Lagrangian density. The classical QCD Lagrangian, for quarks of mass m, as given in [8] is:

$$\mathcal{L}_{QCD} = -\frac{1}{4}F_{\mu\nu}^a F^{a\mu\nu} + \sum_{\text{flavours}} \bar{q}_i(i\slashed{D} - m)_{ij} q_j \ , \tag{2.1}$$

where it is assumed that the SU(3) gauge symmetry is unbroken. $F_{\mu\nu}^a$ is the field strength tensor, $\slashed{D} = \gamma_\mu D^\mu$ and D_μ is the covariant derivative which are defined as:

$$F_{\mu\nu}^a = \partial_\mu A_\nu^a - \partial_\nu A_\mu^a - g f^{abc} A_\mu^b A_\nu^c \ ,$$
$$(D_\mu)_{ij} = \delta_{ij}\partial_\mu + i g_s T_{ij}^a A_\mu^a \ , \tag{2.2}$$

where A_μ^a are the gluon fields, f^{abc} is the structure constant, g_s the strong coupling constant and T_{ij}^a the SU(3) generators. The indices a, b, c, contain the eight degrees of freedom from the colour charge. The non-abelian triple and four-gluon vertices arise from the third term in the definition of the field strength. The mass terms and the coupling constant are the free parameters of the theory. For local transformations of the strong field the QCD Lagrangian is invariant.

The generators can be written as the matrices t or T for the fundamental and adjoint representations, respectively [9]:

$$[t^a, t^b] = i f^{abc} t^c \ , \qquad [T^a, T^b] = i f^{abc} T^c \ , \qquad (T^a)_{bc} = -i f^{abc} \ , \tag{2.3}$$

where the fundamental generators can be represented as $t^a = \lambda^a/2$ via the eight Gell-Mann matrices, λ^a. The normalisation of the generators for SU(N) is chosen to be:

$$\text{Tr}(t^a t^b) = T_R \delta^{ab} \ , \qquad T_R = \frac{1}{2} \ , \tag{2.4}$$

which results in the following:

$$\sum_a (t_{ij}^a t_{jk}^a) = C_F \delta_{ik} \ , \qquad C_F = \frac{N^2 - 1}{2N} \ ,$$
$$\text{Tr}(T^c T^d) = \sum_{a,b} f^{abc} f^{abd} = C_A \delta^{cd} \ , \qquad C_A = N \ . \tag{2.5}$$

For the chosen normalisation and given the SU(3) symmetry, the values are:

$$C_F = \frac{4}{3} \ , \quad C_A = 3 \ , \tag{2.6}$$

The relative splitting probabilities for a quark and a gluon can be described by these factors, where they correspond to the probabilities for a gluon emission from a quark and a gluon emission from a gluon. A gluon splitting into two quarks has the probability described by the factor T_R. The probability of splitting is the same for all colours. The values given above depend on the normalisation chosen for the generators therefore it is more meaningful to refer to ratios of these values than just the values themselves. These ratios correspond to experimental cross sections, which gives evidence for the theory of QCD.

Usually, when QCD is used to describe a process in high-energy physics, perturbative QCD (pQCD) is actually being used that makes use of the concepts of perturbation theory. It is not possible to describe most non-perturbative processes with QCD. To use pQCD the strong coupling must be small, which is only true for processes with large momentum transfers, Q, *i.e.* $Q \gg \Lambda_{QCD}$. Λ_{QCD} is defined as the energy scale at which non-perturbative effects become important, which is $\mathcal{O}(200)$ MeV. The strong coupling, α_s, can be defined as a function of Q^2 to leading order as [8]:

$$\alpha_s(Q^2) \equiv \frac{g_s^2(Q^2)}{4\pi} = \frac{1}{\beta_0 \ln(Q^2/\Lambda_{QCD}^2)} \ , \tag{2.7}$$

where β_0 is a coefficient that depends on the renormalisation scheme used. The scale dependence of the strong coupling is known as the running coupling that is due to the introduction of a second mass scale through the renormalisation of the theory. The value of α_s becomes smaller as Q increases. This inverse relationship means that QCD is an asymptotically free theory and that for large values of Q, perturbation theory can always be applied. The most commonly used renormalisation scheme is the modified minimal subtraction scheme ($\overline{\text{MS}}$), that regulates ultraviolet loop divergences by reducing the number of dimensions to $d = 4 - 2\epsilon$ [9]:

$$\frac{\mathrm{d}^4 k}{(2\pi)^4} \to (\mu)^{2\epsilon} \frac{\mathrm{d}^{4-2\epsilon} k}{(2\pi)^{4-2\epsilon}} \ , \tag{2.8}$$

where $\epsilon = 2 - n/2$ and $n < 4$. Poles arise from the loop integrals of the form $\mathrm{d}^n k/[k^2 + m^2]^2$ when $\epsilon = 0$, that for the minimal subtraction scheme are subtracted out and the bare coupling is replaced by the renormalised coupling, $\alpha_s(\mu^2)$. Additionally, the constants that accompany the poles are subtracted, in the case of the modified minimal subtraction scheme. The choice of renormalisation scheme results in different values for the Λ parameter in the definition of the coupling, and thus different values for the coupling.

At the high-energy scales at which pQCD is applicable, it is possible to investigate physics at a sub-nuclear scale. This enables the description of hadrons via parton density functions (PDFs), which describe the distribution of partons as a function of the momentum fraction carried by each parton. A QCD cross section can be calculated by convoluting tree-level amplitudes with the relevant PDFs, which are independent of the hard subprocess.

2.1.1. Cross Sections and Amplitudes

The most common aspect of QCD to be experimentally measured are cross sections. As an introduction, the total cross section for $e^+e^- \to$ hadrons will be discussed. This cross section can be calculated using pQCD and is expected to have small non-perturbative corrections due the the large scale from the combined momenta of the electron and positron. It is also an inclusive quantity that results in the cancellation of IR divergences, as discussed in Sec. 2.2, and can provide a precise measurement of the strong coupling. Cross sections for a specific number of jets in the final state can be defined and compared to experimental data. Jet cross sections are of particular interest as a way to probe the behaviour of the triple gluon vertex. To determine a cross section analytically it is necessary to determine which amplitudes will contribute. This can involve both electroweak and strong mediators.

Amplitudes in general are described by a series of increasingly complex Feynman diagrams, that can be organised according to the power of coupling they contain. For QCD amplitudes, the amplitude squared is proportional to the simplest set of diagrams of $\mathcal{O}(\alpha_s^n)$, where the value of n depends on the process. This results in the leading order (LO) contribution to the cross section. The next-to-leading order (NLO) approximation corresponds to the diagrams $\mathcal{O}(\alpha_s^{n+1})$ *etc.* Increasing the order of the calculation usually increases the accuracy and results

in better theory predictions for experiments. For $e^+e^- \to q\bar{q}g$, the lowest order of α_s^n is $n = 1$, as is the case for most tree-level QCD processes. Though for the total e^+e^- annihilation cross section the leading contribution is the QED interaction. The matrix elements for a QCD process can be written down using the Feynman rules given in Sec. 2.3.1 and can be used to determine the cross section.

The leading contribution to the total hadronic cross section is obtained by summing over all possible flavours and colours of the quark-antiquark pairs in the final state, where higher order corrections involve gluon interactions. For electron-positron annihilation to two general fermions, $e^+e^- \to f\bar{f}$, $f \neq e$, ignoring weak effects as they can assumed to be small, the differential cross section for the s-channel can be written as [9]:

$$\frac{\mathrm{d}\sigma}{\mathrm{d}\cos\theta} = \frac{\pi\alpha^2 Q_f^2}{2s}(1 + \cos^2\theta) \ , \tag{2.9}$$

where in the centre of mass frame, θ is the scattering angle, s is the scattering energy squared and α is the electromagnetic coupling. Upon integration over θ, the cross section is given by:

$$\sigma_0 = \frac{4\pi\alpha^2}{3s}Q_f^2 \ . \tag{2.10}$$

This cross section does not yet contain any QCD effects that enter at $\mathcal{O}(\alpha_s)$ and require the inclusion of real and virtual gluon emissions from the final-state quarks. The phase space for the real-emission diagrams can be written as [9]:

$$\mathrm{d}\Phi_3 = \frac{1}{(2\pi)^5}\frac{s}{32}\ \mathrm{d}\alpha\ \mathrm{d}\cos\beta\ \mathrm{d}\gamma\ \mathrm{d}x_1\ \mathrm{d}x_2 \ , \tag{2.11}$$

where α, β and γ are Euler angles and $x_1 = 2E_q/\sqrt{s}$, $x_2 = 2E_{\bar{q}}/\sqrt{s}$. By integrating out the angles from the matrix element squared, the total cross section can be expressed in terms of x_1 and x_2.

$$\sigma^{q\bar{q}g} = \sigma_0\ 3\sum_q Q_q^2 \int \mathrm{d}x_1\ \mathrm{d}x_2\ C_F\ \frac{\alpha_s}{2\pi}\frac{x_1^2 + x_2^2}{(1 - x_1)(1 - x_2)} \ . \tag{2.12}$$

The region of integration is defined by $0 \leq x_1, x_2 \leq 1$ and $x_1 + x_2 \geq 1$ and divergences arise at the integration boundaries where $x_1, x_2 = 1$. These divergences can also be expressed in terms of the gluon energy, E_g, and the angle between the gluon and quark i, θ_{ig}:

$$\begin{aligned}
1 - x_1 &= \frac{x_2 E_g(1 - \cos(\theta_{2g}))}{\sqrt{s}} \ , \\
1 - x_2 &= \frac{x_1 E_g(1 - \cos(\theta_{1g}))}{\sqrt{s}} \ .
\end{aligned} \tag{2.13}$$

Divergences then arise in regions of phase space where the emitted gluon is collinear to the quark, $\theta_{ig} \to 0$, or the gluon is soft, $E_g \to 0$. The singularities that result in these two cases appear in both real and virtual contributions and will be discussed in detail in Sec. 2.2.

2.2. Infrared Singularities

Soft and collinear divergences are referred to collectively as IR divergences. The term 'soft' implies that the energy of the emitted parton $\ll Q$, where Q describes the hard scale, and 'collinear' refers to the case when the angle between any two partons is zero. It is also possible to have collinear divergences involving more than two partons, *i.e.* triple collinear cases. For calculations in perturbation theory it is desirable to work with IR safe observables. IR safety

is when there is a small sensitivity to hadronisation and the IR divergences cancel in the perturbative calculation.

For sufficiently inclusive observables these divergences cancel in the massless limit, as established by Bloch and Nordsieck [10] who developed a mechanism for constructing IR finite cross sections. The IR divergences cancel between the real and virtual parts of the cross section when summed over all degenerate physical states. This is due to the use of dimensional regularisation to increase the number of dimensions to greater than four, which results in poles due to the IR singularities at $n = 4$ dimensions. This concept was later extended by Kinoshita [11] and Lee and Nauenberg [12] in parallel, which led to the naming of the Kinoshita-Lee-Nauenberg (KLN) theorem. The KLN theorem shows that inclusive jet cross sections are finite and that the finiteness can be extended to both initial and final-state interactions [13]. Instead of using cross sections, the KLN theorem uses transition probabilities, which are illustrated for a set of states, $D(E_0)$, where the energy range is:

$$E_0 - \epsilon < E < E_0 + \epsilon \qquad (2.14)$$

Then the probability density per unit volume for a transition from j to i, p_{ij}, can be used to define the finite quantity:

$$P(E_0, \epsilon) = \sum_{i,j \in D(E_0)} p_{ij} \,, \qquad (2.15)$$

in the massless limit. For the KLN theorem to apply, an average over the initial states has to be included. This is possible for hadronic initial states if they are constructed to include the averaging. Cross sections containing initial state hadrons depend on the momentum scales of the initial state. At these momentum scales the effective coupling can be large and so the cross section cannot be well determined using perturbation theory. This momentum dependence still allows the cross section to be IR finite, due to the averaging over states, but it cannot be considered to be IR safe in the zero mass limit [13].

For exclusive observables the divergences do not cancel completely and large logarithms arise, written as $L = \ln(Q^2/Q_0^2)$. For $Q^2 \gg Q_0^2$, $\alpha_s(Q^2)L$ is approximately equal to one, which can prevent the perturbation theory, at a given order in α_s, from converging. An alternative approach is to instead expand the differential cross section in powers of $\alpha_s L$, that results in the leading logarithm approximation (LLA) where the results are often referred to as leading log (LL), next-to-leading log (NLL) *etc.* This expansion can be written as [8]:

$$d\sigma = \sum_n a_n(\alpha_s L)^n + \alpha_s(Q^2) \sum_n b_n(\alpha_s L)^n + ... \qquad (2.16)$$

Determining such contributions to a cross section is known as resummation, as the contributions at each order need to be summed. This method is particularly valuable in regions of phase space that are poorly described by the leading-order approximation.

In the context of Feynman amplitudes, the propagator factors that arise from the emissions from external lines contain IR singularities *e.g.* for an emitted gluon:

$$\frac{1}{(p \pm q)^2 - m^2} = \frac{\pm 1}{2p \cdot q} = \frac{\pm 1}{2\omega E(1 - v cos\theta)}, \qquad (2.17)$$

where ω is the gluon energy and E and v describe the emitter parton. The divergences contained are for a soft gluon emission as $\omega \ll Q$ and for a collinear emission where $\theta \to 0$ for the massless case.

To categorise terms and their contributions to soft and collinear divergences it is helpful to introduce a scaling parameter, λ, that in both the soft and collinear cases can be considered

	$p_i \| p_j$	$p_j \to 0$
$p_i \cdot p_j$	λ^2	λ
$p_j \cdot p_k$	1	λ

Table 2.1.: Scaling in soft and collinear limits from SCET conventions.

to go to zero when a limit is taken. The scaling used in this thesis is inspired by SCET conventions [14] and is given in Table 2.1, where p_i is the momentum of particle i. The first column describes the case where i and j are collinear and the second column describes the case where j is soft. This scaling can also be applied to parameters in the context of a kinematic mapping shown in Sec. 5.2.

2.2.1. Soft and Collinear Factorisation

Factorisation is the concept of separation between short and long-range effects. It can be described by the factorisation theorem. Both collinear and soft emissions can be factorised from a hard amplitude and examples of this are shown in Sec. 4.3. Soft and collinear factorisation are specific examples of the factorisation theorem given in Eq. (3.6), which applies to all processes occurring at different scales.

For the emission of a sufficiently soft gluon with momentum k from a hard parton with momentum p_i, where $k \ll p_i$, terms proportional to k in the amplitude can be neglected. This results in the eikonal approximation, which applies to both gluon and quark emitters due to the low resolution of the soft gluon. The total of the emissions from all hard partons in a N-parton final state gives [8]:

$$
\mathcal{M}^{(N+1)} = g_s \epsilon^*(k)_\mu \left(\sum_{i=1}^{N} \hat{T}_i^a \frac{p_i^\mu}{p_i \cdot k} \right) \times \mathcal{M}^{(N)} \; , \tag{2.18}
$$

where $\hat{T}_i^a$ is the appropriate colour charge operator for parton i. The matrix-element squared can be written, after summing over gluon polarisations, as:

$$
|\mathcal{M}^{(N+1)}|^2 = g_s^2 J \cdot J^\dagger |\mathcal{M}^{(N)}|^2 \; , \tag{2.19}
$$

where $J^{a\mu}(k; p_i) = \sum_i \hat{T}_i^a \left(\frac{p_i^\mu}{p_i \cdot k} - \frac{n^\mu}{n \cdot k} \right)$ and n^μ is the gauge vector. J is known as the eikonal current. The term in the eikonal current that is proportional to n^μ does not contribute in a colour neutral system or when the Feynman gauge is used.

Collinear factorisation is possible when an emitted gluon is collinear to a hard parton, that can also be described as the angle between the two momenta going to zero [9]. For a proton-proton collision, with a final state defined by X and Y, producing a collinear gluon, the differential cross section factorises as:

$$
\mathrm{d}\sigma(pp \to Y + g + X) \tag{2.20}
$$
$$
= \mathrm{d}\sigma(pp \to Y + X) \int \frac{\mathrm{d}p_\perp^2}{p_\perp^2} \frac{\mathrm{d}z}{z} \frac{\alpha_s}{2\pi} C_F \frac{f(\frac{x_a}{z}, t)}{f_a(x_a, t)} P(z) \; ,
$$

where f are the distribution functions for the partons involved. The parts containing the collinear behaviour are referred to as splitting functions, $P(z)$, and are described in Sec. 4.1.1.

This factorisation expression is based on the DGLAP evolution equations, which are introduced in Sec. 4.1.

It is possible to factorise at both cross-section and amplitude level, where the collinear factorisation at amplitude level gives factors that represent different components of the splitting functions, that can be added to give the cross-section level expression. The work in this thesis focuses on the amplitude level due to the additional colour information that can be retained. To determine the cross section, there is always an implicit summing over colour and spins that results in an averaged matrix-element squared. For some exclusive observables, the information from specific amplitudes is needed to give accurate predictions.

To calculate the cross section with IR divergences, methods have been developed to subtract the singular terms and integrate them separately. The two most common methods are dipole subtraction [15], as discussed in Sec. 4.2, and FKS subtraction [16]. These operate by subtracting the terms that give the IR divergences before integration, then adding them back in their integrated form. The divergences can be described by a counter term, for which it is possible to determine an expression analytically. The counter terms to be subtracted make use of the splitting functions and eikonal functions that describe the singular behaviour. An alternative to subtraction methods is slicing methods, such as in [17], where the phase space is cut into different regions above and below a cut parameter, that separates the part of the cross section sensitive to IR divergences.

2.3. Notation

This section outlines the notation used in this thesis, that is of particular relevance for the QCD diagrams calculated in the following chapters. The Feynman rules for QCD are gauge dependent, so it is first necessary to introduce the relevant gauges. The two types of gauge that are commonly used in QCD calculations are covariant and axial gauges. The gluon polarisation tensor, $d^{\mu\nu}(p)$, takes different forms for the covariant and axial gauges [8]:

- Covariant gauge: $d^{\mu\nu}(p) = -\eta^{\mu\nu} + (1-\xi)\dfrac{p^\mu p^\nu}{p^2 + i\epsilon}$

- Axial gauge: $d^{\mu\nu}(p) = -\eta^{\mu\nu} + \dfrac{n^\mu p^\nu + p^\mu n^\nu}{n \cdot p} - \dfrac{n^2 + \xi p^2}{(n \cdot p)^2} p^\mu p^\nu.$

For a covariant gauge where the gauge parameter, $\xi = 1$, gives the Feynman gauge, that results in the gluon polarisation tensor, $d^{\mu\nu}(p) = -\eta^{\mu\nu}$. For an axial gauge, ghosts terms decouple given $n \cdot A = 0$ and the light-cone gauge is given by the case where $\xi = 0$, $n^2 = 0$, that gives $d^{\mu\nu}(p) = -\eta^{\mu\nu} + \dfrac{n^\mu p^\nu + p^\mu n^\nu}{n \cdot p}$. Now that the gauges are defined, the Feynman rules can be discussed and it will be shown where the differences between the gauges appear.

2.3.1. Feynman Rules

The Feynman rules of QCD are defined via the operator given by [9]:

$$S = i \int \mathcal{L} \, \mathrm{d}^4 x \tag{2.21}$$

This operator can be separated into two parts, corresponding to the free part and the interacting part of the theory. Where the propagators are determined from the free part, S_0, and the interactions are determined from the interacting part, S_I.

$$S = S_0 + S_I = i \int \mathcal{L}_0 \, \mathrm{d}^4 x + i \int \mathcal{L}_I \, \mathrm{d}^4 x \tag{2.22}$$

The QCD Feynman rules, which apply to both covariant and axial gauges are [9]:

$$\mu, a \quad p \quad \nu, b \quad\qquad = \delta^{ab} \frac{i}{p^2 + i\epsilon} d^{\mu\nu}(p) \ , \tag{2.23a}$$

$$\beta, l \quad p \quad \alpha, k \quad\qquad = \delta^{kl} \frac{i(\not{p} + m)_{\alpha\beta}}{p^2 - m^2 + i\epsilon} \ , \tag{2.23b}$$

$$= -g_s f^{abc} \left[g_{\alpha\beta}(p_a - p_b)_\gamma + g_{\beta\gamma}(p_b - p_c)_\alpha + g_{\gamma\alpha}(p_c - p_a)_\beta \right] \ , \tag{2.23c}$$

$$= -i g_s (t^c)_{kl} (\gamma^\lambda)_{\alpha\beta} \ , \tag{2.23d}$$

where f^{abc} is the structure constant introduced in Eq. (2.5) which can also be written as:

$$f^{abc} = -\frac{i}{T_F} \mathrm{Tr} \left\{ T^a T^b T^c - T^c T^b T^a \right\} \ . \tag{2.24}$$

The Feynman rules for the ghost propagator and quark-ghost vertex are given below, which only contribute when a covariant gauge is used,

$$a \quad p \quad b \quad\qquad = \delta^{ab} \frac{i}{(p^2 + i\epsilon)} \ , \tag{2.25a}$$

$$= g_s f^{abc} q^\lambda \ . \tag{2.25b}$$

The labelling conventions for open indices used in this thesis are defined for quarks and gluons, where the exchanged gluon is always labelled with polarisation λ and colour c. The labelling used is as follows:

- Quark emitter: α, β and k, l,

- Quark spectator: γ, δ and m, n,

- Gluon spectator: μ, ν and a, b ,

- Gluon spectator: ρ, σ and d, e ,

where the emitter refers to the parton that emits the soft or collinear momentum. The spectator is the other parton involved in the dipole. Additionally, square brackets are used to assign the momenta to a hard line and keep track of the indices that connect to the hard amplitude. $[\not{p}_i]_{\alpha\beta}$ describes the momentum flowing through the line connecting the indices α and β.

2.3.2. Colour Algebra

The generators of the colour charge were introduced in Sec. 2.1 and relevant relations given in Eq. (2.3). Here, the notation for combinations of colour charges is introduced, which will

be used in the calculations throughout this thesis. Colour charges for both quarks and gluons can be written as $\mathbf{T}_i^a$, where the index i refers to the parton and a indexes the generators. Additional upper and lower indices can be used to indicate outgoing colour and anti-colour, respectively [8]:

$$\left(\mathbf{T}_{i=q}^a\right)^\alpha{}_\beta = (t^a)^\alpha{}_\beta \; , \qquad \left(\mathbf{T}_{i=\bar{q}}^a\right)_\alpha{}^\beta = -(t^a)^\beta{}_\alpha \; , \qquad \left(\mathbf{T}_{i=g}^a\right)_{bc} = -if^a{}_{bc} \; . \tag{2.26}$$

The generators take the form of matrices and are, by convention, multiplied in order against the flow of the corresponding fermions. Products between the charges can be written as:

$$\mathbf{T}_i \cdot \mathbf{T}_j = \mathbf{T}_i^a \mathbf{T}_j^a \; , \qquad \mathbf{T}_i \cdot \mathbf{T}_j = \mathbf{T}_j \cdot \mathbf{T}_i \; , \qquad \mathbf{T}_i^2 = \mathbf{T}_i \cdot \mathbf{T}_i = C_i \; , \tag{2.27}$$

where $C_i = C_F$ for a quark and $C_i = C_A$ for a gluon, which correspond to the fundamental and adjoint representations respectively. A final-state amplitude squared, summed over colour and spins can be written as:

$$|\mathcal{M}_m|^2 = {}_m\langle 1, ..., m | 1, ..., m \rangle_m \tag{2.28}$$

By definition each vector, $|1, ..., m\rangle_m$, is a colour-singlet state [15]. When colour conservation is applied to a generator acting on such a singlet state, the result is:

$$\sum_{i=1}^{m} \mathbf{T}_i |\mathcal{M}\rangle_m = 0 \; . \tag{2.29}$$

The above expression is only true when the generators act on an amplitude *i.e.* it is not an operator identity. In the context two partons in the final state, labelled i and j, where $i \neq j$, charge conservation can be used for the generators to give: $\sum_{j \neq i} \mathbf{T}_j = -\mathbf{T}_i$. Examples of this notation for factors arising from quark-gluon vertices are:

$$(t_i^c)_{lr}(t_i^c)_{rk} = \mathbf{T}_i^2 \; , \qquad\qquad (t_i^c)^k{}_l (t_j^c)^m{}_n = -\mathbf{T}_i \cdot \mathbf{T}_j \; . \tag{2.30}$$

For triple gluon vertices, the structure constant, f^{abc}, represents the colours involved. When two gluon vertices are combined, this gives:

$$\sum_{c,d} f^{acd} f^{bcd} = C_A \delta^{ab} \; . \tag{2.31}$$

2.3.3. Cutting Rules

The Cutkosky cutting rules were first defined in the context of determining discontinuities of Feynman amplitudes in [18]. They are primarily used to simplify the calculation of the imaginary part of a loop diagram, however, the same rules can be applied to all amplitudes. In the context of this thesis, the cutting rules will be used to calculate the splitting diagrams when dealing with on-shell momenta, particularly for the determination of collinear splitting functions. The rules for loop diagrams, as given in [19], are:

1. Cut through the diagram in all ways that can put all intermediate propagators on-shell without violating momentum conservation.

2. For each cut, replace $\dfrac{1}{p^2 - m^2 + i\epsilon} \rightarrow -2\pi i \, \delta(p^2 - m^2)\theta(p^0)$.

3. Sum over all cuts.

4. The result is the discontinuity of the loop amplitude $\text{Disc}(\mathcal{A}) = -2\,\text{Im}\mathcal{A}$.

The derivation of these rules in shown in detail, and an example for a loop diagram given in [19].

The cutting rules make use of the fact that a Feynman propagator is real except from when the particle is on-shell, shown by:

$$\text{Im} \frac{1}{p^2 - m^2 + i\epsilon} = -\pi\delta(p^2 - m^2) \tag{2.32}$$

For internal lines to be put on-shell a dashed line or 'cut' is drawn through the lines. The cut diagrams used in this thesis to investigate emissions from hard momenta are a representation of the squared tree-level amplitudes for possible emissions such as:

$$(2.33)$$

Where the shaded 'blobs' represent the hard amplitude and the dashed line is the 'cut' that puts the gluon and quark propagators on-shell. These diagrams are a combination of the amplitude and its conjugate, which are joined together at the 'cut'. There are also multiple diagrams for each amplitude because there are multiple ways to combine each amplitude with its conjugate. In this context the following rules apply:

1. No loop-momentum integration is introduced.

2. On each side of the cut, the signs for the momenta and vertex factors are opposite.

3. Cut propagators give the factors:

   - Fermion: $\slashed{p} + m$

   - Gauge boson: $d^{\mu\nu}(q)$

4. Trace over closed fermion lines.

In this case using the cutting rules simplifies the squared amplitudes and means that the spin and polarisation sums do not need to be carried out explicitly. The emissions themselves are the point of interest, so the diagrams can be calculated for a generic hard amplitude that factorises from the IR emissions.

Monte Carlo Event Generators

This chapter details the function and methods of Monte Carlo (MC) event generators, and gives an introduction to parton showers, which are discussed in more detail in Chapter 4. Firstly in Sec. 3.1, the basic concepts of MC methods are explained and the suitability of these methods for complex particle simulations is illustrated. Then in Sec. 3.2, the different components of MC event generators are described with a particular focus on the parton shower algorithm in Sec. 3.2.1 and the methods used to describe non-perturbative physics in Sec. 3.2.3.

3.1. Monte Carlo Methods

MC methods are a group of methods based on the principle of repeated random sampling. They have applications in optimisation and numerical integration problems. These methods are particularly useful when the problem is analytically unsolvable, however, because they are only approximate methods there is always an associated error. The accuracy of the solution generally improves with time and the number of samples. MC methods make use of random numbers to randomise the sampling, that can be efficient for solving complex integrals. Some MC methods make use of a 'Markov Chain', that is defined as a sequence of possible events where the probability of each event depends only on the previous event. Markov Chain MC methods are used to simulate random objects with specific probability distributions. The name 'Monte Carlo' was first used by Von Neumann and Ulam, as published in [20]. Given a probability density:

$$\mathrm{d}P(x) = f(x)\mathrm{d}x \ , \tag{3.1}$$

the probability distribution $\approx$ area, is described by:

$$F(x) = \int_{x_0}^{x} f(x)\mathrm{d}x \ . \tag{3.2}$$

This can be evaluated by the 'Hit and Miss' algorithm, a method of calculating the integral via a random walk of points, which generates a sequence across the probability density, $P(x)$. The error of the result is estimated from the variance of the mean, which is $\mathcal{O}(1/\sqrt{N})$ [21]. This is an inefficient method as it samples uniformly across the range of interest and has a large error for cases with a large variance. However, this approach can be used for any

density that is bounded from above. In its simplest form MC integration is facilitated by
writing integrals as an average over the points in a specific range:

$$F(x) = \int_{x_0}^{x_1} f(x)\mathrm{d}x \approx (x_1 - x_0)\frac{1}{N}\sum_{i=1}^{N} f(x_i) \; . \tag{3.3}$$

The values of x_i from 1 to N are randomly distributed between x_0 and x_1. The estimate
converges to the true value in the limit that $N \to \infty$ [22]. For large enough values of N, the
convergence is independent of the integration-volume dimension. In this case, the error is
proportional to $1/\sqrt{N}$, which is given from the variance of the mean. Thus the error can be
reduced by reducing the variance of the integrand. Methods of variance reduction, such as
importance sampling, use non-uniform sampling, which aims to sample more in the regions
where the integrand is large. For an n-dimensional integral:

$$\int f(\vec{x})\mathrm{d}^n x = \int \frac{f(\vec{x})}{p(\vec{x})} \cdot p(\vec{x})\mathrm{d}^n x = \int \frac{f(\vec{x})}{p(\vec{x})} \cdot \mathrm{d}P(\vec{x}) \; , \tag{3.4}$$

the variance can be reduced by sampling $\vec{x}$ with respect to the probability density function
$p(\vec{x})$, where $p(\vec{x})$ is restricted to positive values [22]. An estimate of the integral is given by:

$$E = \frac{1}{N}\sum_{i=1}^{N} \frac{f(x_i)}{p(x_i)} \; , \tag{3.5}$$

where the aim is to choose the function $p(x)$, as similar as possible to $f(x)$. Importance
sampling is most effective when there is some knowledge of the function to be integrated. For
cases where this is not possible, adaptive methods have been developed, such as the VEGAS
algorithm [23]. This algorithm is adaptative, *i.e.* learns continuously about the function whilst
sampling, which enables it to process integrals with higher dimensions. The integration space
is subdivided into a grid that is then optimised via sampling iterations. The optimal grid
has an increased sampling rate in regions where the integrand is large. An estimate of the
integral is then obtained using the optimised grid.

There are other methods and algorithms that also aim to optimise the sampling, that are
better suited to specific function types. MC methods are suited to particle physics problems,
as these problems often involve complex integrals that cannot be solved analytically. To
calculate hard processes it is easy to implement cuts via MC methods and the phase space
integral can be approximated via a product with dimensions of the degrees of freedom. In
the next section, MC event generators for particle physics are described.

3.2. Monte Carlo Event Generators

MC methods are used effectively in the simulation of particle collisions within the framework
of MC event generators. These event generators are composed of many different parts that
each carry out a specific task to evaluate the simulation steps in the collision and subsequent
decay of colliding particles. The hard process is contained within a phase space of $3n - 4$
dimensions, where n are the degrees of freedom given by the number of produced particles
and the flavour and spin information from the final state. When including the parton shower
and hadronisation in the simulation there are many more dimensions involved. Such a high
dimensional integration problem is best dealt with using MC techniques. A comprehensive
review of available MC event generators can be found in [24].

Event generators use the factorisation theorem, that allows different processes to be separated
due to their different energy scales. This means that perturbative and non-perturbative

physics can be separated. Non-perturbative components, including PDFs and hadronisation, describe physics below scales $\mathcal{O}(1\ \text{GeV})$. Perturbative physics describes the hard process, at scales $\gg$ GeV, that correspond to lengths of fractions of fm, when α_s is assumed to be small. The parton shower also contains perturbative physics and connects the hard process to hadronisation by evolving the parton branching down to a scale $\mathcal{O}(\text{GeV})$, at the limit of perturbation theory. The factorisation theorem can be illustrated for the cross section of two hadrons with momenta P_1 and P_2 as [9]:

$$\sigma(P_1, P_2) = \sum_{i,j} \int \mathrm{d}x_1 \mathrm{d}x_2 f_i(x_1, \mu^2) f_j(x_2, \mu^2) \hat{\sigma}_{ij}(p_1, p_2, \alpha_s(\mu^2), Q^2/\mu^2) , \qquad (3.6)$$

where $\hat{\sigma}_{ij}$ is the short distance cross section as a function of the parton momenta $p_i = x_i P_i$, which can be calculated perturbatively. The scale of the hard scattering is given by Q and the functions $f_i(x, \mu^2)$ are the quark and gluon PDFs defined at a factorisation scale μ.

A generic differential cross section in the context of MC event generators can be factorised into the following contributions:

$$d\sigma = d\sigma_{\text{hard}}(Q) \times \text{PS}(Q \to \mu) \times \text{Had}(\mu \to \Lambda) \times ... \qquad (3.7)$$

where the first term represents the hard cross section, the second term the parton shower, the third term hadronisation and the ellipsis represents other non-perturbative terms. There are multi-purpose event generators that aim to simulate the full process of a particle collision. Other programs focus of one of the above components of the cross section. The commonly used multi-purpose generators include Pythia [3], Herwig [4,5] and Sherpa [6,7].

The hard cross section can be calculated using perturbation theory for inclusive observables. For an exclusive final state, MC event generators are used, as they can implement the cuts necessary to obtain the final state of interest. As an input to the event generator, the LO matrix-elements squared are used, which can be provided by external matrix-element generators. There are dedicated MC programs to generate matrix elements and phase space (*e.g.* MadGraph [25]). These programs then interface to the multi-purpose event generators, although the generators often have built in matrix-element generators. For high-multiplicity final states, dedicated programs are needed to efficiently generate and evaluate the matrix elements. PDFs are integrated via the PDF sets available from LHAPDF [26], however, each generator chooses a default set because the choice of PDF can affect the tuning of the parton shower and hadronisation model.

3.2.1. Shower Algorithm

The next step after the hard process is the parton shower, that connects the hard and non-perturbative scales via a series of emissions that radiate energy, as illustrated in Fig. 3.1. The hard scale is usually $\mathcal{O}(1\ \text{TeV})$ and the parton showers then evolve down to the IR cut-off, which is generally $\mathcal{O}(1\ \text{GeV})$ because this corresponds to the scale defined by QCD at which partons become confined to hadrons. The aim is to include higher order effects not described by the LO or NLO matrix element, such as the resummation of leading logarithmic contributions. Parton showers are discussed in more detail in Chapter 4.

The key components of a parton shower are the kinematic mapping and the emission kernels or splitting functions. Emission kernels, $P(z)$, such as in Eq. (4.12), describe the rate of emission for a propagating quark or gluon to emit an additional quark or gluon as a function of the momentum fraction z. The mapping facilitates the factorisation of emissions within the phase space by relating the momenta after the emission to those before the emission. Parton showers are at high enough energy scales to allow use of perturbation theory and are
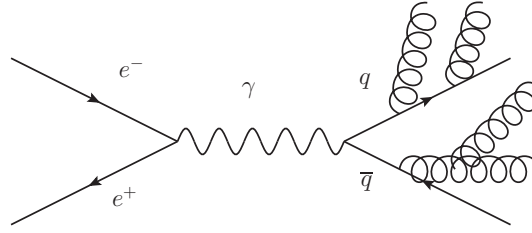
Figure 3.1.: Diagram of an e^+e^- collision and possible parton shower

consistent with energy and momentum conservation. The choice of evolution variable and recoil scheme is important, as these can have a large effect on the result from the shower. Recoil methods are of interest to this thesis and will be discussed in subsequent chapters. The total branching probability for parton i is given by [24]:

$$d\mathcal{P}_i = \int_{p^2_{\perp min}}^{p^2_{\perp max}} \frac{\mathrm{d}p^2_\perp}{p^2_\perp} \int_{z_{min}}^{z_{max}} \mathrm{d}z \frac{\alpha_s}{2\pi} P_{ji}(z) \tag{3.8}$$

for an emitted parton with momentum fraction, $(1-z) \in [z_{min}, z_{max}]$, and $p_\perp \in [p_{\perp min}, p_{\perp max}]$.

As shown in the previous section, MC methods can use probabilities to estimate an integral and are used in the parton shower to formulate the evolution algorithm. The Sudakov form factor is used to describe the probability for parton i to evolve from a scale t_0 to t without an emission and is defined as [9]:

$$\Delta_i(t) \equiv \exp\left(-\sum_j \int_{t_0}^t \frac{\mathrm{d}t'}{t'} \int dz \frac{\alpha_s}{2\pi} \hat{P}_{ji}(z) \right) \tag{3.9}$$

where $\hat{P}_{ji}$ is the unregularised splitting function for $i \to j$. Using this probability it is possible to write an integral equation for the parton distribution, $f(x,t)$, in terms of the initial parton distribution, $f(x,t_0)$:

$$f(x,t) = \Delta(t)f(x,t_0) + \int \frac{dt'}{t'} \frac{\Delta(t)}{\Delta(t')} \int dz \frac{\alpha_s}{2\pi} \hat{P}(z)f(x/z,t') \tag{3.10}$$

With this knowledge, a simple MC branching algorithm for parton evolution from $(t_1, x_1) \to (t_2, x_2)$ can be designed, where t_i is the virtual mass scale and x_i the momentum fraction [9]:

1. Solve $\dfrac{\Delta(t_2)}{\Delta(t_1)} = \mathcal{R}$ for t_2, where $\mathcal{R}$ is a random number between $[0, 1]$.

2. If $t_2 > Q^2$, the hard subprocess scale, stop branching.

3. Otherwise, generate momentum fraction $z = x_2/x_1$ with a probability distribution proportional to $(\alpha_s/2\pi)\hat{P}(z)$.

4. Repeat until hard scale is reached.

These steps describe the process for upward or space-like evolution, which applies to what is called initial state radiation (ISR), that can occur for high-energy partons before the hard collision. Partons emitted in both the initial and final states can result in further branching, however, in this case the variable t evolves downwards to a cut-off scale t_0 and not upwards

towards the hard-process scale. The probability of evolving downwards from t_2 to t_1 without branching is given by $\Delta(t_1)/\Delta(t_2)$, which can be used to solve for t_1 in the same way as described above.

A modified version of the form factor and algorithm can also be used for backward evolution as discussed in [27,28]. Backward evolution is more efficient for describing space-like cascades because it starts at the momentum fraction of the final parton and uses this to generate the momentum fractions of the previous partons. One of the main differences between forward and backward evolution is that the form factor needs to account for the local parton density $f(x,t)$, that gives the probability for backwards evolution from (t_2, x) to (t_1, x) without branching as:

$$\Pi(t_1, t_2; x) = \frac{f(x, t_1)\Delta(t_2)}{f(x, t_2)\Delta(t_1)} \ . \tag{3.11}$$

This has the effect of suppressing branching at large values of x and enhancing branching at low values of x. In this sense, the parton distributions are used as a guide to generate the correct shower for an initial state.

3.2.2. Matching and Merging

The result of parton showers is an approximation of higher order corrections to the hard matrix element. A better description of observables can often be given by replacing this approximation with exact pQCD calculations. Two methods used for such replacements are matching and merging, described as [29]:

- Matching - parton showering of the result of the subtraction of the parton shower at fixed order from a higher-order matrix element calculation.

- Merging - the parton shower is combined with the hard matrix elements for different particle multiplicities, to which cuts have been applied to regulate the soft and collinear divergences.

Both methods remove double counting, in the matching case via the subtraction and in the merging case by applying vetos to the parton shower.

Matching schemes such as MC@NLO [30] and POWHEG [31] match NLO calculations to the parton shower and subtract doubly counted terms. The NLO calculation makes use of IR subtraction to include soft and collinear emissions, an example of which is shown in Sec. 4.2. Matrix-element calculations are more accurate than parton showers at high $p_\perp$ but the matched result does not account for beyond LL effects, that can still have large contributions, as in the case of Higgs production.

Merging methods, such as the CKKW algorithm [32], select parton shower events with a $p_\perp$ below a cut-off energy, Q_{cut}, and shower the events from tree-level matrix elements with $p_\perp$ higher than the cut off. Then the two samples are merged with a discontinuity at Q_{cut}, where smearing of the merging scales can be used to avoid the discontinuity. It is important that the jet algorithm used is IR safe so that the jet configuration does not change if the initial parton is replaced by a cluster of collinear partons. A review of jet algorithms can be found in [33]. The showering process has to identify a configuration that corresponds to the correct final state from the matrix-element calculation, to which further radiation can be added.

3.2.3. Hadronisation

At energies below 1 GeV, perturbation theory no longer holds and non-perturbative hadronisation models must be used. Hadronisation aims to produce final-state hadrons from the

partonic input, which is the end product of the parton shower. The two most commonly used hadronisation models are the cluster and string models.

The cluster hadronisation model is based on the principle of preconfinement of parton showers [34], which shows that colour singlets can be formed from the colour structure of the shower at any evolution scale, $Q_0 \ll Q$, with an invariant-mass scale only dependent on Q_0 and Λ_{QCD}. To create these colour singlets, all gluons are first split into $q\bar{q}$ pairs. These are then grouped to form the 'clusters'. These clusters undergo cluster fission to produce smaller clusters, then hadrons depending on the mass of the cluster. There are two commonly used versions of the cluster model, in Herwig [35] and Sherpa [36], that follow the same basic approach but have different detailed treatment of issues such as high mass clusters.

The Lund string model [37, 38], as used in Pythia [3], transforms the partons directly to hadrons and uses a string model to describe this process. The model is based on the idea of linear confinement, which is expected for QCD at large distances. This can be illustrated as a flux tube with constant energy per unit length, that is stretched between two quarks. The resulting linear potential can be written as, $V(r) = \kappa r$, where κ is the string constant known from hadron-mass spectroscopy to be $\kappa \approx 1$ GeV/fm ≈ 0.2 GeV^2. For the case of a back-to-back $q\bar{q}$ pair the string can be stretched to some length, $r \approx 5 - 10$ fm, in the quarks' rest frame, until it breaks to produce a new $q'\bar{q}'$ pair. This processes repeats until n primary hadrons are formed from adjacent $q\bar{q}$ pairs.

3.2.4. Decays and Soft Interactions

After hadronisation there are hadronic decays, that decay the hadrons into more stable particles detected by experiments. These decays can include electromagnetic, strong and weak processes, and result in hundreds of different particles via thousands of different decay modes. Options to control the output of these decays encompass the inclusion of heavy quarks, heavier baryon multiplets and intermediate decay modes [24]. Specialised eternal packages can be used for both hadron decays, EvtGEN [39], and tau decays, TAUOLA [40] which can be important for analyses involving heavy hadrons or tau decays.

There are many soft interactions, particularly in pp collisions, which are not necessarily associated with the hard scattering. These soft interactions are generally divided into two categories, elastic and inelastic. Elastic scattering implies only an exchange of momenta by emission or annihilation of particles. Inelastic describes all cases where there is some change in the particle content. The inelastic final states can be categorised as diffractive or non-diffractive, where a topology from an excitation of beam particles is considered to be diffractive and can be further specified depending on how many particles are excited [24]. Minimum-bias events are used to measure such soft-physics interactions, because these are selected to be as inclusive as possible. Underlying event (UE) is a term used to describe all interactions in an event other that the hard collision. Models of multiple parton interactions (MPI) aim to describe the case where more than one pair of partons interact in the same collision. Most current implementations of MPI models follow the same principles first outlined in [41], that includes defining the double-parton cross section, which can be calculated perturbatively.

Parton Showers Background

Parton showers were briefly introduced in the previous chapter, in the context of MC event generators and MC methods. A simple example of an MC evolution algorithm is given in Sec. 3.2.1. However, before MC event generators were developed the formalism of parton evolution was established using concepts from field theory. The foundations of this evolution are based on the DGLAP formalism, that contains the so called Altarelli-Parisi (AP) splitting functions from [42]. In this chapter, the known single-emission splitting functions are introduced, in the context of DGLAP evolution in Sec. 4.1. The study of soft and collinear factorisation led to the development of the dipole formalism, discussed in Sec. 4.3, which makes use of the AP splitting functions. This formalism and the splitting functions are of particular interest in this thesis as they are used as reference points for the development of new methods. The current status of dipole showers is outlined in Sec. 4.4, followed by a discussion of future directions in Sec. 4.5, which aim to improve upon the existing paradigm.

For the complex final states observed at the LHC, there is no analytical way to predict these collisions, due to QCD colour confinement effects at large distances. However, MC event generators have been developed to give a good approximation of such QCD effects. Electroweak effects also need to be considered for higher-order corrections, such as bremsstrahlung of soft photons from charged particles in the final state. Due to the large mass of the weak mediators higher-order corrections for weak interactions can be larger than expected [13]. It is possible to integrate both QED and QCD radiation within a shower, where the QED showering pairs are dictated by the particle charge as opposed to colour in the QCD case. There is resulting competition in different regions of phase space between the two types of radiation, that can be used to probe the ordering variable used for the parton shower [43]. This thesis focuses on QCD radiation, however, most of the concepts can also be applied to the QED case by considering only abelian terms.

4.1. DGLAP evolution

As was discussed in Sec. 2.2.1, a QCD amplitude can be factorised into different components at different energy scales. The definition of a factorisation scale, often written as μ_F, results

in a scale dependence of the PDFs. This behaviour is described by the DGLAP equations [42, 44–46], for PDFs with a changing factorisation scale, t, in the collinear limit:

$$t\frac{\partial}{\partial t}q(x,t) = \frac{\alpha_s(t)}{2\pi}\int_x^1 \frac{d\xi}{\xi}P\left(\frac{x}{\xi}\right)q(\xi,t) \ . \tag{4.1}$$

$P = P_{qq}^{(0)}$, and is the first term of P_{qq}, the Altarelli-Parisi splitting function given in Eq. (4.12), when perturbatively expanded in the running coupling as [9]:

$$P_{qq}(z,\alpha_s) = P_{qq}^{(0)}(z) + \frac{\alpha_s}{2\pi}P_{qq}^{(1)}(z) + ... \tag{4.2}$$

The function in Eq. (4.2) describes the branching between quark distributions, but it is possible to define such a splitting function for each possible branching between quarks and gluons. The DGLAP equation can also be written as a matrix equation for quarks, antiquarks and gluons.

MC event generators utilise the concept of DGLAP evolution and via repeated use of Eq. (4.1) can produce an arbitrary number of parton splittings, which leads to a multi-particle final state. The issue with the DGLAP equations are that they are only true for the strictly collinear case, which is not compatible with conserved momentum and a finite factorisation scale. This can be solved by using a recoil method to define a relation between the momenta of the emitted particle and other particles in the same state. These 'spectator' partons absorb kinetic energy from the recoil to allow an on-shell emitter to produce two new on-shell particles. There is also the issue of the resolution scale set by QCD of Λ_{QCD}, this requires that the evolution has to be cut off at a scale of order Λ_{QCD} and restricts the integration range in comparison to the inclusive approach proposed by the DGLAP equations. The practical implementation of the shower kinematics will be discussed in the following sections.

4.1.1. Altarelli-Parisi Splitting Functions

The single emission Altarelli-Parisi splitting functions, $P_{ba}(z)$, describe the probability of the emission of a collinear parton a from parton b, as a function of the momentum fraction z. In the context of collinear emissions, they usually refer to the leading order contribution from Eq. (4.2). The splitting functions are defined at the collinear limit, where the virtuality $y = 0$. Due to flavour symmetry and charge conjugation invariance the following relations exist between splitting functions [8]:

$$P_{qq} = P_{\bar{q}\bar{q}} \ , \qquad P_{q\bar{q}} = P_{\bar{q}q} \ , \tag{4.3}$$

$$P_{qg} = P_{\bar{q}g} \ , \qquad P_{gq} = P_{g\bar{q}} \ . \tag{4.4}$$

To conserve momentum and flavour with each emission between partons b and a, a second parton is produced. This second parton can be ignored for PDF evolution, but in a parton shower this contributes to both ISR and final-state radiation (FSR) and is included in the final state. The regularised splitting functions, $P_{ba}(z)$, are given by:

$$P_{qq} = C_F\left[\frac{1+z^2}{(1-z)_+} - \frac{3}{2}\delta(1-z)\right] \ , \qquad P_{qg} = C_F\left[\frac{1+(1-z)^2}{z}\right] \ , \tag{4.5}$$

$$P_{gq} = T_R\left[z^2 + (1-z)\right] \ , \qquad P_{gg} = 2\,C_A\left[\frac{z}{(1-z)_+} + \frac{1-z}{z} + z(1-z)\right]$$

$$+ \delta(1-z)\left(\frac{11}{6}C_A - \frac{2}{3}n_f T_R\right) \ .$$

At $z = 1$ both P_{qq} and P_{gg} have to be treated as distribution functions and the plus prescription is defined as [8]:

$$F(z)_+ = F(z) - \delta(1-z) \int_0^1 \mathrm{d}y F(y) \ . \tag{4.6}$$

A second form of the splitting function is that in the context of factorisation with spin correlations where the function, $\hat{P}_{ab}(z, k_\perp; \epsilon)$, is dependent on the momentum fraction, transverse momentum and helicity. The relevant splitting is given by [15] :

$$a(p) \rightarrow b(zp + k_\perp + \mathcal{O}(k_\perp^2)) + c((1-z)p - k_\perp + O(k_\perp^2)) \ ,$$

and the splititng functions take the form:

$$\langle s| \hat{P}_{qq}(z, k_\perp; \epsilon) |s'\rangle = \delta_{ss'} C_F \left[\frac{1+z^2}{1-z} - \epsilon(1-z) \right] \ , \tag{4.7}$$

$$\langle s| \hat{P}_{qg}(z, k_\perp; \epsilon) |s'\rangle = \delta_{ss'} C_F \left[\frac{1+(1-z)^2}{z} - \epsilon z \right] \ , \tag{4.8}$$

$$\langle \mu| \hat{P}_{gq}(z, k_\perp; \epsilon) |\nu\rangle = T_R \left[-g_\mu^\nu + 4z(1-z)\frac{k_\perp^\mu k_\perp^\nu}{k_\perp^2} \right] \ ,$$

$$\langle \mu| \hat{P}_{gg}(z, k_\perp; \epsilon) |\nu\rangle = 2C_A \left[-g^{\mu\nu} \left(\frac{z}{1-z} + \frac{1-z}{z} \right) - 2(1-\epsilon)z(1-z)\frac{k_\perp^\mu k_\perp^\nu}{k_\perp^2} \right] \ . \tag{4.9}$$

The indices in the bra-ket refer to the relevant spin indices for parent parton a, which for a fermion are s, s' and for a gluon are μ, ν. It is then possible to perform the d-dimensional average over polarisations of parton a that leads to the third and more well known form of the splitting functions. For fermions this averaging gives a factor of $\delta_{ss'}/2$ and for gluons the factor is:

$$\frac{1}{d-2} d_{\mu\nu}(p) = \frac{1}{2(1-\epsilon)} (-g_{\mu\nu} + \text{gauge terms}) \ , \tag{4.10}$$

where the gauge terms are always proportional to p^μ or p^ν and thus:

$$-g^{\mu\nu} d_{\mu\nu}(p) = d - 2 \ , \qquad -k_\perp^\mu d_{\mu\nu}(p) = k_{\perp\nu}$$
$$p^\mu d_{\mu\nu}(p) = 0 \tag{4.11}$$

The averaging results in the following expressions:

$$\langle \hat{P}_{qq} \rangle = C_F \left[\frac{1+z^2}{1-z} - \epsilon(1-z) \right] \ , \qquad \langle \hat{P}_{qg} \rangle = C_F \left[\frac{1+(1-z)^2}{z} - \epsilon z \right] \ , \tag{4.12}$$

$$\langle \hat{P}_{gq} \rangle = T_R \left[1 - \frac{2z(1-z)}{1-\epsilon} \right] \ , \qquad \langle \hat{P}_{gg} \rangle = 2C_A \left[\frac{z}{1-z} + \frac{1-z}{z} + z(1-z) \right] \ .$$

The angle brackets imply that the average over the polarisations of parton a has been taken. These functions are now only in terms of the momentum fraction z and the dimensional parameter ϵ. The soft limits for the emitter and emission respectively are characterised by the divergences at $z \rightarrow 0, 1$. To describe soft and collinear behaviour, both the splitting functions and the eikonal factors are needed which will be discussed in Sec. 4.3. This can result in double counting in overlapping regions, which needs to be carefully avoided.

4.2. NLO Subtraction

Using the principles of the dipole formalism, outlined in Sec. 4.3, it is possible to define a subtraction scheme for NLO subtraction known as dipole subtraction. Here, this will be shown

in the context of the methods used in [15], which are designed for general jet observables and are inspired by previous methods for three-jet observables from e^+e^- annihilation experiments [47, 48]. These early examples then led to formalisms for hadron collisions up to two-jet observables [49, 50], which were later extended up to three jets [16, 51]. These three-jet methods can in principle be used to describe up to n-jet observables for both lepton and hadron collisions.

The aim of the dipole subtraction method, as developed in [15], is to provide a general subtraction algorithm via dipole factorisation, which allows universal counter-terms to be determined. This formalism can be applied to an arbitrary number of jets in a final state and can also describe multi-particle correlations. It can also be applied to both massive and massless quarks and extended to cases of polarised scattering. First it is necessary to introduce the notation associated with jet cross sections. The leading order cross section is determined from the differential Born cross section, which is fully exclusive according to the Born approximation for the phase space of the quantity of interest [15] :

$$\sigma^{LO} = \int_n \mathrm{d}\sigma^B \ ,$$
(4.13)

for an n particle final state. The NLO cross section can then be written as a combination of the real and virtual parts, where the virtual parts correspond to one-loop corrections at this order:

$$\sigma^{NLO} \equiv \int \mathrm{d}\sigma^{NLO} = \int_{n+1} \mathrm{d}\sigma^R + \int_n \mathrm{d}\sigma^V \ .$$
(4.14)

Using renormalisation, the ultraviolet poles in the virtual contributions can be removed and after dimensional regularistion the only double poles, $1/\epsilon^2$, remaining are those arising from the soft and collinear cases. These poles can be subtracted by using a local counter-term $\mathrm{d}\sigma^A$, which contains the singular behaviour from $\mathrm{d}\sigma^R$, giving:

$$\sigma^{NLO} = \int_{n+1} \left[\left(\mathrm{d}\sigma^R\right)_{\epsilon=0} - \left(\mathrm{d}\sigma^A\right)_{\epsilon=0} \right] + \int_n \left[\mathrm{d}\sigma^V + \int_1 \mathrm{d}\sigma^A \right]_{\epsilon=0} \ .$$
(4.15)

The counter-term has to be analytically integrable over the single-parton subspace to cancel the divergences in the virtual contributions. This subtraction of the poles then makes the numerical integration of both the $n + 1$ and the n-parton phase spaces possible. Such a counter-term can be implemented in an MC event generator that generates events with both $n + 1$ and n final-state partons. The counter-term needs to be established independently of the process of interest and match the singular behaviour of the real part in d dimensions exactly. For dipole factorisation the counter-term can be defined as:

$$\mathrm{d}\sigma^A = \sum_{\mathrm{dipoles}} \mathrm{d}\sigma^B \otimes \mathrm{d}V_{\mathrm{dipole}} \ ,$$
(4.16)

where $\mathrm{d}V_{dipole}$ contains universal dipole factors that can describe the singular behaviour of $\mathrm{d}\sigma^R$. The observable dependence is contained in the Born part, which is combined with the dipole factors via the convolution of phase space and summing over colour and spin. The dipole configurations are defined by taking an n-parton state and allowing one of the partons to decay into two, giving a configuration with $n + 1$ partons. A mapping can then be implemented to connect the $n + 1$ to n-parton phase space times a single-parton phase space. This facilitates the cancellation of the virtual poles contained in the factor $\boldsymbol{I}$:

$$\int_{n+1} \mathrm{d}\sigma^A = \sum_{\mathrm{dipoles}} \int_n \mathrm{d}\sigma^B \otimes \int_1 \mathrm{d}V_{\mathrm{dipole}} = \int_n \left[\mathrm{d}\sigma^B \otimes \boldsymbol{I} \right] \ .$$
(4.17)

Once the expressions for the factors dV_{dipole} and $\boldsymbol{I}$ are determined they can be implemented for NLO subtraction. The implementation requires knowledge of the virtual and real contributions for the observable of interest, as well as colour and helicity projections of the Born-level matrix element. The virtual contributions need to be evaluated in d dimensions but the real contributions can be evaluated in four dimensions, as it is known that the poles exactly cancel.

The Born-level cross section for a jet observable, in d-dimensions with no initial-state hadrons, can be written in terms of the QCD tree-level matrix element, $\mathcal{M}_n$, as [15]:

$$\mathrm{d}\sigma^B = \mathcal{N}_{in} \sum_{\{n\}} \mathrm{d}\phi_n(p_1, ..., p_n; Q) \frac{1}{S_{\{n\}}} |\mathcal{M}_n(p_1, ..., p_n)|^2 F_J^{(n)}(p_1, ..., p_n) \ , \tag{4.18}$$

where $\mathcal{N}_{in}$ contains factors that are QCD independent, $\{n\}$ contains all configurations with n partons, ϕ_n is the n-parton phase space and $S_{\{m\}}$ is the Bose symmetry factor for identical partons in the final state. The jet function, $F_J^{(n)}(p_1, ..., p_n)$, defines the jet observable of interest in terms of the final-state partons.

Using the dipole factorisation formula in Eq. (4.27), combined with the Born-level cross section from Eq. (4.18), the counter term $\mathrm{d}\sigma^A$ can be expressed as:

$$\begin{aligned}
\mathrm{d}\sigma^A = \mathcal{N}_{in} \sum_{\{n+1\}} \mathrm{d}\phi_{n+1}(p_1, ..., p_{n+1}; Q) \frac{1}{S_{\{n+1\}}} \\
\times \sum_{(\text{pairs } i,j)} \sum_{k \neq i,j} \mathcal{D}_{ij,k}(p_1, ..., p_{n+1}) F_J^{(n)}(p_1, ..., \tilde{p}_{ij}, \tilde{p}_k, ..., p_{n+1}) \ ,
\end{aligned} \tag{4.19}$$

where $\mathcal{D}_{ij,k}$ is the dipole contribution as given in Eq. (4.27). $F_J^{(n)}$ is the jet function for the n-parton state that results from combining the momenta p_i and p_j into $\tilde{p}_{ij}$. This counter term can be used to cancel the singularities in the real part of the cross section, $\mathrm{d}\sigma^R$. The jet function plays an important role in regularising the dipole singularities, so that it is necessary for $\mathrm{d}\sigma^R$ to be proportional to $F_J^{(n+1)}$ and $\mathrm{d}\sigma^A$ to $F_J^{(n)}$. The actual mechanism does not depend on the form of the jet function. Within an MC algorithm, the role of the jet functions is to bin weighted events according to the jet observable. When a singular region is approached, the bins for the functions $F_J^{(n+1)}$ and $F_J^{(n)}$ become the same and the weights cancel.

4.3. Dipole Formalism

To construct the counter terms needed for NLO subtraction the relevant soft and collinear behaviour needs to be established. In the context of dipole subtraction from [15], this is done by factorising the singular emissions from a dipole, to relate an amplitude with $n + 1$ partons in the final state to that with n partons. For an amplitude squared this can be written as:

$$|\mathcal{M}_{n+1}|^2 \rightarrow |\mathcal{M}_n|^2 \otimes \boldsymbol{V}_{ij,k} \ , \tag{4.20}$$

where $\boldsymbol{V}_{ij,k}$ is a factor containing the singular factors for 'emitter' parton ij and 'spectator' parton k. The dipole factorisation makes use of the known concepts of soft and collinear factorisation, which were introduced in Sec. 2.2.1. These concepts are shown in the context of a soft or collinear emission in a multi-parton final state in Sec. 4.3.1.

4.3.1. Soft and Collinear Factorisation of an Emission

For the case of a soft emission within an $(n+1)$-parton final state, the soft momentum can be parametrised as $p_j = \lambda q$, where in the soft limit $\lambda \to 0$. The soft emission can be factorised from the matrix element to give the expression:

$$\langle \mathcal{M}_{n+1} | \mathcal{M}_{n+1} \rangle \to - \frac{1}{\lambda^2} 4\pi\mu^{2\epsilon}\alpha_s \langle \mathcal{M}_n | [\boldsymbol{J}^\mu(q)]^\dagger \boldsymbol{J}_\mu(q) | \mathcal{M}_n \rangle + ... \ , \tag{4.21}$$

that contains the leading soft-singular terms and the ellipsis refers to sub-leading terms. The component which factorises is the eikonal current $\boldsymbol{J}_\mu(q)$, that is given by:

$$\boldsymbol{J}^\mu(q) = \sum_i \mathbf{T}_i \frac{p_i^\mu}{pi \cdot q} + \mathbf{T}_a \frac{p_a^\mu}{p_a \cdot q} + ... \ . \tag{4.22}$$

This factorisation is not exact due to colour correlations, as the eikonal current is dependent on the colour of the hard partons. In this definition, initial-state momenta are included, and are denoted by p_a and the ellipsis. In further discussions only the final state will be considered, where these terms can be neglected. The matrix elements are only defined when momentum is conserved. Eq. (4.21) holds in the strict soft limit, where $\lambda = 0$, away from this limit, momentum conservation needs to be carefully implemented to facilitate the factorisation. In the massless limit the eikonal current squared can be written as:

$$[\boldsymbol{J}^\mu(q)]^\dagger \boldsymbol{J}_\mu(q) = \sum_{k,i} \mathbf{T}_k \cdot \mathbf{T}_i \frac{p_k \cdot p_i}{(p_k \cdot q)(p_i \cdot q)} \ . \tag{4.23}$$

To separate the collinear singularities, that correspond to q collinear to p_i or p_k, the above expression can be rewritten as:

$$\begin{aligned}
\sum_{k,i} \mathbf{T}_k \cdot \mathbf{T}_i \frac{p_k \cdot p_i}{(p_k \cdot q)(p_i \cdot q)} &= \sum_{k,i} \mathbf{T}_k \cdot \mathbf{T}_i \left[\frac{p_k \cdot p_i}{(p_k \cdot q)(p_i + p_k) \cdot q} + \frac{p_k \cdot p_i}{(p_i \cdot q)(p_i + p_k) \cdot q} \right] \\
&= \sum_{i,k\neq i} \frac{2}{p_i \cdot q} \mathbf{T}_k \cdot \mathbf{T}_i \frac{p_k \cdot p_i}{(p_i + p_k) \cdot q} \ .
\end{aligned} \tag{4.24}$$

At this point the dipole structure can already be seen, as the terms in Eq. (4.24) depend on the emission momentum q and the momenta p_i and p_k, that can be labelled as the emitter and spectator respectively.

In the collinear limit, a Sudakov decomposition [52] can be used for the final-state momenta p_i and p_j. The limit in which the final-state momenta become collinear, corresponds to $k_\perp \to 0$ [15]:

$$p_i^\mu = zp^\mu - \frac{k_\perp^2}{z(2p \cdot n)}n^\mu + k_\perp^\mu \ , \tag{4.25a}$$

$$p_j^\mu = (1-z)p^\mu - \frac{k_\perp^2}{(1-z)(2p \cdot n)}n^\mu - k_\perp^\mu \ , \tag{4.25b}$$

$$2p_i \cdot p_j = - \frac{k_\perp^2}{z(1-z)} \ , \tag{4.25c}$$

where p and n are light-like vectors. p gives the collinear direction and $k_\perp$ is the transverse component *i.e.* $k_\perp^2 < 0$, $k_\perp \cdot p = k_\perp \cdot n = 0$. For a final-state matrix element with $n+1$ partons, factorisation is possible by replacing partons i and j with one parton labelled ij which can be written as:

$$\langle \mathcal{M}_{n+1} | \mathcal{M}_{n+1} \rangle \to \frac{1}{p_i \cdot p_j} 4\pi\mu^{2\epsilon}\alpha_s \langle \mathcal{M}_n | \hat{P}_{(ij),i}(z, k_\perp, \epsilon) | \mathcal{M}_n \rangle \ , \tag{4.26}$$

where $\hat{P}_{(ij),i}$ are the spin dependent Altarelli-Parisi splitting functions in d-dimensions as given in Eq. (4.7). The splitting functions describe the collinear splitting of $ij \rightarrow i + j$ and depend on the momentum fraction z, the transverse momentum $k_\perp$ and the helicity of the parton ij. The resulting spin correlations prevent the full factorisation of the amplitude from the splitting function.

4.3.2. Dipole Factorisation

For an emission from a dipole composed of two final-state partons, it is possible to combine the methods described above to form a dipole factorisation formula. This is essentially an expansion of the expression in Eq. (4.20), as a sum over spectator partons k, and is written as [15]:

$$\langle \mathcal{M}_{n+1} | \mathcal{M}_{n+1} \rangle = \sum_{k \neq i,j} \mathcal{D}_{ij,k}(p_1, ..., p_{n+1}) + \text{finite terms} ,$$

$$\mathcal{D}_{ij,k} = -\frac{1}{S_{ij}} \langle \mathcal{M}_n | \mathcal{C}_{ij,k} \boldsymbol{V}_{ij,k} | \mathcal{M}_n \rangle ,$$

(4.27)

where $S_{ij} = (p_i + p_j)^2$ and $\mathcal{C}_{ij,k}$ contains the relevant colour structure. The finite terms are those that are non-singular in the limit $p_i \cdot p_j \rightarrow 0$.

The mapping used for this dipole, in a final state without any initial-state partons, to describe the splitting $\tilde{p}_{ij} \rightarrow p_i + p_j$, is:

$$\tilde{p}_{ij}^\mu = p_i^\mu + p_j - \frac{y_{ij,k}}{1 - y_{ij,k}} p_k^\mu , \tag{4.28a}$$

$$\tilde{p}_k^\mu = \frac{1}{1 - y_{ij,k}} p_k^\mu , \tag{4.28b}$$

where p_k is the spectator momentum and $y_{ij,k}$ is given by:

$$y_{ij,k} = \frac{p_i \cdot p_j}{p_i \cdot p_j + p_j \cdot p_k + p_k \cdot p_i} . \tag{4.29}$$

The total momentum before and after the emission is conserved, *i.e.* $p_i + p_j + p_k = \tilde{p}_{ij} + \tilde{p}_k$ and both the emitter and spectator momenta are on-shell. In Eq. (4.27), $\boldsymbol{V}_{ij,k}$ corresponds to splitting matrices in the helicity space of the emitter that depend on $y_{ij,k}$, z_i and z_j. The variable z_i is defined as:

$$z_i = \frac{p_i \cdot p_k}{p_j \cdot p_k + p_i \cdot p_k} = \frac{p_i \tilde{p}_k}{\tilde{p}_{ij} \tilde{p}_k} , \tag{4.30}$$

and $z_j = 1 - z_i$. These variables take different forms in the soft and collinear limits to reproduce the expected factorisation expressions from Sec. 4.3.1.

In the collinear limit, Eq. (4.27) can be related to the known splitting functions, from Eq. (4.5). The dipole variables in the collinear limit can be written as:

$$z_i = 1 - z_j \rightarrow z ,$$

$$y_{ij,k} \rightarrow -\frac{k_\perp^2}{2z(1-z)p \cdot p_k} ,$$

$$\tilde{p}_k \rightarrow p_k , \qquad \tilde{p}_{ij} \rightarrow p .$$

(4.31)

This results in $\boldsymbol{V}_{ij,k}$ being equivalent to:

$$\boldsymbol{V}_{ij,k} \rightarrow 8\pi \mu^{2\epsilon} \alpha_s \hat{P}_{(ij),i}(z, k_\perp; \epsilon) , \tag{4.32}$$

where $\hat{P}_{(ij),i}$ are the collinear splitting functions. This expression can be inserted into Eq. (4.27) to give the collinear factorisation result from Eq. (4.26).

In the soft limit, the dipole variables become:

$$
\begin{aligned}
z_i \to 1 \;, \qquad z_j \to 0 \;, \qquad y_{ij,k} \to 0 \;, \\
\tilde{p}_k \to p_k \;, \qquad \tilde{p}_{ij} \to p_i \;,
\end{aligned}
\tag{4.33}
$$

where the momentum $p_j = \lambda q$ and $\lambda \to 0$. The expression for $\boldsymbol{V}_{ij,k}$ can then be written as:

$$
\lambda \boldsymbol{V}_{ij,k} \to 16\pi\mu^{2\epsilon}\alpha_s \boldsymbol{T}_{ij}^2 \frac{p_k \cdot p_i}{(p_i + p_k) \cdot q} \;.
\tag{4.34}
$$

When this is inserted into Eq. (4.27), the soft eikonal factor from Eq. (4.24) is reproduced. This shows that dipole factorisation can reproduce both the soft and collinear factorisation results.

The splitting kernels $\boldsymbol{V}_{ij,k}$ are helicity dependent, which gives rise to azimuthal correlations that are essential for determining the local counter-term $\mathrm{d}\sigma^A$. There are different factorisation formulae and mappings used for different dipoles, *e.g.* final-final, initial-final, final-initial, initial-initial, that are given in [15]. The discussion in this section is applies to the massless case, that is relevant to the work in this thesis. The massive case is addressed in [53].

4.4. Comparison of Existing Parton Showers

As was introduced in Sec. 3.2.1, parton showers facilitate the decay of high energy partons from the hard process via a shower algorithm. This algorithm requires the known splitting functions, from Sec. 4.1.1, and must evolve using an evolution variable of choice. The kinematic mapping used is also an important choice as this determines how the recoil from the emissions is distributed.

There are two main type of parton showers, angular-ordered and dipole showers, where for angular-ordered showers the emissions are ordered in decreasing angle. Angular ordering is motivated by colour coherence, that shows that for a hard scattering process the colour lines will be scattered through a small angle. This leads to a suppression of large-angle radiation, which is analogous to the QED Chudakov effect. Analysis of antenna radiation shows the property of angular ordering for soft emissions, *i.e.* each emission is emitted at an angle less than the angle between the two antenna particles. To implement these properties in a parton shower, a coherent-branching algorithm can be used, where the evolution variable is proportional to the opening angle of the emission. Coherent branching can describe soft and collinear emissions, where each parton radiates proportional to its colour charge squared.

Some dipole showers implement colour coherence via an angular veto, that imposes angular ordering. This also relates to the choice of evolution variable, *e.g.* $\theta, p_\perp$, that for angular-ordered showers has to be directly related to the angle between emission and emitter. For dipole showers there is more flexibility in the choice of ordering variable, however, the most common choice is some form of the transverse momentum of the emission relative to the emitter.

Another important feature that differs between parton-shower methods is the distribution of recoil. An angular-ordered shower distributes the recoil globally across all partons in the initial or final state. The design of a dipole shower is usually such that the recoil is shared between the dipole partners and therefore locally within the dipole frame. Both Pythia and Sherpa have a default dipole shower with local recoil, whereas Herwig has a default angular-ordered

shower but also offers a dipole shower. There are also two shower plug-ins, VINCIA [54, 55] and Dire [56], which are both compatible with Pythia, Dire is also compatible with Sherpa.

Both angular and dipole showers agree in the soft and collinear limits, however, there are inconsistencies in small regions of phase space away from these limits, that are increasingly important for non-global observables. The work in this thesis is directly applicable to dipole showers and therefore the discussion here will focus on the concepts used in dipole showers. The first implementation of a dipole approach was in Ariadne [57], which is based on the concept of a colour flow composed of colour lines between colour-singlet pairs. In the soft-gluon and large-N_c limit each colour line emits independently. Transverse momentum is the natural ordering variable to use for dipole showers, as the dipole approximation is valid when the transverse momentum of the emission, with respect to the emitter, is much smaller than the scales of the preceding parent emissions.

The Ariadne shower makes use of the colour dipole model from [58], where the recoil from an emission is absorbed by both partons of the emitting dipole, although the transverse recoils are distributed differently depending on the type of dipole *i.e.* $q - g$ or $g - g$. The ordering variable used is the transverse momentum, $p_\perp$, which is defined as [24]:

$$p_\perp^2 = S_{\text{dip}}(1 - x_1)(1 - x_2) , \tag{4.35}$$

where S_{dip} is the invariant mass squared of the dipole and $x_i = 2E_i/\sqrt{S_{\text{dip}}}$. The rapidity can then be defined as:

$$y = \frac{1}{2} \ln \frac{1 - x_1}{1 - x_2} , \tag{4.36}$$

which gives an approximation of the splitting function as $D(p_\perp, y) \propto \mathrm{d}y \, \mathrm{d}\ln p_\perp$, to be used in the shower algorithm. The Pythia 8 shower, from [59], also uses transverse momentum as the ordering variable but it is defined slightly differently for initial and final state radiation (ISR/FSR):

$$
\begin{aligned}
p_{\perp\text{evol}}^2 &= (1 - z)Q^2 \to \text{ISR} , \\
p_{\perp\text{evol}}^2 &= z(1 - z)Q^2 \to \text{FSR} ,
\end{aligned} \tag{4.37}
$$

where Q^2 is the virtuality of the off-shell intermediate parton and z is the momentum fraction.

Both the Herwig dipole shower [60] and the shower in Sherpa [61] are based on the Catani-Seymour (CS) dipole formalism [15, 53], that is outlined in Sec. 4.3. The dipole subtraction terms are used to derive shower splitting operators via the large-N_c limit and performing the sum and average over spins. The four possible dipole combinations between the initial and final states have to be accounted for and are labelled according to FF, IF, FI and II, where initial = I and final = F. The transverse momentum of an emission relative to the emitter beam particle is used as the evolution variable. Some of the benefits of this type of shower include local momentum conservation due to the recoil being balanced within the dipole and the eikonal factor from soft factorisation maps to two CS dipoles, which is in agreement with the soft colour coherence for QCD.

There are still many areas to be improved, that are poorly described by existing parton showers. Some of the flaws and potential ways forward to fix these issues are described in the next section.

4.5. Challenges and Potential Solutions

Parton showers are built using soft and collinear approximations. They are by definition not exact and are not designed to deal with hard wide-angle radiation or multi-jet final states

which are important for some observables. They are also only valid within a limited energy range, down to the scale at which perturbation theory no longer holds and hadronisation models need to be used. The main purpose of parton showers is to include leading logarithmic contributions and to be process independent. They are restricted to MC integration and perturbative scales. In comparison, resummation methods are analytical calculations at low $p_\perp$ that can re-sum all logs. They can probe to higher orders in perturbation theory, which then also leads to non-perturbative structures. The problem with resummation is that the low $p_\perp$ factorisation is process dependent and requires inclusive final states.

Therefore, to describe exclusive final states, parton showers are needed as a vital part of MC event generators. As observables from experiments are measured with increasing precision, the development of the simulations has to compete to increase the accuracy of the event generator predictions. One obvious way to do this is to include higher order corrections to the hard matrix element. As discussed in Sec. 3.2.2, it is necessary to match or merge these higher-order calculations with the parton shower to avoid double counting. To include higher order corrections in parton showers they need to go beyond $2 \rightarrow 3$ splittings, which is the current standard in dipole showers. The next order of splittings includes the $2 \rightarrow 4$ branchings with both one and two emitters, that results in splitting functions accurate to $\mathcal{O}(\alpha_s^2)$.

The collinear two-emission splitting functions were calculated by Catani and Grazzini and given in [62]. In recent years there have been steps towards including second-order emissions in parton showers, in the context of the VINCIA antenna shower [63] a showering algorithm has been developed to include higher-order branching. Also for the Dire framework [64] an algorithm has been shown that makes use of the splitting functions to describe triple-collinear emissions. The implementation was tested in combination with Pythia and Sherpa, with a potential for $\sim 1\%$ effects in differential jet rates. However, as of yet there has been no integration of second-order splittings in the default parton shower of an event generator or in a matching or merging method.

Current parton shower approaches lack a systematic expansion of uncertainties to higher orders, that makes the numerical size of theoretical uncertainties very difficult to measure. Especially as showers are tuned to experimental observables, they can often be very precise, but potentially with large uncertainties. To avoid theory uncertainties becoming dominant in MC simulations, it is necessary to address this within parton showers.

Another issue with current showers is the lack of proper treatment of colour and azimuthal correlations. The splitting functions and algorithms used in parton shower are defined at the cross-section level which implies colour and spin averaging. This affects the colour evolution in the shower and also the subsequent cluster formation, as cluster are formed from colour singlets that are close in phase space. To account for MPI events in Herwig, a colour reconnection model was introduced in [65], to connect partons that are close in phase space but originate from different hard processes. However, this could also be correcting the colour evolution from the parton shower and covering up the loss of information about the colour correlations, that needs to be addressed at the level of each emission.

Fundamental issues with the logarithmic accuracy of both dipole [66] and angular ordered showers [67] have recently been highlighted, which calls for a restructuring of currently applied methods. For global observables, issues arise for next-to-leading logarithms (NLL) at leading colour and for leading logarithms (LL) at next-to-leading colour. Dipole showers can describe non-global and global observables correctly at LL accuracy, at leading colour, but not at NLL accuracy. Angular ordered showers are also only LL accurate for both non-global and global observables. There are specific errors from angular ordered showers at NLL accuracy, that are due to the failure of coherent branching for the non-global case. The most clear example of where dipole showers fail is that for two emissions from a $q\bar{q}$ dipole, where both emissions are

either soft or collinear and are widely separated in rapidity. The double emission probability in this case should have the colour factor C_F^2. What is actually produced by dipole showers in the soft-collinear region of phase space is the factor $C_F C_A/2$ which gives an incorrect contribution at sub-leading colour.

Jet substructure studies often require access to a large range of energy scales that can only be predicted by parton showers. It is important that these predictions are accurate and that the issues introduced above are addressed. One potential source of problems is that dipole showers are designed so that the spectator only absorbs longitudinal recoil. This results in a loss of the original jet direction, as the emitter is shifted as it absorbs the transverse recoil. To have a parton shower that is NLL accurate, for non-global observables, it is necessary to be able to resolve two emissions separately. Whereas for global observables, azimuthal averaging can still be used to provide an accurate shower. This implies that to describe both non-global and global observables to higher logarithmic accuracy, serious redevelopment is required at the level of the kinematic mapping and of the parton-evolution algorithm.

Based on proposed criteria for parton showers to be accurate at next-to-leading logarithmic (NLL) order, two new showers, PanLocal and PanGlobal [68], with local and global recoil respectively, were developed. These criteria are defined in the large-N_C limit and for NLL accuracy require that in the limit where every pair of emissions has distinct values for at least one of the logarithmic variables (*e.g.* energy, angle), the shower can correctly reproduce the squared tree-level matrix element. Additionally, the showers are required to reproduce analytical NLL resummations for recursively infrared and collinear safe observables (rIRC) [69], which is a measure of the virtual corrections. For both the local and global-recoil showers agreement is shown with analytical NLL calculations of global and non-global observables.

There has also been activity in the development of an amplitude-level parton branching algorithm [70], with the aim to go beyond leading colour and include spin correlations. The soft-gluon evolution algorithm from [71] is used as a starting point and improved to include collinear emissions, spin dependence and recoil. This can provide a clear link between resummation calculations and parton showers and can be systematically improved to include NLL accuracy. Subsequently, a new dipole shower was derived in [72] that combines aspects of existing dipole and angular ordered showers and can describe observables to NLL accuracy as well as the wide-angle soft radiation pattern at leading colour. It is however, defined at leading colour, which limits the capabilities of the shower. The MC code CVolver [73] makes use of the improved parton branching algorithm to include terms beyond leading colour. It builds on work on colour-flow evolution for soft gluons from [74], which uses the colour-flow basis. The results produced show deviation from the leading-colour approximation for soft-gluon effects in jet-veto cross sections.

Within this thesis steps are taken to develop a new kinematic mapping to be implemented in parton showers, that aims to distribute recoil globally and facilitate amplitude-level factorisation without explicitly taking soft or collinear limits. This mapping is also part of a larger framework [75], to factorise soft and collinear emissions, that aims to provide a solution that can also be extended to higher orders. The Herwig implementation of the new mapping for the single-emission case is shown in Chapter 8. Some results are shown of the analysis of cluster mass and jet variables for the multiple-emission mapping and two other new mappings compared to the Herwig dipole and angular-ordered showers.

Single-Emission Factorisation

The factorisation of soft and collinear emissions from an amplitude is facilitated by a kinematic mapping, which is commonly a Sudakov decomposition as used in [15]. The typical features of such a mapping are the relations for the momenta after an emission parametrised in terms of the momenta before the emission. In Sec. 5.1 the combinatorics of the single-emission diagrams, that can give singular contributions to the cross section, are outlined. The grouping of these contributions into an emission kernel, defined by a collinear combination, is shown, with the help of partitioning factors to separate the collinear sectors. In this chapter, two different single-emission mappings will be discussed. Firstly, in Sec. 5.2 a slightly modified version of the Sudakov decomposition that still treats the recoil locally within the dipole is introduced. Secondly, in Sec. 5.3 a mapping with global recoil treatment via a Lorentz transformation and more general parameters for the soft and collinear behaviour is developed. Results for the first mapping are shown in detail to confirm the correct collinear behaviour and the ability to determine the single-emission splitting functions. For the second mapping the calculations were repeated and similar results obtained. Additionally, the phase-space factorisation, shown in Sec. 5.3.1, was calculated for the mapping with the Lorentz transformation, as this is needed for the phase-space integration and cannot be directly obtained from known results.

5.1. Combinatorics and Partitioning

The aim here is to show how dipole factorisation, as outlined in Sec. 4.3, can be reproduced using the cut diagram formalism, as given in Sec. 2.3.3, with an applied partitioning of singularities. Considering a cross section containing the tree-level QCD matrix element $|\mathcal{M}_{n+1}|^2$, as shown in Eq. (4.20), the singular behaviour can be factorised to give $|\mathcal{M}_n|^2$ and a singular factor dependent on the momenta and quantum numbers of the final-state partons.

As in the dipole formalism, three partons are labelled, i, j, k, where any of the three could become singular and a sum is taken over these indices to include all the final-state partons. To factorise from an $n + 1$ to an n-parton state, one of the partons must be labelled as the emission and the other two are the emitter and spectator. The different combinations that

can give IR-singular contributions to the cross section, can be represented by the following sub-amplitudes:

$$\sigma[n] = \int \Big[\sum_{i<j} \mathcal{M}(i,j)\mathcal{M}^*(i,j) + \sum_{i<j<k} 2\mathrm{Re}\{\mathcal{M}(i,j)\mathcal{M}^*(j,k) \tag{5.1}$$

$$+ \mathcal{M}(i,j)\mathcal{M}^*(i,k) + \mathcal{M}(i,k)\mathcal{M}^*(j,k)\} \Big] u(1,...,n+1)d\phi(1,...,n+1)$$

$$+ \text{finite terms}$$

$$+ \text{finite terms} ,$$

where u is the measurement function and $d\phi$ is the phase space. The lines in the diagrams correspond to a generic parton and the 'blobs' represent the n-parton hard amplitude. These sub-amplitudes can be further expanded with the use of an explicit splitting operator, $\mathbf{Sp}_{ab} = \mathbf{Sp}(q_a, q_b, q_a + q_b)$, that defines the splitting of a parton with momentum $q_a + q_b$, into two partons a and b, with momenta q_a and q_b respectively. Multiple splittings can be described by the combination of splitting operators, which is shown in Sec. 6.1. The diagrams from Eq. (5.1) can then be expressed using the single-emission splitting operator as:

$$\mathcal{M}(i,j)\mathcal{M}^*(j,k) = \langle\tilde{\mathcal{M}}| \mathbf{Sp}_{jk}^\dagger \mathbf{Sp}_{ij} |\tilde{\mathcal{M}}\rangle = \quad \text{} . \tag{5.2}$$

To be able to construct a collinear splitting kernel, all diagrams containing terms that contribute to the collinear limit of interest need to be added together. The different collinear limits in a diagram can be separated using partitioning factors which add up to one. The partitioning factors, w_{ij}, are illustrated for one of the exchange amplitudes below:

$$\langle\tilde{\mathcal{M}}| \mathbf{Sp}_{jk}^\dagger \mathbf{Sp}_{ij} |\tilde{\mathcal{M}}\rangle = \langle\tilde{\mathcal{M}}| \mathbf{Sp}_{jk}^\dagger \mathbf{Sp}_{ij} |\tilde{\mathcal{M}}\rangle \left(\frac{w_{ij|jk}}{w_{ij|jk} + w_{jk|ij}} + \frac{w_{jk|ij}}{w_{ij|jk} + w_{jk|ij}} \right) ,$$
$$= \langle\tilde{\mathcal{M}}| \mathbf{Sp}_{jk}^\dagger \mathbf{Sp}_{ij} |\tilde{\mathcal{M}}\rangle \left(\mathbb{P}_{ij}^{d_1} + \mathbb{P}_{jk}^{d_1} \right) . \tag{5.3}$$

The w factors on the numerator cancel one of the invariants on the denominator arising from the propagators. The resulting term is only singular in one collinear limit, i.e. for $w_{ij|jk}$ the (jk) factor is cancelled and only the singularity for (ij) collinear remains. The numerator and denominator terms together make the partitioning factor which can also be labelled as $\mathbb{P}_{ij}^d$ where the indices ij refer to the collinear terms which will be kept for a diagram d. A

generalised version of this partitioning will be discussed in Sec. 6.3. To check that the correct behaviour is given in the collinear limit, this formalism is used to reproduce the collinear splitting functions, $P_{ab}(z)$, that can be obtained from the relevant amplitudes multiplied by partitioning factors. Here $U_{ij,k}$ is defined as an emission kernel containing all collinear contributions from diagrams times partitioning factors, where ij are collinear and k is the spectator parton. This can be written as:

$$U_{ij,k} = \sum_d \mathbb{P}_{ij}^d \mathcal{A}_d \ , \tag{5.4}$$

where the sum is carried out over all singular sub-diagrams in the set $\mathcal{A}_d$, multiplied by a diagram specific partitioning factor $\mathbb{P}_{ij}^d$. This expression, in the case where partons i and j are collinear, can be written in terms of the following amplitude combinations:

$$\begin{aligned}
U_{ij,k} = \langle \tilde{\mathcal{M}} | \mathbf{Sp}_{ij}^\dagger \mathbf{Sp}_{ij} | \tilde{\mathcal{M}} \rangle + 2Re\{ \langle \tilde{\mathcal{M}} | \mathbf{Sp}_{jk}^\dagger \mathbf{Sp}_{ij} | \tilde{\mathcal{M}} \rangle \frac{w_{ij|jk}}{w_{ij|jk} + w_{jk|ij}} \\
+ \langle \tilde{\mathcal{M}} | \mathbf{Sp}_{ik}^\dagger \mathbf{Sp}_{ij} | \tilde{\mathcal{M}} \rangle \frac{w_{ij|ik}}{w_{ij|ik} + w_{ik|ij}} \} \ .
\end{aligned} \tag{5.5}$$

The set of diagrams for this case includes three combinations, one self-energy type and two exchange diagrams. The self-energy type diagram does not need a partitioning factor as it only has one possible collinear pair. Additionally, $(ij) = (ji)$ holds for the expressions above. These emission kernels are distinct from the Altarelli-Parisi splitting functions as they do not require an explicit limit to be taken. However, they can reproduce the known splitting functions in the collinear limit. Combining all the results for the emission kernels allows the cross section to be re-expressed as follows:

$$\sigma[n] = \int \left[\sum_{i<j<k} (U_{ij,k} + U_{ik,j} + U_{jk,i}) \right] u(1, ..., n+1) d\phi(1, ..., n+1) + \text{finite terms} \ . \tag{5.6}$$

The $U_{ij,k}$ kernels can be related to $\mathcal{D}_{ij,k}$ from [15], which is discussed in Sec. 4.3, as when evaluated in the ij collinear limit the result gives a factor that contains the Altarelli-Parisi splitting function times an amplitude with one less parton.

$$U_{ij,k} = \sum_d P_{ij}^d \mathcal{A}_d(n+1) \xrightarrow{p_i \cdot p_j \to 0} -\frac{1}{S_{ij}} \langle \tilde{\mathcal{M}}_n | \mathcal{C}_{ij,k} \hat{V}_{ij,k} | \tilde{\mathcal{M}}_n \rangle \ , \tag{5.7}$$

where $\hat{V}_{ij,k}$ in this case additionally contains the denominator from the partitioning factor. It can be shown that the partitioning factors do not contribute singular terms in any limit and therefore this expression is equivalent to the Catani-Seymour expression in Eq. (4.27).

The behaviour of the emission kernels away from the collinear limit and the colour correlations that arise from an amplitude-level approach, are of interest to this thesis. The colour correlations need to be understood to successfully construct a parton shower beyond NLO including multiple emissions. In the next section the kinematics are outlined that are needed to carry out the full factorisation calculation for one emission. In the next chapter a more generalised approach will be discussed.

5.2. Basic Kinematic Mapping

The mapping shown below is a modification of the basic Sudakov decomposition in Eq. (4.25), that has the same essential function, to factorise collinear and soft emissions from an emitter-spectator dipole. The aim is to investigate the soft and collinear singularities whilst keeping

them accessible *i.e.* without loss of information. Shown here is the ability to reproduce the well known single-emission splitting functions from [42] using this mapping. The mapping defined below describes the relation between momenta before emission, p_i and p_j, and the momenta after emission, q_i, q and q_j which are all on-shell:

$$
\begin{aligned}
q_i &= zp_i + y(1-z)p_j + \sqrt{yz(1-z)}n_\perp \ , \\
q &= (1-z)p_i + yzp_j - \sqrt{yz(1-z)}n_\perp \\
q_j &= (1-y)p_j \ , \\
q_i.q_i &= q_j.q_j = p_i.p_i = p_j.p_j = 0 \ , \\
p_i \cdot n_\perp &= p_j \cdot n_\perp = 0 \ .
\end{aligned}
\tag{5.8}
$$

Some useful identities from the above mapping are:

$$
\begin{aligned}
q_i.q &= y(1 - 2z(1-z))p_i.p_j - yz(1-z)n_\perp^2 j \ , \\
q_j.q &= (1-z)(1-y)p_i.p_j \ , \\
q_i.q_j &= z(1-y)p_i.p_j \ , \\
q_i + q &= p_i + yp_j \ , \\
q_j + q &= (1-z)p_i + (1-y+zy)p_j - \sqrt{yz(1-z)}n_\perp \ .
\end{aligned}
\tag{5.9}
$$

From the on-shell conditions above it can be shown that:

$$
q_i \cdot q_i = 0 = 2yz(1-z)p_i \cdot p_j + yz(1-z)n_\perp^2 \implies n_\perp^2 = -2p_i \cdot p_j \ ,
\tag{5.10}
$$

where it can be considered that $y \to \lambda^2 y$ in the collinear limit and $y, (1-z) \to \lambda y, \lambda(1-z)$ in the soft limit, as discussed in Sec. 2.2. The soft and collinear limits are approached as $\lambda \to 0$, which allows the singular terms to be expanded as a series in powers of λ. The singular terms from a diagram arise from the denominator factors of the propagators, that are proportional to $1/\lambda^2$ for the collinear scaling. In order to calculate the splitting functions only the leading collinear-singular terms need to be included, *i.e.* those $\mathcal{O}(1/\lambda^2)$. As the kinematic mapping will be used to expand the numerator terms of each diagram, it is possible to reduce the expressions by ignoring terms which will give sub-leading terms when combined with the denominator *i.e.* any term in the mapping with a power of $\lambda^{1/2}$ or higher. Ignoring these sub-leading terms gives a reduced form of the mapping which can be used to simplify the calculation for a diagram when it is known that the denominator contains terms $\mathcal{O}(1/\lambda^2)$:

$$
\begin{aligned}
q_i &= zp_i \ , & q_i + q &= p_i + yp_j \ , \\
q &= (1-z)p_i + yzp_j \ , & q_j + q &= (1-z)p_i + p_j \ , \\
q_j &= (1-y)p_j \ .
\end{aligned}
\tag{5.11}
$$

The expressions for the sum of two momenta are particularly useful for the exchange diagram calculations. This mapping, in both the full and reduced forms, will be used in the context of cut diagrams in Sec. 5.2.2 via the Feynman rules and conventions outlined in Sec. 2.3. Next it is important to put the mapping from Eq. (5.8) into the context of the phase space.

5.2.1. Phase Space

The Born-level cross section for a QCD process with n partons in the final state can be expressed in terms of the phase space $\mathrm{d}\phi_n$, the QCD matrix element $\mathcal{M}_n$ and the jet-defining function $F_J^{(n)}$ as [15]:

$$
\mathrm{d}\sigma^B = \mathrm{d}\phi_n \, |\mathcal{M}_n|^2 \, F_J^{(n)} \ .
\tag{5.12}
$$

For a jet observable of interest the jet-defining function, $F_J^{(n)}$, gives its value in terms of the final state partons. The Born-level cross section can be used to give the leading order cross section for an observable via:

$$\sigma^{LO} = \int_n \mathrm{d}\sigma^B \ . \tag{5.13}$$

For an n-parton final state the d-dimensional phase space is written as:

$$\left[\prod_{l=1}^n \frac{\mathrm{d}^d q_l}{(2\pi)^{d-1}}\delta_+(q_l^2)\right] (2\pi)^d\delta^{(d)}(q_1 + ... + q_n - Q) \equiv \mathrm{d}\phi_n(q_1, ..., q_n; Q) \ . \tag{5.14}$$

The aim is to factorise the phase space, including the three partons after the emission, into a dipole phase space and a factor for the singular parton. The expressions given here are essentially a reworking of the phase-space factorisation given in [15], as the mapping given in Eq. (5.8) can be considered to be equivalent to the dipole mapping from Eq. (4.28) in the collinear limit. The final-state phase space includes the following terms, from the three partons with momenta q_i, q and q_j:

$$\mathrm{d}\phi(q_i, q, q_j; Q) = \frac{\mathrm{d}^d q_i}{(2\pi)^{d-1}}\delta_+(q_i^2)\frac{\mathrm{d}^d q}{(2\pi)^{d-1}}\delta_+(q^2)\frac{\mathrm{d}^d q_j}{(2\pi)^{d-1}}\delta_+(q_j^2) \ (2\pi)^d\delta^{(d)}(Q - q_i - q - q_j) \ , \tag{5.15}$$

where Q is the total momentum for the three-parton system which is the same before and after the emission. The plus prescription selects the positive-energy solution, *i.e.* $\delta_+(q_a^2) \equiv \delta(q_a^2)\theta(q_0)$. The phase space can then be rewritten in terms of the momenta before the emission *i.e.* the dipole momenta p_i and p_j, and the emission q:

$$\begin{aligned} \mathrm{d}\phi(q_i, q, q_j; Q) &= \mathrm{d}\phi(p_i, p_j; Q) \ [\mathrm{d}q(p_i, p_j)] \ , \\ &= \mathrm{d}\phi(p_i, p_j; Q) \ \frac{\mathrm{d}^d q}{(2\pi)^{d-1}}\delta_+(q^2)\mathcal{J}(q; p_i, p_j) \ . \end{aligned} \tag{5.16}$$

The Jacobian needed for this phase space is the same as in the Catani-Seymour case, because the mappings are equivalent in the collinear limit. Using the mapping variables z and y, the Jacobian factor can be written as:

$$\mathcal{J}(q; p_i, p_j) = \Theta(1 - z) \ \Theta(1 - y) \ \frac{(1 - y)^{d-3}}{1 - z} \ . \tag{5.17}$$

Using the mapping for q, given in Eq. (5.8), the emission phase space, $\mathrm{d}q$, can be expressed in terms of the kinematic variables. This allows the phase space and splitting function to be easily combined. The phase-space terms that are relevant in this case, are those that remain in the collinear limit in four dimensions, *i.e.* $\epsilon \to 0$. The emission phase space can then be written as:

$$[\mathrm{d}q(p_i, p_j)] = \frac{1}{16\pi^2}\frac{\mathrm{d}p_\perp^2 \, \mathrm{d}z}{z(1 - z)}\int \frac{\mathrm{d}\phi}{2\pi} \ , \tag{5.18}$$

where $\mathrm{d}\phi$ results from taking the four-dimensional limit of the element of solid angle, that is perpendicular to p_i and p_j, given in the d-dimensional expression in [15]. The substitution, $y = p_\perp^2/(z(1 - z)2p_i \cdot p_j)$ has been used, that is a result of the mapped emission momentum being on-shell. This expression will be useful at the end of the next section, where it can combined with the results from the splitting-function calculations.

5.2.2. Results with Basic Mapping

To illustrate the application of this kinematic mapping, it was used to reproduce the spin-averaged splitting functions in the collinear limit for a gluon emission from a quark emitter

and a gluon emission from a gluon emitter *i.e.* $\langle\hat{P}_{qq}\rangle$ and $\langle\hat{P}_{gg}\rangle$ as given in Eq. (4.12). The mapping shown in Eq. (5.8) will be used for the examples in this section and can also be used in the reduced form that applies in the collinear limit. Following the dipole formalism from [15], which is outlined in Sec. 4.3, the diagrams that need to be included can be determined from the combinatorics in Sec. 5.1. The calculation is shown at an amplitude level using the cut diagram formalism outlined in Sec. 2.3.3, where the splitting function is the result of the sum over cut diagrams. For these examples a covariant gauge is used with the gluon polarisation tensor defined as $d_{\mu\nu} = -g_{\mu\nu}$. First the quark-emitter case is discussed and then the gluon-emitter case where the inclusion of the triple gluon vertex increases the complexity of the calculation.

5.2.2.1. Quark Emitter

The possible combinations of indices were investigated in Sec. 5.1, where it was established that there are both self-energy and exchange type diagrams that give singular contributions to the cross section in the collinear limit. There are three possible diagrams that contribute to the calculation of a gluon emission from a quark, these are shown below:

$$|\mathcal{M}_{qg}^{(E)}|^2 = \qquad , \qquad (|\mathcal{M}_{qg}^{(E)}|^2)^\dagger = \qquad , \qquad (5.19)$$

$$|\mathcal{M}_{qg}^{(SE)}|^2 = \qquad , \qquad (5.20)$$

where the superscripts (E) and (SE) label the exchange and self energy amplitudes respectively. These diagrams represent the squared matrix elements of all possible ways a singular emission can connect to partons i and j on both sides of the amplitude for a given observable. However, as was also mentioned in Sec. 5.1, two of these diagrams are equivalent when only considering the real part, namely the exchange diagram and its conjugate, shown in Eq. (5.19). This allows the sum over amplitudes, used to determine the emission kernel $U_{ij,k}$ in Eq. (5.5), to be written as:

$$U_{ij,k} = \sum_{i<j<k} 2\mathrm{Re}|\mathcal{M}_{qg}^{(E)}|^2 + \sum_{i<j}|\mathcal{M}_{qg}^{(SE)}|^2 \ , \qquad (5.21)$$

where here j indexes the emission momentum. In this expression no partitioning factors are used as the aim is to reproduce the splitting functions by taking the explicit collinear limit. Using the QCD Feynman rules, given in Sec. 2.3.1, the exchange amplitude is given by:

$$
\begin{aligned}
|\mathcal{M}_{qg}^{(E)}|^2 &= -g_{\mu\nu}\left[(\slashed{q}_i)(-ig_s\gamma^\mu(t_i^c)^k{}_l)\frac{i(\slashed{q}_i+\slashed{q})}{(q_i+q)^2}\right]_{\alpha\beta}\left[\frac{-i(-\slashed{q}_j-\slashed{q})}{(q_j+q)^2}(ig_s\gamma^\nu(-t_j^c)^m{}_n)(-\slashed{q}_j)\right]_{\gamma\delta} , \\
&= \frac{g_s^2(t_i^c)^k{}_l(t_j^c)^m{}_n}{4(q_i.q)(q_j.q)}[(\slashed{q}_i)\gamma^\lambda(\slashed{q}_i+\slashed{q})]_{\alpha\beta}[(\slashed{q}_j+\slashed{q})\gamma_\lambda(\slashed{q}_j)]_{\gamma\delta} , \\
&= \frac{g_s^2(t_i^c)^k{}_l(t_j^c)^m{}_n}{4(q_i.q)(q_j.q)} \ N_{qg}^{(E)} \ .
\end{aligned}
$$

$$(5.22)$$

The square bracket notation is used here to separate the momenta flowing through each hard line, which after factorising the singular terms should just contain the momenta before emission, p_i and p_j. Simplification and expansion steps are then carried out by commuting the gamma matrices and using the identity $\not{p}_i \not{p}_j = 2p_i.p_j - \not{p}_j \not{p}_i$. As the aim is to reproduce the splitting function where only the leading collinear singular terms contribute, these terms are identified with the help of the scaling as they are proportional to $1/\lambda^2$.

The numerator from Eq. (5.22) can be expanded and mapped using the mapping from Eq. (5.8) to give:

$$
\begin{aligned}
N_{qg}^{(E)} =& [(\not{q}_i)\gamma^\lambda(\not{q}_i + \not{q})]_{\alpha\beta}[(\not{q}_j + \not{q})\gamma_\lambda(\not{q}_j)]_{\gamma\delta} \\
=& [(z\not{p}_i)\gamma^\lambda(\not{p}_i + y\not{p}_j)]_{\alpha\beta}[((1-z)\not{p}_i + \not{p}_j)\gamma_\lambda((1-y)\not{p}_j)]_{\gamma\delta} \\
=& (1-y)[-z\gamma^\lambda\not{p}_i(\not{p}_i + y\not{p}_j) + 2zp_i^\lambda(\not{p}_i + y\not{p}_j)][((1-z)\not{p}_i + \not{p}_j)\gamma_\lambda\not{p}_j] \\
=& (1-y)z\{-y[\gamma^\lambda\not{p}_i\not{p}_j][((1-z)\not{p}_i + \not{p}_j)\gamma_\lambda\not{p}_j] + 2[\not{p}_i + y\not{p}_j][\not{p}_j\not{p}_i\not{p}_j]\} \\
=& (1-y)z\{y[\gamma^\lambda\not{p}_i\not{p}_j][((1-z)\not{p}_i + \not{p}_j)\not{p}_j\gamma_\lambda] - 2y[\gamma^\lambda\not{p}_i\not{p}_j][((1-z)\not{p}_i + \not{p}_j)p_{j\lambda}] \\
& + 4(p_i.p_j)[\not{p}_i + y\not{p}_j][\not{p}_j]\} \\
=& (1-y)z\{y(1-z)[\gamma^\lambda\not{p}_i\not{p}_j][\not{p}_i\not{p}_j\gamma_\lambda] - 2y(1-z)[\not{p}_j\not{p}_i\not{p}_j][\not{p}_i] \\
& - 4y(p_i.p_j)[\not{p}_j][\not{p}_j] + 4(p_i.p_j)[\not{p}_i + y\not{p}_j][\not{p}_j]\} .
\end{aligned}
\tag{5.23}
$$

For the splitting function, only in the leading collinear-singular behaviour is of interest. Therefore, all sub-leading terms that arise can be neglected. The two $[\not{p}_j][\not{p}_j]$ terms cancel, that gives a final form of $N_{qg}^{(E)}$ containing the leading order term relevant to the splitting function. Here the p_j momentum is written with a minus sign because it belongs to the anti-quark. The resulting expression for the numerator is:

$$
N_{qg}^{(E)} = -4(1-y)z(p_i.p_j)[\not{p}_i][-\not{p}_j] .
\tag{5.24}
$$

Substituting this back into the full matrix element gives:

$$
\begin{aligned}
|M_{qg}^{(E)}|^2 =& \sum_{j \neq i} \frac{g_s^2(t_i^c)^k{}_l(t_j^c)^m{}_n}{4(q_i.q)(q_j.q)}(-4)(1-y)z(p_i.p_j)[\not{p}_i]_{\alpha\beta}[-\not{p}_j]_{\gamma\delta} \\
=& \sum_{j \neq i} \frac{-g_s^2(t_i^c)^k{}_l(t_j^c)^m{}_n}{2(q_i.q)} \frac{2z}{1-z}[\not{p}_i]_{\alpha\beta}[-\not{p}_j]_{\gamma\delta} \\
=& \frac{4\pi\alpha_s C_F}{2(q_i.q)} \frac{2z}{1-z}[\not{p}_i]_{\alpha\beta}[-\not{p}_j]_{\gamma\delta} .
\end{aligned}
\tag{5.25}
$$

The exchange diagram and its conjugate give the same result, as here only the real part of the amplitude is considered. This can be accounted for as a factor of two. The matrix element squared for the self-energy-type diagram is expressed as follows:

$$
\begin{aligned}
|M_{qg}^{(SE)}|^2 =& -g_{\mu\nu}[\frac{-i(\not{q}_i + \not{q})}{(q_i + q)^2}(ig_s\gamma^\mu(t_i^c)^r{}_l)(\not{q}_i)(-ig_s\gamma^\nu(t_i^c)^k{}_r)\frac{i(\not{q}_i + \not{q})}{(q_i + q)^2}]_{\alpha\beta}[-\not{q}_j]_{\gamma\delta} \\
=& \frac{-g_s^2(t_i^c)^r{}_l(t_i^c)^k{}_r}{4(q_i.q)^2}[(\not{q}_i + \not{q})\gamma^\mu(\not{q}_i)\gamma_\mu(\not{q}_i + \not{q})]_{\alpha\beta}[-\not{q}_j]_{\gamma\delta} .
\end{aligned}
\tag{5.26}
$$

To establish the collinear-leading terms in the numerator it is first necessary to look at the scaling in the denominator. In the collinear limit a factor of y^2 appears in the denominator after the mapping is applied, that corresponds to a scaling $\mathcal{O}(1/\lambda^4)$:

$$
\frac{1}{(q_i.q)^2} \approx \frac{1}{(\lambda^4)y^2(p_i.p_j)^2} .
\tag{5.27}
$$

The same reduced mapping as used for diagram (E) cannot be used in this case due to the different factors on the denominator. For this diagram only terms with a factor of y^2 will be finite. The numerator in this case can be mapped and expanded as:

$$
\begin{aligned}
N_{qg}^{(SE)} =& [(\slashed{q}_i + \slashed{q})\gamma^\lambda(\slashed{q}_i)\gamma_\lambda(\slashed{q}_i + \slashed{q})]_{\alpha\beta}[-\slashed{q}_j]_{\gamma\delta} \\
=& [(\slashed{p}_i + y\slashed{p}_j)\gamma^\lambda(z\slashed{p}_i + y(1-z)\slashed{p}_j)\gamma_\lambda(\slashed{p}_i + y\slashed{p}_j)][-(1-y)\slashed{p}_j] \\
=& (1-y)[((-\gamma^\lambda(\slashed{p}_i + y\slashed{p}_j)) + 2(p_i^\lambda + yp_j^\lambda))(z\slashed{p}_i + y(1-z)\slashed{p}_j)\gamma_\lambda(\slashed{p}_i + y\slashed{p}_j)][-\slashed{p}_j] \\
=& (1-y)\{[(-\gamma^\lambda(y(1-z)\slashed{p}_i\slashed{p}_j + zy\slashed{p}_j\slashed{p}_i)\gamma_\lambda(\slashed{p}_i + y\slashed{p}_j)] + 2[y^2(1-z)\slashed{p}_j\slashed{p}_i\slashed{p}_j \\
& + yz\slashed{p}_i\slashed{p}_j\slashed{p}_i]\}[-\slashed{p}_j] \\
=& (1-y)y(p_i.p_j)\{[2\gamma^\lambda((1-z)\slashed{p}_i + zy\slashed{p}_j)\gamma_\lambda - 4(z\slashed{p}_i + y(1-z)\slashed{p}_j)] \\
& + 4[y(1-z)\slashed{p}_j + z\slashed{p}_i]\}[-\slashed{p}_j] \\
=& 2(1-y)y(p_i.p_j)[(2-d)((1-z)\slashed{p}_i + zy\slashed{p}_j)][-\slashed{p}_j] \;,
\end{aligned}
\tag{5.28}
$$

where the identity $\gamma^\lambda \slashed{p}_i \gamma_\lambda = (2-d)\slashed{p}_i$ has been used. The $[\slashed{p}_j][\slashed{p}_j]$ term can be neglected as it is finite in this case, where the denominator is proportional to y^2. Considering dimensional regularisation, where $d = 4 - 2\epsilon$, the final result for the numerator is:

$$
N_{qg}^{(SE)} = 4(1-y)y(p_i.p_j)((1-z)(\epsilon-1))[\slashed{p}_i][-\slashed{p}_j] \;.
\tag{5.29}
$$

Substituting this back into the full matrix element gives:

$$
\begin{aligned}
|M_{qg}^{(SE)}|^2 &= \frac{-g_s^2(t_i^c)^r{}_l(t_i^c)^k{}_r}{4(q_i.q)^2}(4(1-y)y(p_i.p_j)(-(1-z)(1-\epsilon)))[\slashed{p}_i]_{\alpha\beta}[-\slashed{p}_j]_{\gamma\delta} \\
&= \frac{g_s^2(t_i^c)^r{}_l(t_i^c)^k{}_r}{2(q_i.q)}(2(1-z)(1-y)(1-\epsilon))[\slashed{p}_i]_{\alpha\beta}[-\slashed{p}_j]_{\gamma\delta} \\
&= \frac{4\pi\alpha_s C_F}{2(q_i.q)}(2(1-z)(1-y)(1-\epsilon))[\slashed{p}_i]_{\alpha\beta}[-\slashed{p}_j]_{\gamma\delta} \;.
\end{aligned}
\tag{5.30}
$$

To add the three contributions together, colour conservation needs to be applied, that allows the colour operators to be simplified as shown in Sec. 2.3.2. This sum applied to the case where parton i is a quark gives:

$$
-\sum_{j\neq i} T_i.T_j = C_F \;.
$$

The sum arises from the dipole factorisation formulae, that imply a sum over all emissions and over all dipoles to describe the cross section. The result for the gluon emission from a quark emitter is obtained by carrying out the sum:

$$
\sum_{i<j<k} 2\mathrm{Re}\left\{|\mathcal{M}_{qg}^{(E)}|^2\right\} + \sum_{i<j}|\mathcal{M}_{qg}^{(SE)}|^2 = \frac{8\pi\alpha_s C_F}{2(q_i.q)}\left(\frac{2z}{1-z} + (1-z)(1-\epsilon)\right)[\slashed{p}_i]_{\alpha\beta}[-\slashed{p}_j]_{\gamma\delta} \;,
\tag{5.31}
$$

plus additional terms that are ignored because they are finite or contain only integrable singularities. The terms in brackets correspond to the z terms from the splitting function for a quark emitter, $\langle\hat{P}_{qq}\rangle$, from Eq. (4.12) and the remaining momenta in square brackets give the factorised dipole amplitude in terms of the momenta before the emission. To reproduce

the full splitting function the phase space also has to be included. The result of combining the phase space factor, from Eq. (5.18), with the matrix element pre-factor gives:

$$
\begin{aligned}
\frac{1}{16\pi^2} &\frac{dp_\perp^2\, dz}{z(1-z)} \int \frac{d\phi}{2\pi} \times \frac{8\pi\alpha_s}{2(q_i.q)} \\
&= \frac{\alpha_s}{2\pi} \frac{dp_\perp^2\, dz}{z(1-z)} (1) \times \frac{z(1-z)}{p_\perp^2}\ , \\
&= \frac{\alpha_s}{2\pi} \frac{dp_\perp^2}{p_\perp^2} dz\ .
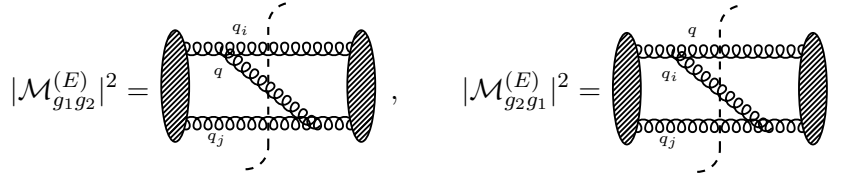\end{aligned}
\tag{5.32}
$$

Resulting in the final form that reproduces $\langle \hat{P}_{qq}(z;\epsilon)\rangle$ and the corresponding phase space factor from [15]:

$$
\frac{\alpha_s dp_\perp^2\, dz}{2\pi p_\perp^2} C_F \left(\frac{2z}{1-z} + (1-z)(1-\epsilon) \right) [\not{p}_i]_{\alpha\beta} [-\not{p}_j]_{\gamma\delta}\ .
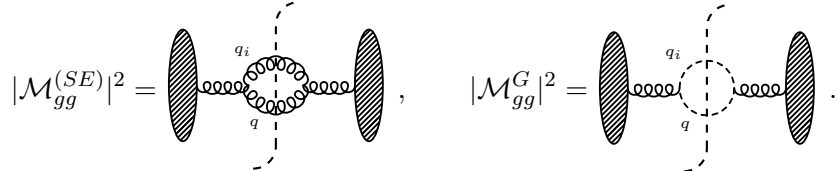\tag{5.33}
$$

This is validation that this mapping reproduces the correct behaviour in the collinear limit. This mapping will go on to act as a starting point for a more complex and powerful mapping that can capture both soft and collinear-singular behaviour for multiple emissions and access a wider range of phase space. The generalised mapping is discussed in Sec. 6.4.

5.2.2.2. Gluon Emitter

The second example shown here is the case of a gluon emitter and a gluon emission, that involves the consideration of four cut diagrams with two triple gluon vertices per diagram. The triple gluon vertex results in a more complicated tensor structure and there are more terms in the final expressions. This case is additionally complicated as the emitter and emission are now indistinguishable, that requires the two cases where momentum q or momentum q_i is the exchanged gluon to be considered. Each of the gluon-exchange diagrams carries a factor of two due to the addition of the conjugate diagram, that is equivalent to twice the real contribution, as was the case for the quark emitter. The self-energy diagram in this case requires the calculation of a ghost-loop diagram, that contains contributions from the loop propagating both clockwise and anti-clockwise. This is due to the choice to carry out this calculation in a covariant gauge. Details of the calculation are given in App. A.1. The diagrams involved are:

$$
|\mathcal{M}_{g_1 g_2}^{(E)}|^2 = \quad\text{}\quad , \qquad |\mathcal{M}_{g_2 g_1}^{(E)}|^2 = \quad\text{}\quad ,
\tag{5.34}
$$

$$
|\mathcal{M}_{gg}^{(SE)}|^2 = \quad\text{}\quad , \qquad |\mathcal{M}_{gg}^{G}|^2 = \quad\text{}\quad .
\tag{5.35}
$$

The collinear leading terms, which as in the previous section are those $\mathcal{O}(1/\lambda^2)$, from the first diagram, are:

$$
|M_{g_1 g_2}^{(E)}|^2 = \frac{-g_s^2(-T_i.T_j)}{4(q_i.q)} \left[g^{\mu\nu} \frac{(p_i)_\sigma (p_i)_\rho}{(p_i \cdot p_j)} \frac{(1-z^2)}{1-z} - 2g^{\mu\nu} g_{\rho\sigma} \frac{(1+z)}{1-z} \right]\ .
\tag{5.36}
$$

This allows the total squared amplitude for gluon splitting to be written as:

$$|M_{\text{split}}|^2 + |M_{\text{self}}|^2 = \sum_i^n \sum_{j\neq i}^n \left\{ 2\operatorname{Re}\left[|M_{g_1g_2}^{(E)}|^2 \right] + 2\operatorname{Re}[|M_{g_2g_1}^{(E)}|^2] + |M_{gg}^{(SE)}|^2 + |M_{gg}^{(G)}|^2 \right\} \ . \tag{5.37}$$

When considering a collinear limit where $y \approx 0$ the contributions from the exchanged-gluon diagrams can be reduced to the following terms:

$$|M_{g_1g_2}^{(E)}|^2 = -T_i.T_j \frac{4\pi\alpha_s}{2(q_i.q)}[(-g^{\mu\nu})\frac{p_{i\sigma}p_{i\rho}}{p_i.p_j}\frac{(1-z^2)}{2(1-z)} + (-g^{\mu\nu})(-g_{\sigma\rho})\left(\frac{1}{1-z} + \frac{z}{1-z}\right)] \ , \tag{5.38}$$

$$|M_{g_2g_1}^{(E)}|^2 = -T_i.T_j \frac{4\pi\alpha_s}{2(q_i.q)}[(-g^{\mu\nu})\frac{p_{i\sigma}p_{i\rho}}{p_i.p_j}\frac{(2-z)}{2} + (-g^{\mu\nu})(-g_{\sigma\rho})\left(\frac{1}{z} + \frac{1-z}{z}\right)] \ .$$

To rearrange the z terms the following expressions are used:

$$\frac{1}{1-z} = 1 + \frac{z}{1-z} \ , \qquad \frac{1}{z} = 1 + \frac{1-z}{z} \ . \tag{5.39}$$

This then results in the $\dfrac{2z}{1-z}$ and $\dfrac{2(1-z)}{z}$ terms expected. The result of adding these two diagrams and ignoring finite contributions gives:

$$\begin{aligned}
|M_{\text{split}}|^2 &= \sum_i^n \sum_{j\neq i}^n 2\operatorname{Re}\left(|M_{g_1g_2}^{(E)}|^2 + |M_{g_2g_1}^{(E)}|^2 \right) \\
&= \frac{8\pi\alpha_s C_A \delta_{ad}\delta_{be}}{2(q_i.q)} \left[(-g^{\mu\nu})(-g_{\sigma\rho})\frac{2z}{1-z} + (-g^{\mu\nu})(-g_{\sigma\rho})\frac{2(1-z)}{z} \right] \ ,
\end{aligned} \tag{5.40}$$

where the sum over j for a gluon emitter results in the colour factor C_A. The next step is to add these diagrams to the gluon self-energy and ghost-loop diagrams that together give the following singular contributions:

$$|M_{\text{self}}|^2 = \frac{16\pi\alpha_s C_A \delta_{ab}}{2(q_i.q)}\left((-g^{\mu\nu}) - 2(1-\epsilon)z(1-z)\frac{n_\perp^\mu n_\perp^\nu}{2(p_i.p_j)} \right) \ , \tag{5.41}$$

where the $n_\perp$ terms are the leading singular contributions that remain after the applying the kinematic mapping to q_i and q. The total combination of the splitting terms above and the self-energy term also containing factors of z, where $(-g_{\sigma\rho})$ can be factored out as it only relates to the spectator gluon, and $2p_i \cdot p_j = n_\perp^2$ has been used to give:

$$\begin{aligned}
|M_{\text{split}}|^2 + |M_{\text{self}}|^2 &= \frac{16\pi\alpha_s C_A \delta_{ad}\delta_{be}}{2(q_i.q)}[-g^{\mu\nu}\left(\frac{z}{1-z} + \frac{(1-z)}{z} \right) \\
&\qquad - 2(1-\epsilon)z(1-z)\frac{n_\perp^\mu n_\perp^\nu}{n_\perp^2}] \ , \\
&= \frac{8\pi\alpha_s}{2(q_i.q)} \langle\mu| \hat{P}_{gg}(z, n_\perp; \epsilon) |\nu\rangle \ .
\end{aligned} \tag{5.42}$$

This reproduces the form of the splitting function that still depends on the spin indices of the gluon, μ and ν, as given in [15]. The process of averaging over the spins removes the $n_\perp$ dependence, as illustrated in Sec. 4.1.1, and gives the spin-averaged splitting function $\langle\hat{P}_{gg}\rangle$, shown in Eq. (4.12).

These two examples, for both a gluon and quark emitter, demonstrate the ability of the mapping to reproduce the correct collinear behaviour. Throughout this process several terms

were ignored because they do not contribute in the collinear limit, they do however give important contributions in the soft and soft-collinear limits. The power of the mapping and the parametrisation of the soft and collinear scaling through the variables y and z gives the flexibility to access other IR-singular terms. This idea will be extended in the next section as the mapping is further developed.

5.3. Mapping with Lorentz Transformation

Although the mapping used in the previous section does have some benefits, it also suffers from some of the same flaws as existing methods, the main one that is addressed here is the recoil. In a traditional dipole method the recoil of the emission is absorbed within the dipole *i.e.* by the emitter and spectator partons. This recoil method can lead to problems for more than one emission when the process is iterated, which is what happens in most parton showers, some such issues are discussed in Sec. 4.4. With the aim here in mind to incorporate more than one emission into the mapping, it is first vital to address the recoil scheme. The solution explored here is to distribute the recoil globally, across all possible spectator partons, via a Lorentz transformation. The momenta before the emission are labelled p, after the emission q and the emission momentum is k_1. Considering the case where there are n momenta before the emission and $(n+1)$ momenta after the emission gives the sets of momenta:

$$\{p_1, ..., p_n\} \to \{q_1, ..., q_n; k_1\} \ , \tag{5.43}$$

where Q is the total momentum defined as:

$$Q = \sum_k p_k = p_i + \sum_{r \neq i} p_r = q_i + k_1 + \sum_{r \neq i} q_r \ . \tag{5.44}$$

To maintain overall energy-momentum conservation either all the momenta before or after the emission need to be transformed. This mapping is constructed with the parameters α_1, β_1 and y to describe the soft and collinear limits and the recoil is distributed via the Lorentz transformation $\Lambda^\mu{}_\nu$ with a scaling factor α. The Lorentz transformation is applied to the emitter and spectator momenta, in this case denoted by p_i and p_r:

$$
\begin{aligned}
k_1^\mu &= \alpha_1 \alpha \Lambda^\mu{}_\nu p_i^\nu + y \beta_1 \ n^\mu + \sqrt{y \alpha_1 \beta_1} n_{\perp,1}^\mu \ , \\
q_i^\mu &= (1 - \alpha_1) \alpha \Lambda^\mu{}_\nu p_i^\nu + y (1 - \beta_1) n^\mu - \sqrt{y \alpha_1 \beta_1} n_{\perp,1}^\mu \ , \\
q_r^\mu &= \alpha \Lambda^\mu{}_\nu p_r^\nu \ , \qquad r = 1, ..., n \ , \qquad r \neq i \ .
\end{aligned}
\tag{5.45}
$$

Where as before the following on-shell conditions apply: $q_i^2 = k_1^2 = q_r^2 = p_i^2 = n^2 = 0$, and $n_\perp$ is defined so that $p_i \cdot n_\perp = n \cdot n_\perp = 0$. The k_1 on-shell condition fixes $n_\perp^2 = -2p_i \cdot n$ and from the on-shell condition for q_i it can be shown that for this case $\beta_1 = 1 - \alpha_1$. Which for $\alpha_1 = (1-z)$ gives the mapping from the previous section, modulo the Lorentz transformation, in terms of y and z without the need for a third parameter. Although for the two or more emission case this does not hold and the β_l parameter is not degenerate.

The Lorentz transformation, $\Lambda^\mu{}_\nu$, needs to be a proper orthochronous transformation to preserve the time ordering of the system. The transformation proposed is based on the solution for transforming a momentum p to momentum $\hat{p}$ given in App. A.2 . For the physical case considered here, the required action of the transformation to fulfil momentum conservation is:

$$\Lambda^\mu{}_\nu Q^\nu = \frac{Q^\mu - y n^\mu}{\alpha} \ . \tag{5.46}$$

In the collinear limit of $y \to 0$, $\alpha \to 1$ this transformation reduces to δ_ν^μ. For full details of $\Lambda^\mu{}_\nu$ see App. A.2. From the form of the transformation it becomes clear that n^μ must be some function of Q and p_i and is required to be on-shell. One suitable solution has the form:

$$n^\mu = Q^\mu - \frac{Q^2}{2p_i.Q}p_i^\mu \ . \tag{5.47}$$

The transformation times the factor α is useful to define, where $\alpha = \sqrt{1-y}$ and the form of n given above has been used:

$$\begin{aligned}
\alpha\Lambda^\mu{}_\nu = {} & p_i^\mu p_{i\nu} \frac{-y^2 Q^2}{4(p_i \cdot Q)^2(1 + \sqrt{1-y} - \frac{y}{2})} + p_i^\mu Q_\nu \frac{y(1 + \sqrt{1-y})}{2p_i \cdot Q(1 + \sqrt{1-y} - \frac{y}{2})} \\
& + Q^\mu p_{i\nu} \frac{(y^2 - y - y\sqrt{1-y})}{2p_i \cdot Q(1 + \sqrt{1-y} - \frac{y}{2})} + \delta_\nu^\mu \sqrt{1-y} \ .
\end{aligned} \tag{5.48}$$

The action of $\Lambda^\mu{}_\nu$ on p_i^ν yields $\frac{1}{\alpha}p_i^\mu$ and hence for the single-emission case the mapping can be simplified using: $\alpha\Lambda^\mu{}_\nu p_i^\nu = p_i^\mu$. This is a useful result, as can be seen in the context of the mapping from Eq. (5.45), as it corresponds to the first component of the emitter and emission.

5.3.1. Phase Space

Once the mapping is established the next step is to look at the phase space. In this case the mapping is not equivalent to the Sudakov decomposition in the collinear limit and so the phase space needs to be investigated in more detail. The general structure of the phase-space factorisation can be carried out in a familiar way. However, the Jacobian for this mapping needs to be determined as this provides the key additional terms and facilitates the factorisation of the emission. To establish the Jacobian for this mapping it is helpful to invert it *i.e.* express p_i and p_k in terms of k_1, q_i and q_k. It can be used that in the single emission case $\alpha_1 = 1 - \beta_1$. Using this and inverting the expressions above for k_1 and q_i gives:

$$\begin{aligned}
p_i^\mu = {} & q_i^\mu + k_1^\mu - yn^\mu \ , \\
p_k^\mu = {} & \frac{1}{\alpha}\Lambda^\mu{}_\nu q_k^\nu \ .
\end{aligned} \tag{5.49}$$

Rewriting like this and using the expression for n given in Eq. (5.47) allows $p_i \cdot Q$ to be written as:

$$p_i \cdot Q = q_i \cdot Q + k_1 \cdot Q - \frac{y}{2}Q^2 \tag{5.50}$$

The general $n + m$ parton phase space considered is:

$$d\phi_{n+m}(q_1, ..., q_n, k_1, ..., k_m | Q) = \left(\prod_{k=1}^{n} \frac{d^d q_k}{(2\pi)^{d-1}}\tilde{\delta}(q_k)\prod_{l=1}^{m}\frac{d^d k_l}{(2\pi)^{d-1}}\tilde{\delta}(k_l)\right)\delta\left(\sum_{k=1}^{n}q_k + \sum_{l=1}^{m}k_l - Q\right) \tag{5.51}$$

where $\tilde{\delta}(q) \equiv \tilde{\delta}(q, 0)$ and $\tilde{\delta}(q, m) = \delta(q^2 - m^2)\theta(q^0)$. The action of the mapping defined above, with the specific choice of $p_{1,n} = \sum_{k=1}^{n} p_k$, gives:

$$n^\mu(p_{1,n}, p_1) = p_{1,n}^\mu - \frac{p_{1,n}^2}{2p_{1,n} \cdot p_1}p_1^\mu \ , \tag{5.52}$$

and an emitter with momentum p_1 and where here $k > 1$:

$$q_k^\mu = \sqrt{1-y} \ \Lambda^\mu{}_\nu(p_{1,n}, p_1)p_k^\nu \qquad q_1^\mu = p_1^\mu - k_{1,m}^\mu + y \ n^\mu(p_{1,n}, p_1) \ . \tag{5.53}$$

The action of the Lorentz transformation gives:

$$\Lambda^{\mu}{}_{\nu}(p_{1,n}, p_1)p_{1,n}^{\nu} = \frac{p_{1,n}^{\mu} - y\, n^{\mu}(p_{1,n}, p_1)}{\sqrt{1-y}} \;, \qquad \Lambda^{\mu}{}_{\nu}(p_{1,n}, p_1)p_1^{\nu} = \frac{1}{\sqrt{1-y}}p_1^{\mu} \;. \tag{5.54}$$

Now the phase space can be rewritten using $q = \sum_{k=2}^{n} q_k$:

$$\mathrm{d}\phi_{n+m}(q_1, ..., q_n, k_1, ..., k_m | Q) = \mathrm{d}\phi_{m+2}(q_1, \{q, m\}, k_1, ..., k_m | Q)\frac{\mathrm{d}m^2}{2\pi}\mathrm{d}\phi_{n-1}(q_2, ..., q_n | q) \;, \tag{5.55}$$

where $\{q, m\}$ now indicates that the momentum q is to be constrained to a mass m. Considering the equivalent expressions for the transformations given in Eq. (5.53):

$$\begin{aligned}
q_k^{\mu} &= \sqrt{1-y}\Lambda^{\mu}{}_{\nu}(p_1 + p, p_1)p_k^{\nu} \;, \qquad q^{\mu} = \sqrt{1-y}\Lambda^{\mu}{}_{\nu}(p_1 + p, p_1)p^{\nu} \;, \\
q_1^{\mu} &= p_1^{\mu} - k_{1,m}^{\mu} + y\, n^{\mu}(p_1 + p, p_1) \;,
\end{aligned} \tag{5.56}$$

gives agreement with the original expressions when $q = q_{2,n}$ and $p = p_{2,n}$. Since the transformation (including y) is now a function of $p_1, p, k_{1,m}$, the factored measure transforms independently as:

$$\mathrm{d}\phi_{n-1}(\sqrt{1-y}\Lambda p_2, ..., \sqrt{1-y}\Lambda p_n | \sqrt{1-y}\Lambda p) = (1-y)^{\frac{(n-1)(d-2)-d}{2}}\mathrm{d}\phi_{n-1}(p_2, ..., p_n | p) \;, \tag{5.57}$$

and by construction $q_1 + q + k_{1,m} = p_1 + p$. y can then be determined from $q_1^2 = p_1^2$. The phase space measure is then written in full as:

$$\prod_{l=1}^{m} \frac{\mathrm{d}^d k_l}{(2\pi)^{d-1}}\tilde{\delta}(k_l) \;\times\; \mathrm{d}\phi_{n-1}(p_2, ..., p_n | p) \frac{\mathrm{d}^d p_1}{(2\pi)^{d-1}}\delta(p_1^2)\,\delta(p_1 + p - Q)\mathrm{d}^d p \;\times$$
$$\frac{(1-y)^{\frac{(n-1)(d-2)-d}{2}}}{(2\pi)^{d-1}}\theta(p_1^0 - k_{1,m}^0 + y\, n^0(p_1 + p, p_1))\delta((1-y)p^2 - m^2)\theta(p^0)\frac{\mathrm{d}m^2}{2\pi}\left|\frac{\partial(q_1, q)}{\partial(p_1, p)}\right| \;. \tag{5.58}$$

For $Q = p_1 + p$ this can be simplified to:

$$\prod_{l=1}^{m} \frac{\mathrm{d}^d k_l}{(2\pi)^{d-1}}\tilde{\delta}(k_l) \;\times\; \mathrm{d}\phi_{n-1}(p_2, ..., p_n | p) \frac{(1-y)^{\frac{(n-1)(d-2)-d}{2}}}{(2\pi)^{2d-1}} \times \mathcal{J} \;. \tag{5.59}$$

The full details of the Jacobian calculation are given in App. A.2.1. In the massless limit the result agrees with the expression given in [15] (for $n = 3$) as shown below:

$$\begin{aligned}
\mathcal{J} &= \frac{p^0 p_1^0}{q^0 q_1^0}(z_{11}z_{22} - z_{21}z_{12})\left(\frac{m^2 - Q^2(-1+y)^2}{m^2 + Q^2(-1+y)}\right)^{d-2} \\
&\overset{m, k^2 \to 0}{=\joinrel=} \frac{(1-y)^{d-3}}{z} \;.
\end{aligned} \tag{5.60}$$

This shows that for the massless limit the phase-space factorisation functions in a very similar way to that of the mapping used by Catani-Seymour and importantly that the mapping can be used for collinear single-emission calculations.

5.3.2. Behaviour in Soft and Collinear Limits

In this section the aim is to again reproduce the single-emission splitting functions that requires the same diagrams to be evaluated as shown in Sec. 5.2.2. However, the recoil is now distributed globally instead of only within the dipole. For the determination of the splitting functions it is relevant to examine how the mapping behaves in the collinear and soft limits. The scaling in the soft and collinear limits was introduced in Sec. 2.2, that when applied to this mapping gives the following scaling:

- Collinear scaling: $y \to \lambda^2 y$

- Soft scaling: $\alpha_1 \to \lambda \alpha_1, y \to \lambda y, \beta_1 \to \lambda \beta_1$

Using the simplification $\alpha \Lambda^\mu{}_\nu p_i^\nu = p_i^\mu$ and $\alpha^2 = (1 - y)$ the invariants for this mapping can be written as:

$$
\begin{aligned}
q_i \cdot k_1 &= (\alpha_1 + \beta_1) y p_i \cdot n \ , \\
q_r \cdot k_1 &= \alpha_1 (1 - y) p_i \cdot p_r + y \beta_1 \alpha \Lambda^\mu{}_\nu p_r^\nu n_\mu + \sqrt{y \alpha_1 \beta_1} \alpha \Lambda^\mu{}_\nu p_r^\nu (n_{\perp,1})_\mu \ , \\
q_i \cdot q_r &= (1 - \alpha_1)(1 - y) p_i \cdot p_r + y(1 - \beta_1) \alpha \Lambda^\mu{}_\nu p_r^\nu n_\mu - \sqrt{y \alpha_1 \beta_1} \alpha \Lambda^\mu{}_\nu p_r^\nu (n_{\perp,1})_\mu \ .
\end{aligned}
\tag{5.61}
$$

The invariants scale in the soft and collinear limits with the factors shown in Table 5.1. Where || indicates that the momenta are collinear and $k_1 \to 0$ is the soft-emission case. For

	$q_i \| k_1$	$k_1 \to 0$	$q_r \| k_1$
$q_i \cdot k_1$	λ^2	λ	1
$q_r \cdot k_1$	1	λ	λ^2
$q_i \cdot q_r$	1	1	1

Table 5.1.: Scaling of the invariants in the soft and collinear limits.

the collinear case in the first column, which is of interest for the single-emission splitting functions, the behaviour is the same as for the mapping discussed in the previous chapter. The results for each of the emission diagrams are equivalent to those from the previous mapping and thus the splitting-function expressions for both a quark and gluon emitter can be obtained as in Sec. 5.2.2.

5.4. Conclusions from the Single-Emission Case

In this chapter two different kinematic mappings have been introduced and examined. The first is used to calculate the collinear splitting functions for a gluon emission from a quark and a gluon emitter, in agreement with the known results from [42]. The y parameter controls the collinearity and z the softness of the emission and the combination of the two parameters describes the spectrum of IR singularities.

The knowledge from this first mapping is then extended, with an important modification to allow for a global treatment of the recoil from the emission. The aim is to develop a new mapping that maintains the important features of the previous mapping and behaves in the same way in the collinear limit but improves upon the recoil treatment and is more easily extended beyond the one emission case. The scaling in the soft and collinear limits is verified to illustrate the consistency of this mapping and a suitable form for the Lorentz transformation is established.

However, the interesting aspect of this mapping is the ability to go beyond the one-emission case, where k_1 is an example of the first emission and this can be easily extended to k_2, k_3 *etc.* The case of multiple emitters can also be considered. A more general mapping based on this one but with some additional improvements is described in Sec. 6.4. The issue with more emissions is then the determination of the splitting functions and inclusion of these in a parton shower. This will be discussed in the next chapters.

The global recoil distribution is already an important modification, although the effect of this is not apparent when only looking at the single-emission splitting functions. The implementation of a global recoil scheme in the context of a parton-shower simulation is shown in Chapter 8. The contrast to local recoil schemes is also strongest for multiple emissions as the issues with current recoil schemes only arise at the two-emission level and beyond.

In the next chapter, the formalism for multiple emissions will be developed and a suitable mapping outlined. This builds on the discussion so far and uses the mapping with the Lorentz transformation as a starting point with some modifications.

The Big Picture

Having discussed the single-emission case in detail, this chapter focuses on the generalisation of the concepts used previously, to the k-emissions case, where k is an arbitrary number of emissions. The factorisation theorem holds for any number of IR emissions. Therefore, if a suitable kinematic mapping can be found, the IR singular momenta can be factorised from the hard amplitude. The first step, in Sec. 6.1, is to extend the factorisation formalism to the two-emission case whilst continuing to work at the matrix-element level. This is then further extended in Sec. 6.2 to the general k-emissions case and the possible pairings of partons are discussed. It is also possible to rewrite these expressions in terms of a density operator, that is a convenient representation for use in showering algorithms, this is shown in Sec. 6.2.1. Then in Sec. 6.3 a partitioning algorithm for the general case is outlined and an example is given for the single-emission case. For the general k-emissions case the kinematic mapping and phase space are defined in Sec. 6.4 and Sec. 6.5 respectively. In Chapter 7, this framework will be applied to the two-emission case.

6.1. Extension to the Two-Emission Case

In the single-emission case, factorisation is discussed in terms of a matrix element with $(n+1)$ partons factorised to a state with n partons, where there is a soft or collinear emission. The factor describing such an emission is $\boldsymbol{V}_{ij,k}$ in the dipole formalism, given in Sec. 4.3. This same concept can be extended to an arbitrary number of emissions.

The process is the same for any number of emissions, namely to factorise IR-singular emissions from a general hard amplitude. This will be shown first for the single and double-emission cases and later for the fully general case. The expression in Eq. (6.1) describes a matrix element with external legs 1 to n, where q_n is the momentum of parton n and α_n contains the colour and spin indices. This is the expansion to second order in α_s that contains the

single and double-emission cases, where the notation $[...]_{\overline{ij}}$ indicates that the set of partons considered does not include partons i and j:

$$\langle q_1...q_n; \alpha_1...\alpha_n | \mathcal{M}(q_1...q_n; \alpha_1...\alpha_n)\rangle$$

$$= g_s \sum_{i<j}^{n} \sum_{\beta} \langle q_i, q_j; \alpha_i, \alpha_j | \mathbf{Sp}(q_i, q_j, q_i + q_j; \alpha_i, \alpha_j, \beta)\rangle \langle [q_1...q_n; \alpha_1...\alpha_n]_{\overline{ij}} | \mathcal{M}([q_1...q_n]_{\overline{ij}}, q_i + q_j; [\alpha_1...\alpha_n]_{\overline{ij}}, \beta)\rangle$$

$$+ g_s^2 \sum_{i<j<k}^{n} \sum_{\beta} \langle q_i, q_j, q_k; \alpha_i, \alpha_j, \alpha_k | \mathbf{Sp}(q_i, q_j, q_k, q_i + q_j + q_k; \alpha_i, \alpha_j, \alpha_k, \beta)\rangle \langle [q_1...q_n; \alpha_1...\alpha_n]_{\overline{ijk}}$$

$$\times | \mathcal{M}([q_1...q_n]_{\overline{ijk}}, q_i + q_j + q_k; [\alpha_1...\alpha_n]_{\overline{ijk}}, \beta)\rangle$$

$$+ g_s^2 \sum_{i<j}^{n} \sum_{\substack{k<l \\ k,l\neq i,j}}^{n} \sum_{\beta,\beta'} \langle q_i, q_j; \alpha_i, \alpha_j | \mathbf{Sp}(q_i, q_j, q_i + q_j; \alpha_i, \alpha_j, \beta_1)\rangle \langle q_k, q_l; \alpha_k, \alpha_l | \mathbf{Sp}(q_k, q_l, q_k + q_l; \alpha_k, \alpha_l, \beta_2)$$

$$\times \langle [q_1...q_n; \alpha_1...\alpha_n]_{\overline{ijkl}} | \mathcal{M}([q_1...q_n]_{\overline{ijkl}}, q_i + q_j, q_k + q_l; [\alpha_1...\alpha_n]_{\overline{ijkl}}, \beta_1, \beta_2)\rangle$$

$$+ \mathcal{O}(g_s^3) + \text{finite terms} .$$

$$(6.1)$$

The first term in Eq. (6.1) describes a single splitting of $(q_i + q_j)$ to q_i and q_j and the second and third terms describe double splittings, sequentially or independently. To establish the diagrams that give singular contributions to the cross section, the expressions above need to be squared. Upon squaring, not all possible combinations contribute as there are restrictions, including those coming from the observable. Some abbreviated notation will be used:

$$\langle q_1...q_n; \alpha_1...\alpha_n | \mathcal{M}(q_1...q_n; \alpha_1...\alpha_n)\rangle = \langle n | \mathcal{M}(n)\rangle ,$$
$$\langle q_i, q_j; \alpha_i, \alpha_j | \mathbf{Sp}(q_i, q_j, q_i + q_j; \alpha_i, \alpha_j, \beta)\rangle = \langle i, j | \mathbf{Sp}(i, j, i+j)\rangle , \qquad (6.2)$$
$$\langle [q_1...q_n; \alpha_1...\alpha_n]_{\overline{ij}} | \mathcal{M}([q_1...q_n]_{\overline{ij}}, q_i + q_j; [\alpha_1...\alpha_n]_{\overline{ij}}, \beta)\rangle = \langle [n]_{\overline{ij}} | \mathcal{M}([n]_{\overline{ij}}, i+j)\rangle .$$

Indices i and j will be used for the original amplitude and k and l used for the conjugate amplitude. Using the above abbreviations, the matrix element can be written as a sum of contributions for single and double splittings up to the order g_s^3. Where 'Single' refers to the one-emission case, 'Triplet' to the two-emission one-emitter case and 'Pairs' is the two-emission two-emitter case, the following is equivalent to Eq. (6.1):

$$\langle n | \mathcal{M}(n)\rangle = \langle n | \mathcal{M}^{\text{Single}}(n)\rangle + \langle n | \mathcal{M}^{\text{Triplet}}(n)\rangle + \langle n | \mathcal{M}^{\text{Pairs}}(n)\rangle + \mathcal{O}(g_s^3) . \qquad (6.3)$$

To illustrate the combinatorics, *i.e.* the relevant diagrams giving singular contributions, an example is shown for the single-emission case that corresponds to the matrix-element squared, but only to the first order in α_s or equivalently g_s^2:

$$\langle n | \mathcal{M}^{\text{Single}}\rangle^2 = g_s^2 \sum_{i<j}^{n} \sum_{\beta} \langle i, j | \mathbf{Sp}(i, j, i+j)\rangle \langle [n]_{\overline{ij}} | \mathcal{M}^{\text{Single}}([n]_{\overline{ij}}, (i+j))\rangle$$

$$\times \sum_{k<l}^{n} \sum_{\beta'} \langle \mathcal{M}^{\text{Single}}([n]_{\overline{kl}}, (k+l)) | [n]_{\overline{kl}}\rangle \mathbf{Sp}^{\dagger}(k, l, k+l) | k, l\rangle \Delta_{ij}^{kl} , \qquad (6.4)$$

$$|\mathcal{M}^S(n)|^2 = \sum_{i<j} \sum_{k<l} \mathcal{M}(i, j)\mathcal{M}^*(k, l)\Delta_{ij}^{kl} .$$

The possible index pairings are:

$$\Delta_{ij}^{kl} = (\delta_{ik}\delta_{jl} + \bar{\delta}_{ik}\delta_{jl} + \delta_{jk} + \delta_{il} + \bar{\delta}_{jl}\delta_{ik}) , \qquad (6.5)$$

where $\bar{\delta}_{ij} \equiv 1 - \delta_{ij}$. These allow the splitting to be expanded to the following:

$$
\begin{aligned}
|\mathcal{M}^S(n)|^2 &= \sum_{i<j}\sum_{k<l}\mathcal{M}(i,j)\mathcal{M}^*(k,l)(\delta_{ik}\delta_{jl} + \bar{\delta}_{ik}\delta_{jl} + \delta_{jk} + \delta_{il} + \bar{\delta}_{jl}\delta_{ik}) \,, \\
&= \sum_{i<j}\mathcal{M}(i,j)\mathcal{M}^*(i,j) + \sum_{i<j,k<j}\mathcal{M}(i,j)\mathcal{M}^*(k,j) \\
&\quad + \sum_{i<j<l}\mathcal{M}(i,j)\mathcal{M}^*(j,l) + \sum_{k<i<j}\mathcal{M}(i,j)\mathcal{M}^*(k,i) \\
&\quad + \sum_{i<j,i<l}\mathcal{M}(i,j)\mathcal{M}^*(i,l) \,.
\end{aligned}
\tag{6.6}
$$

After relabelling the partons and applying an ordered sum over the three indices i,j,k it is possible to rewrite these terms as:

$$
\begin{aligned}
|\mathcal{M}^S(n)|^2 &= \sum_{i<j}\mathcal{M}(i,j)\mathcal{M}^*(i,j) + \sum_{i<j<k}2\mathrm{Re}\{\mathcal{M}(i,j)\mathcal{M}^*(j,k) \\
&\quad + \mathcal{M}(i,j)\mathcal{M}^*(i,k) + \mathcal{M}(i,k)\mathcal{M}^*(j,k)\} \,.
\end{aligned}
\tag{6.7}
$$

The above gives a complete set of all the relevant diagrams for the single-emission case. The examples for the two-emission case can be found in App. B.1.

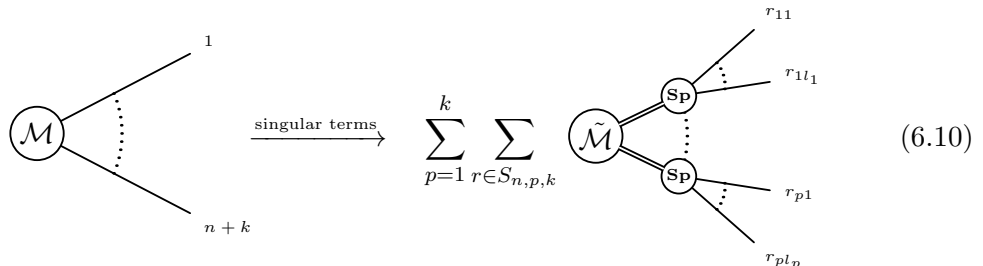## 6.2. General k-emissions Case

The general case can be described by considering a hard process with n external legs and k additional emissions, that can be factorised to the underlying n-particle hard amplitude multiplied by emission diagrams for the singular emissions. The different emission diagrams can be characterised by the splitting function $\mathbf{Sp}$ and a sum over the set of possible splittings $S_{n,q,k}$. For the most general case the number of emitters is not fixed and therefore a sum needs to be carried out over all possible cases, where the number of emitters p can range from 1 to k, where k is the number of emissions. The general amplitude considered here is written as a vector in spin and colour space and for the case of one emitter and k emissions reads:

$$
|\mathcal{M}_{n+k}(p_1...p_{n+k})\rangle = \sum_{p=1}^{k}\sum_{r\in S_{n,p,k}}\mathbf{Sp}_{(q_1|k_{11}|...|k_{1\ell_1})}...\mathbf{Sp}_{(q_p|k_{p1}|...|k_{p\ell_p})}
$$
$$
\times|\mathcal{M}_n(p_1,...,(q_1|k_{11}|...|k_{1\ell_1}),...,(q_p|k_{p1}|...|k_{p\ell_p}),...,p_{n+k})\rangle \,.
\tag{6.8}
$$

Here the notation used is:

$$
(q_i|k_{i1}|...|k_{i\ell_i}) = q_i + k_{i1} + ... + k_{i\ell_i} \,.
\tag{6.9}
$$

For the case where the emissions are infrared singular, *i.e.* contain soft and/or collinear singularities, Eq. (6.8) can be represented diagramatically as:

$$
\tag{6.10}
$$

To obtain the singular behaviour of the cross section, the amplitude vector needs to be combined with its conjugate, either to form a matrix-element squared or a density-operator structure. The method used in the previous sections takes the matrix-element squared approach. The density operator requires the development of a projector formalism, which is discussed in [75]. The density operator has the benefit of being a more generalised framework that is helpful for the the discussion of iterated emissions at the amplitude level.

6.2.1. Projector Formalism

The generalised amplitudes can be combined and written in terms of a density-type operator instead of a squared amplitude, that can operate on external amplitudes. Using the same notation as above, this is written as:

$$|\mathcal{M}_{n+k}(1, ..., n+k)\rangle\langle\mathcal{M}_{n+k}(1, ..., n+k)| =$$

$$\sum_{p=1}^{k}\sum_{\bar{p}=1}^{k}\sum_{r\in S_{n,p,k}}\sum_{\bar{r}\in S_{n,\bar{p},k}}\mathbf{Sp}_{(r_1)}...\mathbf{Sp}_{(r_p)}|\mathcal{M}_n(1, ..., (r_1), ..., (r_p), ..., n+k)\rangle$$

$$\langle\mathcal{M}_n(1, ..., (\bar{r}_1), ..., (\bar{r}_{\bar{p}}), ..., n+k)|\mathbf{Sp}^{\dagger}_{(\bar{r}_1)}...\mathbf{Sp}^{\dagger}_{(\bar{r}_{\bar{p}})} \times \hat{\Delta}^r_{\bar{r}} , \quad (6.11)$$

where the splitting momenta have been abbreviated to $(r_i) = (r_{i1}|...|r_{i\ell_i})$. $\hat{\Delta}^r_{\bar{r}}$ is a generalisation of Eq. (6.5), and takes the form of tensor to single out relevant parton pairings *i.e.* diagram topologies that give rise to singular behaviour in the IR limits.

The tensor expression from [75] is derived using Kronecker-deltas, as in Eq. (6.5). For the permutations σ of a set $\bar{S}_{n,p,k}$, the decomposition of possible combinations is given as:

$$\hat{D}^r_{\bar{r}} \equiv \frac{1}{n_\sigma}\sum_\sigma\prod_{g=1}^{\min(p,\bar{p})}\prod_{l=1}^{l_g}\left(\delta^{r_{gl}}_{\sigma(\bar{r}_{gl})} + b_{\sigma(g)}\bar{\delta}^{r_{gl}}_{\sigma(\bar{r}_{gl})}\right), \qquad (6.12)$$

where the number of permutations is n_σ and $p \leq \bar{p}$. The index g labels the splitting group and the length of that group corresponds to the value of l_g. The parameters b_g give the number of possible unconnected lines for each splitter group. The function $\hat{D}$ can then be used to generate the tensor, $\hat{\Delta}^r_{\bar{r}}$, that contains the permutations for the possible parton combinations:

$$\hat{\Delta}^r_{\bar{r}} \equiv \sum_{n=0}^{\min(p,\bar{p})}\sum_{\bar{g}=1}^{\bar{p}}\frac{\partial^n}{\partial b_{\bar{g}}^n}\hat{D}^r_{\bar{r}}\Big|_{b_{\bar{g}}=0} . \qquad (6.13)$$

For a specific number of emissions, $\hat{\Delta}^r_{\bar{r}}$ can be used to determine all possible combinations of partons which can give diagrams containing singular contributions.

To be able to determine the singular contributions in such a framework, a decomposition is used to separate the different components of the numerator momenta into different 'boxes'. This is particularly effective, because a scaling can then be applied to each component of the external and internal lines in a diagram. When this scaling is compared to the denominator scaling, some contributions can be immediately neglected, which simplifies the calculations. Additionally, it is possible to determine all relevant contributions to the soft and collinear limits without taking either limit explicitly, and to determine the combinations which contribute in an algorithmic way. This formalism is developed and discussed in detail in [75].

The aim of this formalism is to be able to examine parton branching at the amplitude level, as opposed to the standard method of cross-section level subtractions. The cross section result can be obtained from the density operator by tracing over colour and spin indices. For iterated emissions, an amplitude-level treatment is particularly important due to existing knowledge of inaccuracies beyond the one emission case as discussed in Sec. 4.5.

6.3. Partitioning

After all the potentially singular topologies have been identified, it remains to examine the different singular limits they include. In order to be able to describe an emission kernel for one collinear configuration, the relevant terms need to be extracted from the set of contributing diagrams. The emission kernels can then be used to generate probabilistic splittings as part of a parton-shower algorithm, but also retain information about potential spin and colour correlations in both the soft and soft-collinear limits. The calculation of a two-emission splitting kernel is shown in Sec. 7.2 as a cross check for the kinematics and methods used.

The splitting kernel, $\mathbb{U}_{ij}$, is defined as the sum over all possible contributions to a specific collinear limit involving the partons labelled i and j. This is obtained from a set of squared sub-amplitudes for the possible splittings, $\mathcal{A}_d$, multiplied by a partitioning factor, $\mathbb{P}_{ij}^{(d)}$, which is specific to the diagram and collinear configuration. The emission kernel for the ij collinear case for a single emission can be described by:

$$\mathbb{U}_{ij} = \sum_{d \in \mathbf{D}_1} \left[\mathbb{P}_{ij}^{(d)} \mathcal{A}_d \right] . \tag{6.14}$$

Where $\mathcal{A}_d$ are the squared amplitudes, in this case from the set of one-emission diagrams $\mathbf{D}_1$, the same principle can be extended to any number of emissions. The general partitioning functions, where c denotes the singular configuration and d the diagram, can be written as:

$$\mathbb{P}_c^{(d)} \equiv \frac{F_c^{(d)}}{\mathbb{F}^{(d)}}. \tag{6.15}$$

The cancelling factors $F_c^{(d)}$ can be determined from:

$$F_c^{(d)} = \left(\prod_{S_{c'} \in \mathbf{S}_c^d} S_{c'} \, \mathcal{D}(\mathcal{A}_d) \right)^{-1} \varsigma^p, \tag{6.16}$$

where $\mathbf{S}_c^d$ is the set of singular S factors appearing in the denominator of diagram d for a collinear configuration c. The cancelling factor for a specific configuration can be described as the inverse of the singular factors from the denominator of the diagram for that combination, multiplied by the full denominator of the diagram, written here as $\mathcal{D}(\mathcal{A}_d)$. The scale ς^p is introduced to match the mass dimensions from the different factors so that all the factors are dimensionless. The denominator term of the partitioning functions is the sum over all of the cancelling factors:

$$\mathbb{F}^{(d)} \equiv \sum_{c \in \mathbf{C}_d} F_c^{(d)}, \tag{6.17}$$

where $\mathbf{C}_d$ is the set of collinear combinations for which diagram d gives singular contributions. As an example, consider the one-emission exchange diagram described in Sec. 5.2.2.1, this can contribute to two different collinear limits. The two cases are: either the emission is collinear to the emitter or the emission is collinear to the spectator. Using three indices to label the partons, where i corresponds to the emitter, j to the emission and k to the spectator allows the singular behaviour to be described generically. The singular factors are in the denominator of the amplitude and arise from the propagators in the diagrams, they can be described by $S_{ij} = (p_i + p_j)^2$. The denominator terms for the single emission exchange diagram can be written as:

$$\text{Denom}(|\mathcal{M}_{ij}^{(E)}|^2) = \mathcal{D}(\mathcal{A}_{E1}) = \frac{1}{S_{ij} S_{jk}} , \tag{6.18}$$

where each S factor is singular in a different collinear limit. A partitioning factor for each limit can be defined using the cancelling factors which are:

$$F_{ij}^{(E1)} = \left(S_{ij} \frac{1}{S_{ij} S_{jk}} \right)^{-1} = S_{jk} \ , \qquad\qquad F_{jk}^{(E1)} = S_{ij} \ . \qquad\qquad (6.19)$$

Giving partitioning factors:

$$\mathbb{P}_{ij}^{(E1)} = \frac{S_{jk}}{S_{ij} + S_{jk}} \ , \qquad\qquad \mathbb{P}_{jk}^{(E1)} = \frac{S_{ij}}{S_{ij} + S_{jk}} \ . \qquad\qquad (6.20)$$

This allows the contribution from this diagram to the ij-collinear emission kernel to be written as:

$$\mathbb{P}_{ij}^{(E1)} \mathcal{A}_{E1} = \frac{S_{jk}}{S_{ij} + S_{jk}} \frac{\mathcal{N}(\mathcal{A}_{E1})}{\mathcal{D}(\mathcal{A}_{E1})} = \frac{1}{S_{ij}(S_{ij} + S_{jk})} \mathcal{N}(\mathcal{A}_{E1}) \ , \qquad\qquad (6.21)$$

where $\mathcal{N}(\mathcal{A}_{E1})$ contains the numerator terms from this diagram. A further example of the partitioning for a two-emission diagram is given in C.1.

This partitioning formalism is particularly useful for constructing splitting kernels that require contributions from only one collinear limit. When considering a case with multiple emissions there are more possible collinear limits and they can overlap and interact with one another. The partitioning is needed to separate these overlapping collinear singularities smoothly whilst retaining the correct soft behaviour. To effectively factorise the IR emissions, the partitioning formalism has to fulfil several requirements that will be discussed below.

6.3.1. Partitioning Checks

One of the most important conditions is that the partitioning factors themselves should not give collinear-singular contributions, *i.e.* they are non-singular in all possible collinear limits. Additionally the partitioning should not affect the soft-collinear and soft limits. The checks shown below are for the two-emission case, however, these conditions should hold generally for any number of emissions.

For all of the two-emission exchange amplitudes, given in App. B.2, for which there is a defined partitioning factor, via the formalism given above, the behaviour of the propagator factors from the conjugate recoiler in the collinear limit was checked. The aim is to show that there are only sub-leading contributions from the partitioning factor denominator in the collinear limit corresponding to the emissions being collinear to the recoiler. The scaling was checked for all ten double-exchange single-spectator topologies that are relevant in the triple-collinear QCD case. In all cases the scaling was found to be either finite or $\mathcal{O}(1/\lambda^2)$ which are sub-leading contributions, where for the two-emission case the leading collinear contributions are $\mathcal{O}(1/\lambda^4)$.

In Table 6.1 the scaling of the different invariants in different limits is shown, this was used when determining the scaling of the partitioning factors. The following limits were tested, not only to check the collinear behaviour, but also to ensure that the scaling in the double-soft and soft-collinear cases is not affected by the partitioning:

- Collinear triplets: $(ijk), (ijl), (ikl), (jkl)$

- Collinear pairs: $(ij, kl), (ik, jl), (il, jk)$

- Double soft: $(ij), (ik), (il), (jk), (jl), (kl)$

- Soft-collinear: $(ij, k/l), (ik, j/l), (il, j/k), (jk, i/l), (jl, i/k), (kl, i/j)$

Limit	S_{ij}	S_{ik}	S_{jk}	S_{il}	S_{jl}	S_{kl}
Collinear $i\|\|j\|\|k$	λ^2	λ^2	λ^2	1	1	1
Collinear $i\|\|j, k\|\|l$	λ^2	1	1	1	1	λ^2
Double soft $(i,j \to 0)$	λ^2	λ	λ	λ	λ	1
Soft-collinear $i\|\|j, (k \to 0)$	λ^2	λ	λ	1	1	λ

Table 6.1.: Scaling of invariants in different IR limits, from [75].

The leading scaling in the collinear, soft and soft-collinear limits for all of the two-emission topologies is $\mathcal{O}(1/\lambda^4)$, when both numerator and denominator terms are included. The denominator multiplied by the partitioning factor scales differently in the collinear limit for two different groups of the exchange topologies. Those containing a self-energy like loop have a scaling of $\mathcal{O}(1/\lambda^6)$ in the collinear limit. However, when combined with the leading terms from the numerator the total collinear scaling is $\mathcal{O}(1/\lambda^4)$, due to the corresponding $\mathcal{O}(\lambda^2)$ terms in the numerator. The other exchange diagrams have a collinear scaling $\mathcal{O}(1/\lambda^4)$ from just the denominator and partitioning factor, and contain only $\mathcal{O}(1)$ terms in the numerator.

	CC	CS	SC	SS
$\{A_1\}$	$1/\lambda^4$	$1/\lambda^4$	$1/\lambda^2$	$1/\lambda^4$
$\{A_2\}$	$1/\lambda^4$	$1/\lambda^3$	$1/\lambda^3$	$1/\lambda^4$
$\{A_3\}$	$1/\lambda^4$	$1/\lambda^3$	$1/\lambda^2$	$1/\lambda^4$
$\{A_4\}$	$1/\lambda^6$	$1/\lambda^4$	$1/\lambda^3$	$1/\lambda^5$
$\{A_5\}$	$1/\lambda^6$	$1/\lambda^3$	$1/\lambda^3$	$1/\lambda^6$
$\{B_1\}$	$1/\lambda^6$	$1/\lambda^6$	$1/\lambda^3$	$1/\lambda^4$
$\{B_2\}$	$1/\lambda^6$	$1/\lambda^4$	$1/\lambda^5$	$1/\lambda^4$
$\{E_1\}$	$1/\lambda^8$	$1/\lambda^6$	$1/\lambda^4$	$1/\lambda^4$
$\{E_2\}$	$1/\lambda^8$	$1/\lambda^5$	$1/\lambda^5$	$1/\lambda^4$
$\{E_3\}$	$1/\lambda^8$	$1/\lambda^5$	$1/\lambda^4$	$1/\lambda^5$

Table 6.2.: Scaling for denominator times partitioning factor of two-emission single-emitter topologies.

In Table 6.2 the scaling for each of the two-emission single-emitter topologies in the possible limits are shown. The limits can be described by labelling the hard parton i and the second and first emissions j and k respectively. 'CC' is the double collinear limit where $i\|\|j\|\|k$, 'SS' is the double soft limit where both j and k are soft, 'CS' is the soft-collinear case where of i and j are collinear and k is soft and 'SC' is the alternative soft-collinear combination where i and k are collinear and j is soft.

Then for the two-emission two-emitter topologies the scaling of the denominator times partitioning factor is given in Table 6.3. Here the indices have to be reinterpreted as the hard

partons are labelled i and l and the emissions are j and k from i and l respectively. The indices involved in each limit are modified correspondingly, 'CC' is for i collinear to j and k collinear to l, 'CS' is the soft-collinear combination of j collinear to i and k soft, 'SC' is the soft-collinear combination of k collinear to l and j soft and 'SS' is the double soft limit for both emissions, j and k, soft. This knowledge of the scaling behaviour for the denominator

	CC	CS	SC	SS
$\{B_3\}$	$1/\lambda^6$	$1/\lambda^4$	$1/\lambda^6$	$1/\lambda^4$
$\{B_4\}$	$1/\lambda^4$	$1/\lambda^3$	$1/\lambda^4$	$1/\lambda^3$
$\{X\}$	$1/\lambda^4$	$1/\lambda^4$	$1/\lambda^4$	$1/\lambda^4$
$\{E_4\}$	$1/\lambda^8$	$1/\lambda^6$	$1/\lambda^6$	$1/\lambda^4$

Table 6.3.: Scaling for denominator times partitioning factor of two-emission two-emitter topologies.

and partitioning, makes is easy to determine which terms from the numerator are leading in each of the limits for each topology. The contributions from the partitioning factors are of order $(1/\lambda^2)$ or less and therefore do not affect the behaviour in any of the possible limits as they are always sub-leading. The self-energy type topologies do not require partitioning as they only contain one type of collinear singularity. Though they also display similar scaling behaviour to the exchange diagrams with a self-energy type loop, *i.e.* $\mathcal{O}(1/\lambda^8)$ denominator scaling in the collinear limit which is combined with numerator terms to give total collinear scaling $\mathcal{O}(1/\lambda^4)$.

Additional details of the partitioning checks carried out are given in [75]. A possible application of the splitting kernels would be the implementation in a multiple-emission parton shower, that needs to be combined with a kinematic mapping to facilitate the factorisation. One possible such mapping is discussed in the next section.

6.4. Kinematics for k-emissions

For the k-emissions case the concepts applied to the single-emission mapping are extended to a generalised picture of an emitter with any number of emissions, as illustrated in Eq. (6.10). Where each emitter is part of a system of emitter and spectator momenta, which partially absorb the recoil. The final-state system is described by a set $\mathbf{S}$ of "splitters" or emitters q_i, the sets of emisisons $\mathbf{E}_i$ associated to each emitter and containing momenta k_{il} and finally a set $\mathbf{R}$ of recoil momenta q_r. The kinematic mapping that relates the momenta before any emission to those after k-emissions is written in terms of the light-cone momenta p_i and n_i, transverse momenta $n_{\perp,l}^{(i)}$ and recoil momentum p_r:

$$
\begin{aligned}
q_r &\equiv \frac{1}{\hat{\alpha}}\Lambda p_r \ , \\
q_i &\equiv \frac{1}{\hat{\alpha}}\Lambda \left[(1 - A_i)p_i + \left(y_i - (1 - A_i)B_i\right)n_i - \sqrt{1 - A_i}\,\tilde{n}_\perp^{(i)}\right] \ , \\
k_{il} &\equiv \frac{1}{\hat{\alpha}}\Lambda \left[\alpha_{il}\,p_i + (1 - A_i)\beta_{il}\,n_i + \sqrt{1 - A_i}\,\sqrt{\alpha_{il}\beta_{il}}\,n_{\perp,l}^{(i)}\right] \ .
\end{aligned}
\tag{6.22}
$$

Where the following abbreviations are used:

$$
A_i \equiv \sum_{l \in \mathbf{E}_i} \alpha_{il} \ , \quad B_i \equiv \sum_{l \in \mathbf{E}_i} \beta_{il} \ , \quad \tilde{n}_\perp^{(i)} \equiv \sum_{l \in \mathbf{E}_i} \sqrt{\alpha_{il}\beta_{il}}\,n_{\perp,l}^{(i)} \ .
\tag{6.23}
$$

This momentum mapping is the same as that presented in [75]. The use of the light-cone momenta is to preserve the backward direction from the hard process and with that correctly distribute the recoil for multiple emissions. Here, as in Sec. 5.3, a Lorentz transformation is used to conserve the total momentum and the momenta p_i, p_r, n_i, q_i, q_r and k_{il} are assumed to be on-shell. The changes compared to the previous version include applying the transformation to all of the momenta before emission, including the backwards and transverse momenta. The y dependence was removed from the transverse and the backward momentum components to ensure consistency of the collinear scaling across the momenta. The $(1 - A_i)$ factors were added to ensure that the definition of y_i does not contain any additional singularities. The conservation of the total momentum transfer, Q, for this mapping is written as:

$$Q = \sum_{i \in \mathbf{S}} \left(q_i + \sum_{l \in \mathbf{E}_i} k_{il} \right) + \sum_{r \in \mathbf{R}} q_r = \frac{1}{\hat{\alpha}} \Lambda \left[\sum_{i \in \mathbf{S}} (p_i + y_i n_i) + \sum_{r \in \mathbf{R}} p_r \right] . \tag{6.24}$$

The action of the transformation therefore has to fulfil:

$$\Lambda^{\mu}{}_{\nu} [Q^{\nu} + N^{\nu}] = \hat{\alpha} Q^{\mu}, \tag{6.25}$$

where $N = \sum_{i \in \mathbf{S}} y_i n_i$. Given that Λ is a proper orthochronous transformation the scaling factor $\hat{\alpha}$ can be defined as:

$$\hat{\alpha} = \sqrt{\frac{(Q + N)^2}{Q^2}} . \tag{6.26}$$

The full expression for the Lorentz transformation is:

$$\begin{aligned}
\Lambda^{\mu}{}_{\nu} = g^{\mu}{}_{\nu} &- \frac{(N^{\mu} + Q^{\mu})(N_{\nu} + (\hat{\alpha} + 1)Q_{\nu}) + \hat{\alpha}^2 Q^{\mu} Q_{\nu}}{N^2 + (\hat{\alpha} + 2)N \cdot Q + (\hat{\alpha} + 1)Q^2} \\
&+ \frac{\hat{\alpha} Q^{\mu}(N_{\nu} + Q_{\nu})(N^2 + 2(\hat{\alpha} + 1)N \cdot Q + (2\hat{\alpha} + 1)Q^2)}{(N^2 + 2N \cdot Q + Q^2)(N^2 + (\hat{\alpha} + 2)N \cdot Q + (\hat{\alpha} + 1)Q^2)} .
\end{aligned} \tag{6.27}$$

The choice of the backward light-cone vector is constrained to be on-shell and backwards, *i.e.* $p_i \cdot n_i$ should be large. There is more than one possible form of this vector but for the examples in later sections n_i is chosen to be:

$$n_i^{\mu} = Q^{\mu} - \frac{Q^2}{2 p_i \cdot Q} p_i^{\mu}. \tag{6.28}$$

The transverse component from the mapping is defined as being perpendicular to the light-cone momenta and therefore, $p_i \cdot n_{\perp,l}^{(i)} = n_i \cdot n_{\perp,l}^{(i)} = 0$. Expanding the expression for k_{il} as an on-shell momentum fixes the square of the transverse component to be $\left(n_{\perp,l}^{(i)} \right)^2 = -2 p_i \cdot n_i$. From applying the on-shell conditions for the momenta k_{il} and q_i, y_i can be parametrised as:

$$y_i = (1 - A_i)B_i - \frac{(\tilde{n}_{\perp}^{(i)})^2}{2 p_i \cdot n_i} . \tag{6.29}$$

The mapping coefficients α_{il}, β_{il} and y_i all have values between 0 and 1 and parametrise the soft and collinear limits. The scaling of the parameters, where $K_i = \sum_l k_{il}$, in each of the limits is given in Table 6.4. The y_i scaling only applies if all of the emissions from that emitter are collinear or soft, because the definition of y_i contains the sum over β_{il}. In the soft collinear limit the α_{il} and β_{il} parameters scale correspondingly to the emission as above, and y_i scales as in the soft case, due to the contribution from the soft β_{il}. The choice of mapping coefficients changes the number of degrees of freedom available, this has an impact on the phase space integration. The phase space for this mapping will be outlined in the next section.

	α_{il}	β_{il}	y_i
K_i soft	λ	λ	λ
K_i, q_i collinear	1	λ^2	λ^2

Table 6.4.: Scaling for mapping parameters in soft and collinear limits.

6.5. Phase Space for k-emissions

Here, the factorised final-state phase space is defined for the mapping given in Eq. (6.22), with on-shell momenta as defined in the previous section. The total momenta for the emitters and recoilers before emission and the mass of the recoil momenta, m, are defined as:

$$P_S = \sum_{i \in \mathbf{S}} p_i \ , \qquad P_R = \sum_{r \in \mathbf{R}} p_r \ , \qquad Q_R = \frac{1}{\hat{\alpha}} \Lambda P_R \ ,$$
$$Q_R^2 = m^2 \ , \qquad P_R^2 = \hat{\alpha}^2 m^2 \ . \tag{6.30}$$

The full final-state phase space, for the sets of momenta including the emitters, recoilers and emissions, where $\{q_i\}_{\mathbf{S}} = \{q_1, ..., q_n\}$ for $i \in \mathbf{S}$, is written in terms of the momenta before the emission and the emission phase space:

$$\mathrm{d}\phi\left(\{q_i\}_{\mathbf{S}}, \{q_r\}_{\mathbf{R}}, \{k_{il}\}_{\mathbf{E}_i} | Q\right)$$
$$= \mathrm{d}\phi\left(\{p\}_{\mathbf{R}} | P_R\right) \hat{\alpha}^{d - n_R(d-2)} (2\pi)^d \delta\left(P_S + P_R - Q\right)$$
$$\times \frac{\mathrm{d}m^2}{2\pi} \frac{\mathrm{d}^{d-1}P_R}{(2\pi)^{d-1} 2\omega(\vec{P}_R, \hat{\alpha}m)} \frac{\omega(\vec{P}_R, \hat{\alpha}m)}{\omega(\vec{Q}_R, m)} \Theta(Q_R^0)$$
$$\times \prod_{i \in \mathbf{S}} \frac{\mathrm{d}^{d-1}p_i}{(2\pi)^{d-1} 2\omega(\vec{p}_i)} \frac{\omega(\vec{p}_i)}{\omega(\vec{q}_i)} \Theta(i^0) \left| \frac{\partial(\{\vec{q}\}_{\mathbf{S}}, \vec{Q}_R)}{\partial(\{\vec{p}\}_{\mathbf{S}}, \vec{P}_R)} \right| \prod_{l \in \mathbf{E}_i} \frac{\mathrm{d}^{d-1}k_{il}}{(2\pi)^{d-1} 2\omega(\vec{k}_{il})} \Theta(k_{il}^0). \tag{6.31}$$

Further details of the phase space factorisation are described in [75] including the Jacobian calculation for this mapping. The resulting Jacobian is:

$$|\mathcal{J}| = \frac{\hat{\alpha}^{1-d}}{4} (2p_i \cdot n_i)^{\frac{d-1}{2}} (\alpha_{il}\beta_{il})^{\frac{d-4}{2}} (1 - A_i)^{\frac{d-2}{2}} \left(\alpha_{il} + \tilde{\beta}_{il}\right) \ . \tag{6.32}$$

This is needed to determine the phase space of the emission momenta that factorise from the total phase space, and to regulate IR divergences when integrating over the phase space. The resulting expression for the emission phase space is:

$$[\mathrm{d}k_{il}] = \frac{1}{(2\pi)^{d-1}} \Theta(\alpha_{il}) \Theta(\beta_{il}) \frac{\hat{\alpha}^{2-d}}{4} [2p_i \cdot n_i (1 - A_i)]^{\frac{d-2}{2}} (\alpha_{il}\beta_{il})^{\frac{d-4}{2}} \mathrm{d}\alpha_{il} \, \mathrm{d}\beta_{il} \, \mathrm{d}\Omega^{d-3} \ . \tag{6.33}$$

The phase-space factorisation is an important component of the parton evolution using this mapping and needs to be included in the parton-shower code to give the correct behaviour. This is relevant for any implementation of the methods discussed in this Chapter.

6.6. Conclusions from the Big Picture

Here, the development of a kinematic mapping for k-emissions has been shown and corresponding methods established to enumerate the diagrams relevant to the IR singular limits.

A partitioning framework has been introduced to separate overlapping collinear sectors. The aim is to provide a mapping that can expose soft and collinear-singular contributions for all possible cases within one method, so that the limits can be correctly reproduced without loss of information about the regions between different limits.

The motivation for developing such a mapping includes the issues raised in Sec. 4.5, and was inspired by aspects of both dipole and angular-ordered showers. One benefit of using the light-cone parametrisation of p and n is that the backwards direction of the hard process can be preserved, which is important when describing multiple emissions. This mapping and associated framework is well suited to be combined with the parton branching algorithm from [70], as it is designed at the amplitude level with the goal of keeping all information about the colour evolution. A first implementation of this mapping for the one-emission case is shown in Chapter 8, which gives a useful comparison to the existing dipole and angular-ordered showers in Herwig. However, it is not expected that this has any large affect on the shower output as the emission kernels and branching algorithm used in Herwig remain unchanged. A more promising option for the implementation of the mapping is the code, CVolver [73], that is designed around the amplitude-level branching algorithm mentioned above. Such an implementation is left for future work.

This chapter starts by outlining the kinematics for two emissions in the one and two-emitter cases, in Sec. 7.1. Then a result using the one-emitter two-emissions mapping is given in Sec. 7.2, that shows that this mapping reproduces the correct collinear-singular behaviour. Having obtained the result for the collinear limit, it is helpful to show the relation between the splitting function and the soft and soft-collinear functions, discussed in Sec. 7.3. Understanding the singular terms in each of the IR limits allows subtraction terms to be constructed, and illustrates the overlap between the different singular limits.

7.1. Two-Emission Kinematics

The two-emission case includes diagrams with either one emitter or two emitters and one or two spectators. To fully describe the soft and collinear behaviour at this order, all of the possible combinations are required. Here the mapping is outlined, for the momenta after the emissions in terms of the momenta before the emissions, p_i, p_r, and two additional vectors to describe the backward and transverse directions, n_i and $n_{\perp,l}^{(i)}$, respectively.

The generalised mapping in Sec. 6.4, for massless partons, is shown here for the case of a single emitter and two emissions where q_r is the spectator, q_i the emitter and k_{i1}, k_{i2} are the emission momenta:

$$q_r = \frac{1}{\hat{\alpha}} \Lambda p_r \ ,$$

$$q_i = \frac{1}{\hat{\alpha}} \Lambda \bigg[(1 - \alpha_{i1} - \alpha_{i2}) \, p_i + (y_i - (1 - \alpha_{i1} - \alpha_{i2})(\beta_{i1} + \beta_{i2})) \, n_i$$
$$- \sqrt{(1 - \alpha_{i1} - \alpha_{i2})} \left(\sqrt{\alpha_{i1}\beta_{i1}} n_{\perp,1}^{(i)} + \sqrt{\alpha_{i2}\beta_{i2}} n_{\perp,2}^{(i)} \right) \bigg] \ , \tag{7.1}$$

$$k_{i1} = \frac{1}{\hat{\alpha}} \Lambda \bigg[\alpha_{i1} p_i + (1 - \alpha_{i1} - \alpha_{i2})\beta_{i1} \ n_i + \sqrt{(1 - \alpha_{i1} - \alpha_{i2})} \sqrt{\alpha_{i1}\beta_{i1}} n_{\perp,1}^{(i)} \bigg] \ ,$$

$$k_{i2} = \frac{1}{\hat{\alpha}} \Lambda \bigg[\alpha_{i2} p_i + (1 - \alpha_{i1} - \alpha_{i2})\beta_{i2} \ n_i + \sqrt{(1 - \alpha_{i1} - \alpha_{i2})} \sqrt{\alpha_{i2}\beta_{i2}} n_{\perp,2}^{(i)} \bigg] \ ,$$

where as in the previous chapter, $p_i, p_r, n_i, q_i, q_r, k_{i1}$ and k_{i2} are on-shell and p_i and n_i are transverse to all $n_{\perp,l}^{(i)}$. The choice of $n_i = Q - \frac{Q^2}{2p_i \cdot Q} p_i$ gives $\hat{\alpha} = \sqrt{1 + y_i}$.

Solving the q_i on-shell condition for y_i and using invariants to simplify the expression gives:

$$y_i = \frac{S(k_{i1}, k_{i2}) + S(q_i, k_{i1}) + S(q_i, k_{i2})}{2n_i \cdot p_i} \ , \tag{7.2}$$

where the invariants $S(q_a, q_b) = (q_a + q_b)^2$.

The mapping for two emissions and two emitters is parametrised as:

$$q_r = \frac{1}{\hat{\alpha}} \Lambda p_r \ ,$$

$$q_i = \frac{1}{\hat{\alpha}} \Lambda \left[(1 - \alpha_{i1})p_i + \left(y_i - (1 - \alpha_{i1})\beta_{i1} \right) n_i - \sqrt{(1 - \alpha_{i1})}\sqrt{\alpha_{i1}\beta_{i1}} n_{\perp,1}^{(i)} \right] \ ,$$

$$k_{i1} = \frac{1}{\hat{\alpha}} \Lambda \left[\alpha_{i1}p_i + (1 - \alpha_{i1})\beta_{i1} \ n_i + \sqrt{(1 - \alpha_{i1})}\sqrt{\alpha_{i1}\beta_{i1}} n_{\perp,1}^{(i)} \right] \ , \tag{7.3}$$

$$q_j = \frac{1}{\hat{\alpha}} \Lambda \left[(1 - \alpha_{j1})p_j + \left(y_j - (1 - \alpha_{j1})\beta_{j1} \right) n_j - \sqrt{(1 - \alpha_{j1})}\sqrt{\alpha_{j1}\beta_{j1}} n_{\perp,2}^{(j)} \right] \ ,$$

$$k_{j1} = \frac{1}{\hat{\alpha}} \Lambda \left[\alpha_{j1}p_j + (1 - \alpha_{j1})\beta_{j1} \ n_j + \sqrt{(1 - \alpha_{j1})}\sqrt{\alpha_{j1}\beta_{j1}} n_{\perp,1}^{(j)} \right] \ .$$

For the same choice of n_i and n_j, in this case $\hat{\alpha} = \sqrt{1 + y_i + y_j + \frac{y_i y_j}{2p_i \cdot Q p_j \cdot Q} p_i \cdot p_j}$.

Each emitter in the two-emitter mapping has almost identical properties to the emitter in the single-emission case. The on-shell condition for the emitters in this case results in $y_i = \beta_{i1}$ and $y_j = \beta_{j1}$.

For both the one and two-emitter cases, the invariants, $S(i, j)$, which appear in the amplitude expressions, can be written as an expansion of the mapping variables, that allows the scaling to be checked. The scaling for α_{il}, β_{il} and y_i remain the same as in Table 6.4 and give the corresponding scaling of the invariants, *i.e.* for two collinear or two soft momenta $\mathcal{O}(\lambda^2)$ and for a single soft momentum $\mathcal{O}(\lambda)$.

7.2. Two-Emission Splitting Function Result

As an illustration of the function of the two-emission mapping, the triple-collinear splitting function for the emission of two gluons from a quark was determined, using the one-emitter two-emission mapping given in the previous section. As discussed in Sec. 6.1, there are many different exchange diagrams for the two-emission case, including combinations of the one and two-emitter amplitudes. In the previous examples for the one-emission case a covariant gauge was used, however, for two emissions the number of exchange diagrams greatly increases and the calculations become more complicated. Therefore, for the two-emission case a light-cone gauge was chosen, that results in only the self-energy type diagrams contributing in the collinear limit. This simplifies the calculation and uses the gauge terms to include the terms that would contribute from the exchange diagrams in a covariant gauge. The gluon polarisation tensor, for the light-cone gauge used, takes the form:

$$d^{\mu\nu}(q) = -g^{\mu\nu} + \frac{q^\mu n^\nu + n^\mu q^\nu}{q \cdot n} \ , \tag{7.4}$$

as introduced in Sec. 2.3, where n^μ is an arbitrary gauge vector.

The generalised collinear-factorisation formula, given in [62] for m collinear partons, is analogous to the single collinear factorisation formalism as discussed in [15]:

$$|\mathcal{M}_{a_1,...,a_m,...}(p_1, ..., p_m, ...)|^2 \simeq \left(\frac{8\pi\alpha_S}{s_{1...m}} \mu^{2\varepsilon} \right)^{m-1} \mathcal{T}_{a,...}^{ss'}(xp, ...) \ \hat{P}_{a_1...a_m}^{ss'} \ , \tag{7.5}$$

where μ is the dimensional regularisation scale, $\mathcal{T}$ is the spin polarisation tensor describing the flavour a of the parent parton, $\hat{P}$ is the d-dimensional spin-dependent splitting function, and $s_{1...m}$ is equivalent to the S_{ij} factors already introduced, for up to m partons. x is the sum over all x_i, that is a factor used in the kinematics given in [62]. In the following, the spin averaged splitting functions, $\langle \hat{P}_{a_1...a_m} \rangle$, will be discussed, that are obtained by averaging over all possible polarisations. There are no spin correlations for the case of a parent fermion. For a parent gluon averaging over the spin correlations requires use of the gluon polarisation tensor as given in Eq. (7.4).

The spin-averaged splitting function $\langle \hat{P}_{ggq} \rangle$, as given in [62] contains an abelian and a non-abelian part, distinguished by the factors C_F^2 and $C_F C_A$. Firstly, the diagrams, from [75], that contribute to the abelian terms are:

$$\left\{ \quad + \quad \left[\quad + (1 \leftrightarrow 2) \right] \right\}_{C_F^2} \tag{7.6}$$

$$= \frac{1}{\lambda^4} \left(\frac{8\pi\alpha_S}{\hat{\alpha} S_{i12}} \mu^{2\varepsilon} \right)^2 C_F^2 \langle \hat{P}_{ggq}^{(\mathrm{ab})} \rangle \hat{\slashed{p}}_i + \mathcal{O}\left(\frac{1}{\lambda^3} \right), \tag{7.7}$$

where the second diagram also has non-abelian contributions but here only the abelian terms are taken. The abelian part of the splitting function is given by:

$$
\begin{aligned}
\langle \hat{P}_{ggq}^{(\mathrm{ab})} \rangle = & \left\{ \frac{S_{i12}^2}{2 S_{i2} S_{i1}} (1 - \alpha_{i1} - \alpha_{i2}) \left(-\frac{\epsilon(\alpha_{i2}^2 + \alpha_{i1}^2)}{\alpha_{i1}\alpha_{i2}} + \frac{(1 - \alpha_{i1} - \alpha_{i2})^2 + 1}{\alpha_{i1}\alpha_{i2}} - \epsilon(\epsilon+1) \right) \right. \\
& + \frac{S_{i12}}{S_{i2}} \left(\frac{(1-\alpha_{i2})(1-\alpha_{i1}-\alpha_{i2}) + (1-\alpha_{i1})^3}{\alpha_{i1}\alpha_{i2}} - \frac{(1-\alpha_{i1})}{\alpha_{i1}\alpha_{i2}} \epsilon(\alpha_{i2}^2 + \alpha_{i2}\alpha_{i1} + \alpha_{i1}^2) \right. \\
& \left. + (2 - \alpha_{i1} - \alpha_{i2})\epsilon^2 \right) + (1-\epsilon)\left(\epsilon - \frac{S_{i1}(1-\epsilon)}{S_{i2}} \right) \right\} + (1 \leftrightarrow 2) .
\end{aligned}
\tag{7.8}
$$

The following terms factorise from the calculation of the diagrams: $\mu^{4\varepsilon}/\hat{\alpha}^2 S_{i12}^2$, which includes the regulator, as well as a factor of g_s^2 that results in the corresponding coefficient given in Eq. (7.5) for the $m = 3$ case times $1/\hat{\alpha}^2$, which is the scaling factor from the mapping. The leading collinear terms are those with a scaling proportional to $1/\lambda^4$, that agree with the full expression in [62].

The evaluation of the cut-diagram amplitudes was carried out in a very similar way to the single emission examples shown in Sec. 5.2.2. The general method can be described by the following steps:

1. Write down the amplitude for the cut diagram using the cutting rules.

2. Expand the numerator algebra then apply the kinematic mapping.

3. Apply the kernel-appropriate partitioning factor to denominator.

4. Apply the appropriate collinear scaling to the numerator and expand to leading order.

5. Map the invariants and cancel possible terms between numerator and denominator.

To complete the splitting function the non-abelian terms also have to be determined. The diagram above now contributes its non-abelian terms and the other diagrams are those arising

from the known self-energy topologies, given in Fig. B.1, containing a triple gluon vertex, that are illustrated below:

$$= \left(\frac{8\pi\alpha_S}{\hat{\alpha}S_{i12}} \mu^{2\varepsilon} \right)^2 C_A C_F \langle \hat{P}_{ggq}^{(\mathrm{nab})} \rangle \hat{\not{p}}_i + \mathcal{O}\left(\frac{1}{\lambda^3} \right) \,, \tag{7.9}$$

where the non-abelian part of the splitting function is given by:

$$
\begin{aligned}
\langle \hat{P}_{ggq}^{(\mathrm{nab})} \rangle = \Bigg\{ & (1-\epsilon)\left(\frac{t_{12,i}^2}{4S_{12}^2} - \frac{\epsilon}{2} + \frac{1}{4} \right) + \frac{S_{i12}}{2S_{12}} \left(\frac{(1-\epsilon)\left(\alpha_{i2}\left(\alpha_{i2}^2 - 2\alpha_{i2} + 2\right) - \alpha_{i1}\left(\alpha_{i1}^2 - 6\alpha_{i1} + 6\right)\right)}{\alpha_{i1}(\alpha_{i1} + \alpha_{i2})} \right. \\
& + \frac{2\epsilon((1 - \alpha_{i1} - \alpha_{i2})(\alpha_{i2} - 2\alpha_{i1}) - \alpha_{i1})}{\alpha_{i1}(\alpha_{i1} + \alpha_{i2})} \Bigg) + \frac{S_{i12}}{2S_{i2}} \left[(1 - \alpha_{i1})\epsilon \left(\frac{\alpha_{i2}^2 + \alpha_{i1}^2}{\alpha_{i1}\alpha_{i2}} - \epsilon \right) \right. \\
& - \frac{(1 - \alpha_{i2})(1 - \alpha_{i1} - \alpha_{i2}) + (1 - \alpha_{i1})^3}{\alpha_{i1}\alpha_{i2}} + \frac{(1 - \epsilon)\left((1 - \alpha_{i1})^3 - \alpha_{i1} + (1 - \alpha_{i1} - \alpha_{i2})^2\right)}{\alpha_{i1}(\alpha_{i1} + \alpha_{i2})} \\
& - \epsilon \left(-\alpha_{i2} + \frac{2(1 - \alpha_{i1})(\alpha_{i1} - (1 - \alpha_{i1} - \alpha_{i2}))}{\alpha_{i1}(\alpha_{i1} + \alpha_{i2})} + \alpha_{i1} \right) \Bigg] \\
& + \frac{S_{i12}^2}{2S_{12}S_{i2}} \left(\frac{\alpha_{i1}^2(1 - \epsilon) + 2(1 - \alpha_{i1})}{\alpha_{i1} + \alpha_{i2}} + \frac{(\alpha_{i1} + \alpha_{i2})^2(1 - \epsilon) + 2(1 - \alpha_{i1} - \alpha_{i2})}{\alpha_{i1}} \right) \\
& - \frac{S_{i12}^2}{4S_{i2}S_{i1}}(1 - \alpha_{i1} - \alpha_{i2}) \left(\frac{(\alpha_{i1} + \alpha_{i2})^2(1 - \epsilon) + 2(1 - \alpha_{i1} - \alpha_{i2})}{\alpha_{i1}\alpha_{i2}} + (1 - \epsilon)\epsilon \right) \Bigg\} \\
& + (1 \leftrightarrow 2) \,,
\end{aligned}
\tag{7.10}
$$

and:

$$t_{12,i} \equiv 2\frac{\alpha_{i2}S_{i1} - \alpha_{i1}S_{i2}}{\alpha_{i1} + \alpha_{i2}} + \frac{\alpha_{i2} - \alpha_{i1}}{\alpha_{i1} + \alpha_{i2}}S_{12} \,. \tag{7.11}$$

The same steps as before were applied to these amplitudes and the result in the collinear limit agrees with the non-abelian terms in the expression derived by Catani-Grazzini (CG) [62]. The expressions given here are equivalent to those from CG when the following substitutions are used:

$$
\begin{aligned}
\alpha_{i1} &= z_2 \,, & \alpha_{i2} &= z_1 \,, & \alpha_{i1} + \alpha_{i2} &= 1 - z_3 \,, \\
S_{i12} &= s_{123} \,, & S_{i2} &= s_{13} \,, & S_{i1} &= s_{23} \,.
\end{aligned}
\tag{7.12}
$$

This result verifies that the kinematic mapping developed has the correct behaviour in the collinear limit, as well as being able to describe other singular behaviour. What is now useful to examine is the relationship between the two-emission splitting function and the double-soft and soft-collinear functions, as full understanding of these functions is needed to subtract IR singularities.

7.3. Comparison of IR Limits

Having focused on the collinear limit in the previous section, in this section the double-soft and soft-collinear limits and the relations between the different limits will be looked at in detail. As was discussed in Sec. 4.2, to calculate higher-order cross sections it is necessary to construct a counter term that contains the singular behaviour of the real part of the cross section. The singular behaviour includes all possible IR limits, *i.e.* soft, collinear and soft-collinear, these need to be understood to construct the counter term. The splitting functions that factorise in the collinear limit also contain soft terms and so it is necessary to look at the soft limit to determine the purely soft and purely collinear terms.

In this section a comparison is made of the terms from the splitting function in both the double-soft and the soft-collinear limits with the double-soft and soft-collinear functions. This comparison gives valuable information about how these terms can be used in a subtraction scheme. There is an extended discussion of the double-soft and soft-collinear functions in [62], that is the basis for most of the following discussion.

The results in Sec. 7.2 reproduce the spin-averaged splitting function, $\langle \hat{P}_{g_1 g_2 q_3} \rangle$, where the momenta are labelled as, $p_3 = q_i$, $p_1 = q_2$ and $p_2 = q_1$ in relation to the diagrams and mapping given in the previous sections. The kinematic parametrisation of the momenta used by CG is as follows:

$$p_i = x_i p - \frac{k_{\perp i}^2}{2n \cdot p x_i} n + k_{\perp i} , \qquad z_i = \frac{x_i}{\sum_j x_j} = \frac{n \cdot q_i}{\sum_j n \cdot q_j} .$$
(7.13)

For this mapping in the collinear limit the momenta p_i can be approximated by $p_i \to x_i p$. The relations between the variables used here and those from Eq. (7.1) are given below, as well as the relations between the invariants that will be used to describe the IR functions:

$$\begin{aligned}
z_1 &= \alpha_{i2} , & z_2 &= \alpha_{i1} , & z_3 &= 1 - \alpha_{i1} - \alpha_{i2} , \\
s_{123} &= S_{i12} , & s_{13} &= S_{i2} , & s_{23} &= S_{i1} ,
\end{aligned}$$
(7.14)

where $s_{ij} = (p_i + p_j)^2$. These variables are used to allow a direct comparison to the expressions given in [62], where the factorisation in each of the limits of interest is shown. The aim in this section is to show the connection between the terms that factorise in the different limits and how they can be combined to give terms that are singular in only one limit.

7.3.1. Double-Soft Limit

In both the soft and soft-collinear cases the emissions factorise from the amplitude and the terms that factorise are described by the soft and soft-collinear currents respectively. At the single-emission level the soft current consists of an eikonal function. For two emissions the factorisation is more complicated, as there is a double-eikonal term and a more complicated double-soft function, which together give the soft current. For a generic squared amplitude, where the soft gluons have momenta q_1 and q_2, the factorised terms are described by the square of the two-gluon soft current, that is given by:

$$[J_{\mu\rho}^{a_1 a_2}(q_1, q_2)]^\dagger d^{\mu\nu}(q_1) d^{\rho\sigma}(q_2) J_{\nu\sigma}^{a_1 a_2}(q_1, q_2) = \frac{1}{2} \{\mathbf{J}^2(q_1), \mathbf{J}^2(q_2)\}$$
$$- C_A \sum_{i,j=1}^n \mathbf{T}_i \cdot \mathbf{T}_j \, \mathcal{S}_{ij}(q_1, q_2) + ...$$
(7.15)

Here a_1 and a_2 are the colour indices of the two soft gluons and the lower indices of J are the corresponding spin indices. The '...' refers to terms that are proportional to the total colour

charge and do not contribute in the factorised case. It can also be seen that the second term on the right-hand side is purely non-abelian and that in the abelian case only the first term contributes. The two-gluon soft function is given by:

$$\mathcal{S}_{ij}(q_1, q_2) = 2\Bigg(\frac{1}{s_{12}s_{13}} \frac{n \cdot q_3(n \cdot q_1 + 2n \cdot q_2)}{n \cdot q_2(n \cdot q_1 + n \cdot q_2)} - \frac{1}{s_{13}s_{23}} \frac{(n \cdot q_3)^2}{2n \cdot q_1 n \cdot q_2}$$
$$+ \frac{1}{(n \cdot q_1 + n \cdot q_2)(s_{13} + s_{23})} \left[\frac{1}{s_{12}} \frac{n \cdot q_3(n \cdot q_1 - 3n \cdot q_2)}{n \cdot q_2} - \frac{1}{s_{13}} \frac{(n \cdot q_3)^2}{n \cdot q_1} \right]$$
$$+ \frac{1}{s_{12}^2} \frac{(1-\epsilon)((n \cdot q_1 s_{23} - n \cdot q_2 s_{13})^2 + n \cdot q_1 n \cdot q_2(s_{13} + s_{23})^2 + s_{13}s_{23}(n \cdot q_1 + n \cdot q_2)^2)}{(n \cdot q_1 + n \cdot q_2)^2(s_{13} + s_{23})^2} \Bigg)$$
$$+ (1 \leftrightarrow 2) \ . \tag{7.16}$$

The changes made with respect to the expression given in [62] are that $q_i = q_3$ *i.e.* the quark momentum, and the j direction has been relabelled as n to allow for direct comparison with the splitting function. Additionally, the colour factor for the two-gluon soft function is determined by summing over j, setting $j = n$ and applying colour conservation gives:

$$- C_A \sum_{i,j=1}^{n} \mathbf{T}_i \cdot \mathbf{T}_j = C_F C_A \ . \tag{7.17}$$

To look at the double-soft behaviour of the splitting function the scaling of the invariants in the double-soft case needs to be established and applied to the splitting function. From the two-gluon double-soft factorisation it is expected that the abelian part of the splitting function will reproduce the double-eikonal and the non-abelian part will give the two-gluon soft function $\mathcal{S}_{ij}(q_1, q_2)$. Given that in the soft limit $\lambda \to 0$, the mapping invariants scale as follows:

$$s_{12} \to \lambda^2 s_{12}, \qquad\qquad\qquad s_{13}, s_{23} \to \lambda s_{13}, \lambda s_{23} \ ,$$
$$s_{123} \to (\lambda^2 s_{12} + \lambda s_{13} + \lambda s_{23}) \ , \qquad n \cdot p_1, n \cdot p_2 \to \lambda n \cdot p_1, \lambda n \cdot p_2 \ . \tag{7.18}$$

Applying this scaling to the abelian and non-abelian parts of the splitting function separately and only keeping the leading terms gives:

$$\langle \hat{P}_{g_1 g_2 q_3}^{(ab)} \rangle \Big|_{SS} = \frac{(n \cdot q_3)^2(s_{13} + 3s_{23})}{n \cdot q_1 n \cdot q_2 s_{13} s_{23}(s_{13} + s_{23})} + (1 \leftrightarrow 2) = \frac{4(n \cdot q_3)^2}{n \cdot q_1 n \cdot q_2 s_{13} s_{23}} \ ,$$
$$\langle \hat{P}_{g_1 g_2 q_3}^{(nab)} \rangle \Big|_{SS} = \frac{1}{s_{12}s_{13}} \frac{n \cdot q_3(n \cdot q_1 + 2n \cdot q_2)}{n \cdot q_2(n \cdot q_1 + n \cdot q_2)} - \frac{1}{s_{13}s_{23}} \frac{(n \cdot q_3)^2}{2n \cdot q_1 n \cdot q_2}$$
$$+ \frac{1}{(n \cdot q_1 + n \cdot q_2)(s_{13} + s_{23})} \left[\frac{1}{s_{12}} \frac{n \cdot q_3(n \cdot q_1 - 3n \cdot q_2)}{n \cdot q_2} - \frac{1}{s_{13}} \frac{(n \cdot q_3)^2}{n \cdot q_1} \right]$$
$$+ \frac{1}{(s_{13} + s_{23})^2} \left[\frac{1}{s_{12}^2} \frac{(1-\epsilon)(n \cdot q_1 s_{23} - n \cdot q_2 s_{13})^2}{(n \cdot q_1 + n \cdot q_2)^2} \right] + (1 \leftrightarrow 2) \ , \tag{7.19}$$

where SS indicates that the behaviour is evaluated in the double-soft limit. The abelian part of the splitting function gives an eikonal, as expected. Once colour conservation is considered, all terms from $\langle \hat{P}_{g_1 g_2 q_3}^{(nab)} \rangle \Big|_{SS}$ agree with those in $\mathcal{S}_{ij}$, as the sum over i and j causes the additional terms in the soft function to vanish. This agreement illustrates the overlap between the soft and collinear limits, that is important to be aware of when constructing subtraction terms. However, there is another possible overlap with the soft-collinear limit, which now also needs to be examined.

7.3.2. Soft-Collinear Limit

The aim here is to compare the two-emission splitting function, for the emission of two collinear gluons from a quark, to the corresponding soft-collinear case of one soft gluon and one collinear gluon. This can however be formulated more generally for any amplitude with a soft gluon and two collinear partons. For a generic squared amplitude, with a soft gluon, q, and collinear partons p_1 and p_2, the soft-collinear factorisation can be described by the following, as given in [62]:

$$
\begin{aligned}
&|\mathcal{M}_{g,a_1,a_2,...,a_n}(q,p_1,p_2,...,p_n)|^2 \\
&\simeq -\frac{2}{s_{12}}(4\pi\mu^{2\epsilon}\alpha_s)^2 \langle\mathcal{M}_{a,...,a_n}(p,...,p_n)| \hat{\mathbf{P}}_{a_1,a_2}[\mathbf{J}^\dagger_{(12)\mu}(q)\mathbf{J}^\mu_{(12)}(q)] |\mathcal{M}_{a,...,a_n}(p,...,p_n)\rangle ,
\end{aligned}
$$
(7.20)

where on the right hand side the collinear partons a_1 and a_2 are replaced by a parent parton a. The terms that factorise are the soft current, $\mathbf{J}^\mu_{(12)}(q)$, and the single-emission splitting function for the collinear partons, $\hat{\mathbf{P}}_{a_1,a_2}$. The terms arising from the soft-current squared that are relevant in this case, are those that are collinear singular, namely:

$$
\mathbf{J}^\dagger_{(12)\mu}(q)\mathbf{J}^\mu_{(12)}(q) \simeq \sum_{i,j=3}^n \mathbf{T}_i \cdot \mathbf{T}_j\, \mathcal{S}_{ij}(q) + 2\sum_{i=3}^n \mathbf{T}_i \cdot \mathbf{T}_{(12)}\mathcal{S}_{i(12)}(q) ,
$$
(7.21)

where $\mathcal{S}_{ij}(q) = 2s_{ij}/(s_{iq}s_{jq})$ and $\mathcal{S}_{i(12)}(q)$ is the corresponding eikonal for the sum of momenta p_1 and p_2 and some other momentum p_i. The full form of this function is given, with some relabelling of the notation above, where here q_1 is soft and q_2 and q_3 are collinear for comparison to the splitting functions:

$$
\begin{aligned}
&\frac{1}{s_{23}}\hat{\mathbf{P}}_{q_3g_2}(z_3)[\mathbf{J}^\dagger_{(23)\mu}(q_1)\mathbf{J}^\mu_{(23)}(q_1)] \\
&= \frac{1}{s_{23}}\hat{\mathbf{P}}_{q_3g_2}(z_3)\left(C_F\mathcal{S}_{n(23)}(q_1) + \frac{C_A}{2}\mathcal{S}_{n2}(q_1) + (C_F - \frac{C_A}{2})\mathcal{S}_{n3}(q_1)\right) \\
&= \frac{\left((n\cdot q_2)^2(1-\epsilon) + 2(n\cdot q_3)^2 + 2n\cdot q_2 n\cdot q_3\right)}{s_{12}s_{13}s_{23}n\cdot q_1 n\cdot q_2(n\cdot q_2 + n\cdot q_3)(s_{12} + s_{13})}[-C_FC_A(s_{12} + s_{13})(n\cdot q_3 s_{12} - n\cdot q_2 s_{13}) \\
&\quad + 2C_F^2 s_{12}(n\cdot q_2 s_{13} + n\cdot q_3(s_{12} + 2s_{13}))] .
\end{aligned}
$$
(7.22)

The single-emission splitting function as a function of z_3 has been rewritten using the expression in terms of n invariants, where q_1 does not contribute because it is the soft momentum, $z_3 = n\cdot q_3/(n\cdot q_2 + n\cdot q_3)$. The next step is to apply the soft-collinear limit to the splitting function to enable a comparison to the soft-collinear factorisation function. The mapping invariants have the following scaling for the limit where q_1 is soft and q_2 and q_3 are collinear:

$$
\begin{aligned}
s_{12}, s_{13} &\to \lambda s_{12}, \lambda s_{13} , \qquad s_{23} \to \lambda^2 s_{23} , \\
n\cdot q_1 &\to \lambda n\cdot q_1 .
\end{aligned}
$$
(7.23)

The scaling given above is then applied to the full two-emission splitting function for two emitted gluons, and results in the following expression:

$$
\begin{aligned}
\langle\hat{P}_{g_1g_2g_3}\rangle\Big|_{S_1C_{23}} &= \frac{\left((n\cdot q_2)^2(1-\epsilon) + 2(n\cdot q_3)^2 + 2n\cdot q_2 n\cdot q_3\right)}{2s_{12}s_{13}s_{23}n\cdot q_1 n\cdot q_2(n\cdot q_2 + n\cdot q_3)(s_{12} + s_{13})} \\
&\quad \times \Big[-C_FC_A(s_{12} + s_{13})(n\cdot q_3 s_{12} - n\cdot q_2 s_{13}) \\
&\quad + 2C_F^2 s_{12}(n\cdot q_2 s_{13} + n\cdot q_3(s_{12} + 2s_{13}))\Big] .
\end{aligned}
$$
(7.24)

This result agrees with the expression from the factorisation formula above, when the relevant momenta are used. The difference of a factor of two is due to differences in the full expressions for the collinear and soft-collinear factorised amplitudes.

7.3.3. Subtraction

The importance of showing the overlap between the collinear splitting function and the double-soft and soft-collinear functions is to facilitate the construction of a subtraction scheme for the singularities arising from these limits. For the two-emission case this would correspond to NNLO subtraction. As an example of how this would function at NNLO, the principles can be explained for the NLO case, where the expressions are more manageable. The dipole subtraction scheme for NLO, from [15], is discussed in Sec. 4.2.

For the subtraction of soft singularities at NNLO the full soft current given in Eq. (7.15) can be used, when combined with the partitioning to ensure the correct singularities are subtracted. The single-emission soft current for a soft gluon with momentum q_1 emitted from a quark with momentum q_2 is the eikonal, $\mathcal{S}_{n2}(q_1)$. To extract the pure collinear part of the single-emission splitting function, the soft eikonal is subtracted from the splitting function times the leading singular denominator as illustrated here:

$$\frac{P_{q_2 g_1}}{s_{12}} - C_F \mathcal{S}_{n2}(q_1) = \frac{C_F n \cdot q_1 (1 - \epsilon)}{(n \cdot q_1 + n \cdot q_2) s_{12}} \ . \tag{7.25}$$

The result here on the right-hand side no longer contains a leading soft singularity, *i.e.* scaling of $\mathcal{O}(1/\lambda^2)$, for the soft limit, where momentum $q_1 \to \lambda q_1$ and $\lambda \to 0$. What remains are terms describing the collinear limit that therefore contain only collinear leading singularities.

This same process can be repeated to extract the purely soft part from the exchange diagrams, when working with a light-cone gauge. Since in this gauge the self-energy diagrams are used to determine the splitting function, the pure soft behaviour must come from the exchange diagrams. The splitting function evaluated in the soft limit is subtracted from the soft-singular terms from the exchange diagram for a gluon emission from a quark with a quark spectator. The resulting terms are:

$$|\mathcal{M}_{g_1 q_i q_r}|^2\big|_{S_1} - C_F \mathcal{S}_{n2}(q_1) = C_F \left[\frac{(q_2 \cdot q_r)}{(q_1 \cdot q_r)(q_1 \cdot q_2)} + \frac{n \cdot q_r}{(q_r \cdot q_1)(n \cdot q_1)} \right] \ , \tag{7.26}$$

where the eikonal $\mathcal{S}_{n2}(q_1)$ corresponds to the soft part of the single-emission splitting function. By considering the splitting function, where momentum q_r is the emitter and taking the soft limit of this, there is another eikonal produced that can be used to subtract the second term on the right-hand side above, *i.e.* $\mathcal{S}_{nr}(q_1)$. This leaves only the eikonal term without the n vector, which corresponds to the metric terms from the exchange diagrams.

A test of the subtractions for the two-emission case was carried out in Mathematica using the results for the two-gluon-emission splitting function. From this process the pure double-soft, soft-collinear and collinear terms can be obtained. The system of subtraction for the two-emission case can be summarised by the following expressions:

$$\begin{aligned}
\mathbb{C}_{jk} &= C_j C_k - S_j S_k\big|_{j+k \text{ coll.}} \ , \\
\mathbb{SC}_{jk} &= S_j C_k + S_j S_k\big|_{j \text{ coll.}} \ , \\
\mathbb{CS}_{jk} &= S_k C_j + S_j S_k\big|_{k \text{ coll.}} \ , \\
\mathbb{S}_{jk} &= S_j S_k - S_j S_k\big|_{j \text{ coll.}} - S_j S_k\big|_{k \text{ coll.}} + S_j S_k\big|_{j+k \text{ coll.}} \ ,
\end{aligned} \tag{7.27}$$

where each line refers to the pure behaviour of two emissions in the triple-collinear, soft-collinear or double-soft limits. $\mathbb{C}_{jk}$ contains the purely collinear terms for the case where the emissions j and k are collinear and $\mathbb{S}_{jk}$ contains the terms for the double-soft limit where j and k are soft. The $\mathbb{SC}$ and $\mathbb{CS}$ terms describe the soft-collinear limit for the two different combinations, j soft and k collinear or j collinear and k soft. The short-hands CC, SS

and *SC* refer to the factorising functions in the triple-collinear, double-soft and soft-collinear limits respectively and the subscripts show which momenta are soft or collinear in each case. The full expressions for the factorising functions in the different limits for the *ggq* case, *i.e.* two gluon emissions from a quark, are given in App. D.

7.4. Conclusions from the Two-Emission Case

This formalism has the potential to be built into a subtraction scheme. There is already a multitude of subtraction schemes available at NNLO, what would be different in this case is the additional information available from an amplitude-level calculation. The treatment of colour correlations is one area in which this approach can improve on that of existing approaches. Additionally, this approach can provide smooth phase-space coverage by including both soft and collinear singularities in the same framework. The work shown here and in Chapter 6 is part of a collaborative effort to develop a formalism for multi-emission kernels at the amplitude level, given in [75]. These kernels are designed to encompass all IR limits within one framework and use QCD amplitudes to allow full-colour evolution to be accessed.

Implementation of this mapping and associated formalism in the context of a parton shower is also of interest. Such an approach, where the soft and collinear singular terms can be factorised at the amplitude level, can be combined with the parton-branching algorithm introduced in [70]. There is also the possibility to implement this mapping in existing showers, although this does restrict the performance due to the use of an existing showering algorithm. An MC implementation of the kinematic mapping, for one emission, in the Herwig dipole shower is shown in the next chapter.

Herwig Implementation

The previous chapters have focused on the development and testing of a kinematic mapping, given in Sec. 6.4, that distributes recoil across all partons in the final state via a Lorentz transformation. To test the performance of this mapping in comparison to the currently available parton showers, it had to be implemented within an MC event generator, in this case Herwig 7. Firstly, the current dipole shower in Herwig is introduced in Sec. 8.1 and the kinematic mapping used is given in Eq. (8.2). Then the multi-emission mapping from Eq. (6.22) is illustrated for the one-emission case in Sec. 8.2, as is suitable for implementation in the parton shower code.

Two other mappings are included in the analysis for comparison, inspired by work from [72], that are closely linked and are essentially only distinguishable by the inclusion of the parameter y'. This parameter takes the value of 1 to give the minimally-modified mapping 'Minmod', or can be set to $y' = y$ to give a mapping which has the same structure as the PanGlobal mapping from [68]. These two mappings are introduced in Sec. 8.3.

Then in Sec. 8.4 the implementation of these new mappings in the Herwig dipole shower is described. To compare the mappings, the implementation was then tested in two analyses, one at the parton level and one at the cluster level. These analyses are introduced in Sec. 8.5 and some first results are shown. The conclusions of the analyses and implementation are given in Sec. 8.6, with a discussion of potential improvements and suggestions for future work.

8.1. Herwig Dipole Shower

The default shower in Herwig is the angular-ordered shower, although it also contains a dipole shower, from [60], which was introduced in Sec. 4.4. The dipole shower is ordered in transverse momentum given by:

$$p_\perp^2 = \frac{2p_i \cdot q q \cdot p_k}{p_i p_k} \ , \tag{8.1}$$

for a gluon emission with momentum q from the dipole (i, k). This ordering reproduces multiple soft, strongly-ordered gluon emissions in the most probable way as defined by the eikonal approximation.

Since the mapping that was developed in previous chapters is in the context of massless final-state radiation, the description here focuses on the massless F-F dipole where both emitter and emission are in the final state. The kinematic mapping used in the dipole shower for final state radiation, which describes the splitting $(p_i, p_r) \rightarrow (q_i, k_{i1}, q_r)$, is:

$$q_i = zp_i + y(1-z)p_r + k_\perp \, , \tag{8.2a}$$

$$k_{i1} = (1-z)p_i + yz \, p_r - k_\perp \, , \tag{8.2b}$$

$$q_r = (1-y)p_r \, , \tag{8.2c}$$

where the emitter, emission and spectator correspond to q_i, k_{i1}, q_r respectively. The transverse component $k_\perp$ is defined so that $k_\perp \cdot p_i = k_\perp \cdot p_r = 0$ and $k_\perp^2 = -p_\perp^2$. The expression for $p_\perp$ in Eq. (8.1), can then be written using the equivalent notation from Eq. (8.2) for the momenta before emission, p_i, p_r, and the emission momentum, k_{i1}. In this case, $\{p_i, p_r\}$ and $\{q_i, k_{i1}, q_r\}$ are on-shell momenta which results in the following expression for y:

$$k_\perp^2 = -2p_i \cdot p_r(1-z)yz \, ,$$
$$y = -\frac{k_\perp^2}{2p_i \cdot p_r z(1-z)} \, . \tag{8.3}$$

From [60], y and z are defined as:

$$y = \frac{p_\perp^2}{z(1-z)s_{ij}} \, , \qquad z = \frac{p_j \cdot q_i}{p_i \cdot p_j} \, , \tag{8.4}$$

which agrees with the expression for y in Eq. (8.3) when $s_{ij} = 2p_i \cdot p_r$. The recoil from the emission is balanced locally within the dipole after each emission, which also means that after each emission all momenta can be put on-shell.

8.2. Multiple Emission Mapping

For implementation in the Herwig dipole-shower infrastructure a mapping for one emission must be used and then iterated via the parton-shower algorithm to produce multiple emissions. The mapping given in Eq. (6.22) is defined for an arbitrary number of emissions, however, it can be written for the one emission case as:

$$q_i = \frac{1}{\hat{\alpha}}\Lambda\left[(1-\alpha_{i1})\,p_i + \left(y_i - (1-\alpha_{i1})\beta_{i1}\right)n_i - \sqrt{1-\alpha_{i1}}\sqrt{\alpha_{i1}\beta_{i1}}n_{\perp,1}^{(i)}\right] \, , \tag{8.5a}$$

$$k_{i1} = \frac{1}{\hat{\alpha}}\Lambda\left[\alpha_{i1}p_i + (1-\alpha_{i1})\beta_{i1}\,n_i + \sqrt{1-\alpha_{i1}}\sqrt{\alpha_{i1}\beta_{i1}}n_{\perp,1}^{(i)}\right] \, , \tag{8.5b}$$

$$q_r = \frac{1}{\hat{\alpha}}\Lambda p_r. \tag{8.5c}$$

where the momenta, $q_i, k_{i1}, q_r, p_i, p_r$ and n_i are on-shell and as before q_i, k_{i1}, q_r correspond to the emitter, emission and spectator. For this case the variable $\beta_{i1} = y_i$ which arises from the on-shell conditions, and α_{i1} is equivalent to $(1-z)$ used in the Herwig code. Solving the mapped expression for $k_{i1}^2 = 0$ gives:

$$(n_{\perp,1}^{(i)})^2 = -2p_i \cdot n_i \, ,$$
$$y_i = -\frac{k_\perp^2}{2p_i \cdot n_i z(1-z)} \, , \tag{8.6}$$

where, $z = (1 - \alpha_{i1})$ and $k_\perp = \sqrt{y_i z (1 - z)} n_{\perp,1}^{(i)}$. The Lorentz transformation is the same as defined in Eq. (6.27), and can be written for the single emission case, where $N = y_i n_i$ and $N^2 = 0$, as:

$$
\Lambda^\mu{}_\nu = g^\mu{}_\nu - \frac{(y_i n_i^\mu + Q^\mu)(y_i n_{i\nu} + (\hat{\alpha} + 1)Q_\nu) + \hat{\alpha}^2 Q^\mu Q_\nu}{(\hat{\alpha} + 2)y_i n_i \cdot Q + (\hat{\alpha} + 1)Q^2}
$$
$$
+ \frac{\hat{\alpha} Q^\mu (y_i n_{i\nu} + Q_\nu)(2(\hat{\alpha} + 1)y_i n_i \cdot Q + (2\hat{\alpha} + 1)Q^2)}{(2y_i n_i \cdot Q + Q^2)((\hat{\alpha} + 2)y_i n_i \cdot Q + (\hat{\alpha} + 1)Q^2)} \; ,
\tag{8.7}
$$

and for this case it can also be shown that $\hat{\alpha} = \sqrt{1 + y_i}$. The expression used for n_i is:

$$
n_i = Q - \frac{Q^2}{2p_i \cdot Q} p_i \; ,
\tag{8.8}
$$

as in Sec. 6.4. The z variable can be used for this mapping in the same way as for the mapping already implemented in Herwig. However, it can be seen above that the expression for y_i is not the same as the definition in Eq. (8.3), and so y has to be defined separately for this mapping. The Lorentz transformation expression is also important for the method to apply the recoil to the momenta.

8.3. Minimally Modified Mapping

Here, the framework for the minimally modified mapping is given, that originates from the shower developed in [72]. This is a dipole shower that combines components of existing dipole and angular ordered showers. Two different versions of the mapping are implemented for the values of $y' = 1$ or $y' = y$. Both versions of the mapping are defined in the massless limit, where q_i is the emitter, k_{i1} is the emission and q_r and q_l are spectators:

$$
q_i = \kappa \Lambda z p_i,
\tag{8.9a}
$$
$$
k_{i1} = \kappa \Lambda ((1 - z) p_i + (1 - y) p_r \pm k_\perp),
\tag{8.9b}
$$
$$
q_r = \kappa \Lambda y' p_r,
\tag{8.9c}
$$
$$
q_l = \kappa \Lambda p_r \quad \forall l \in \text{event} \mid l \neq i, r.
\tag{8.9d}
$$

The sign of $k_\perp$ is an arbitrary choice and is chosen to be minus for this implementation as this agrees with the Herwig dipole-shower mapping. The total momentum in the lab frame is defined as:

$$
Q = \sum_{\forall l \in \text{event}} p_l \; ,
\tag{8.10}
$$

and the total momentum in the dipole frame is given by:

$$
T = Q \pm k_\perp + (1 - y) p_r - (1 - y') p_r \; .
\tag{8.11}
$$

The Lorentz transformation is constructed to conserve momentum in both the dipole and lab frames as:

$$
\kappa \Lambda^\mu{}_\nu T^\nu = Q^\mu \; ,
\tag{8.12}
$$

where κ is a scaling parameter. Momentum conservation requires that the Lorentz transformation takes the form:

$$
\Lambda^\mu{}_\nu = g^\mu{}_\nu + \frac{2\kappa Q^\mu T_\nu}{Q^2} - \frac{2(Q + \kappa T)^\mu (Q + \kappa T)_\nu}{(Q + \kappa T)^2} \approx g^\mu{}_\nu \pm \mathcal{O}(k_\perp) \; ,
\tag{8.13}
$$

which in the collinear limit gives the metric as the leading term. From squaring Eq. (8.12) the expression for κ is found to be:

$$\kappa = \sqrt{\frac{Q^2}{T^2}} \approx 1 - \mathcal{O}(k_\perp^2) \ . \tag{8.14}$$

For the case of the minimal mapping, where $y' = 1$, the requirement that the emissions k_{i1} is on-shell gives:

$$y = 1 \mp \frac{k_\perp^2}{(1-z)2p_i \cdot p_r}. \tag{8.15}$$

The other case, where $y' = y$, has the same expression for y, but the expression for T is different. Introducing the extra factor of y to a spectator parton is expected to affect the showering for hard emissions in the anti-collinear limit. This is a region of phase space that is only relevant at next-to-leading order as it is suppressed by the partitioning from the dipole. The $y' = y$, 'Pglobal' mapping is essentially an analogue of the PanGlobal mapping from [68], which is given by:

$$\bar{p}_k = a_k \tilde{p}_i + b_k \tilde{p}_j + k_\perp \ , \tag{8.16a}$$

$$\bar{p}_i = (1 - a_k)\tilde{p}_i \ , \tag{8.16b}$$

$$\bar{p}_j = (1 - b_k)\tilde{p}_j \ , \tag{8.16c}$$

where a boost is subsequently applied to the $\bar{p}_{i,j,k}$ momenta to conserve momentum. This results in the momenta p_i, p_j, p_k which are equivalent to q_i, q_r, k_{i1} from Eq. (8.9) respectively.

8.4. Implementation

Now that all of the mappings have been introduced, their implementation within the Herwig 7 parton shower can be discussed. As was shown in Sec. 8.1, Herwig contains a dipole shower based on the Catani-Seymour dipole formalism and an angular-ordered shower. The first point of comparison is the dipole shower as this is also where the mapping will be implemented. However, the angular-ordered shower is also included in final plots to show the difference between the two shower approaches.

The dipole-shower infrastructure in Herwig can treat both massive and massless dipoles, as well as all possible combinations of final and initial-state dipoles. As the formalism developed in Sec. 6 is directly applicable to final-final (FF) state dipoles, it was chosen to implement the mappings for this case. The final-final dipole kinematics, in the massless case, are defined within the class 'FFlightkinematics', where there is a defined function to carry out the kinematic mapping. To enable the user to access the different mappings, a switch first had to be included for each dipole that is accessible from the Herwig input file. The switch variable is called 'theRecoilScheme' and has a default value of 0 that corresponds to the standard Herwig dipole shower. The other mappings are associated with the following values:

- theRecoilScheme $= 1 \rightarrow$ 'Multi-emission' mapping
- theRecoilScheme $= 2 \rightarrow$ 'Minmod' mapping $y' = 1$
- theRecoilScheme $= 3 \rightarrow$ 'Pglobal' mapping $y' = y$

For each of the settings given above the relevant kinematic mapping was implemented with the corresponding expressions for y and $k_\perp$. The total momentum in the lab frame, Q had to be introduced as a new variable as well as N for the multi-emission mapping and T for the

'Minmod' and 'Pglobal' mappings, which are needed to define the Lorentz transformation. The scaling factors $\hat{\alpha}$ and κ are defined in the previous sections and these were combined with the transformation into one method. The transformation and scaling are implemented within a method called 'transform' that has the equivalent effect of:

$$\text{transform}(p) \equiv \frac{1}{\hat{\alpha}}\Lambda^{\mu}{}_{\nu}p^{\nu} \; , \tag{8.17}$$

for the multi-emission mapping. For the 'Minmod' and 'Pglobal' mappings κ replaces the $1/\hat{\alpha}$ and the corresponding expression for $\Lambda^{\mu}{}_{\nu}$ is used. There are already boosts defined within Herwig and so the same tools could be used to implement the Lorentz transformation.

As a first test of the implementation the input file was modified to only produce one massless emission and some debugging had to be carried out to ensure that there were no large momentum violations. This implementation of the different mappings can also be combined with the appropriate phase space and splitting functions, this is left to future work and will be discussed in more detail in Sec. 8.6.

8.5. Analysis

The aim here is to compare the different shower mappings at the parton and cluster level. As was shown in Sec. 8.4, the implementation focuses on the kinematic mapping and so statements can only be made based on the effect of the mapping. It is possible that the future inclusion of phase-space effects might also affect results. It would be beneficial to compare the new mappings to data although this will require more rigorous testing and a more complete shower implementation that could be carried out in the future.

All plots shown are from analyses with 100,000 events, which is sufficient for the purpose of comparing the showers to each other. To compare the showers to experimental data more events would usually be required. The generator set up used is for e^+e^- annihilation, as this provides a clean environment in terms of final state QCD radiation, and could be used to compare to LEP data. The LEP Matchbox input file, provided with the Herwig installation, was used and slightly modified for each of the analyses. In both cases the QED initial state radiation was switched off. The plots in this section are made using Rivet [76].

The abbreviations PL and CM refer to the parton-level and cluster-mass analyses respectively and the labelling of the showers used in the plots is as follows:

- Angular = Herwig angular-ordered shower
- Default = Herwig dipole shower Sec. 8.1
- Multi = multi-emission mapping Sec. 8.2
- Minmod = minimally-modified mapping Sec. 8.3, $y' = 1$
- Pglobal = analogue of PanGlobal shower Sec. 8.3, $y' = y$

The two analyses used are custom analyses to look at parton-level and cluster-level observables. The parton-level analysis should show most clearly any direct effects from the parton shower, as the simulated data at this level is the end-result of the shower.

8.5.1. Parton Level

The input file was set up for this analysis with hadronisation and decays switched off as the output from the simulation should be at the parton level. The analysis is designed for e^+e^-

to jets events and gives plots for ALEPH jet rates and event shapes. One of the most common event-shape variables, which is also IR safe, is thrust, that is defined as [77]:

$$T = \max \frac{\sum_i |\vec{p}_i \cdot \vec{n}|}{\sum_i \vec{p}_i} \ , \qquad (8.18)$$

where p_i are final-state parton momenta and n is an arbitrary unit vector. The maximum is obtained for the vector n_T which corresponds to the thrust axis and should lie in the direction of the jet formed by the momenta p_i.

Once the thrust axis has been defined it is possible to define two axes perpendicular to it. These two other axes correspond to two other variables, thrust major, T_{major}, and thrust minor, T_{minor}. The thrust major vector, n_{Ma}, is defined in the same way as the thrust vector, but with the additional condition that n_{Ma} must lie in the plane perpendicular to n_T:

$$T_{\mathrm{major}} = \max_{\vec{n}_{\mathrm{Ma}} \perp \vec{n}_T} \left(\frac{|\vec{p}_i \cdot \vec{n}_{\mathrm{Ma}}|}{\sum_i |\vec{p}_i|} \right) \ . \qquad (8.19)$$

Thrust minor is defined in the same way as the thrust major, except that the minimum instead of the maximum is taken:

$$T_{\mathrm{minor}} = \min_{\vec{n}_{\mathrm{min}} \perp \vec{n}_T} \left(\frac{|\vec{p}_i \cdot \vec{n}_{\mathrm{min}}|}{\sum_i |\vec{p}_i|} \right) \ . \qquad (8.20)$$

The plots for two event-shape variables are shown below, these are $\tau = 1 - T$ and thrust minor. $1 - T$ is used as a measure of the shape of the final state, where $\tau = 0$ describes back-to-back jets and $\tau > 0$ is a measure of how isotropic the final state is.
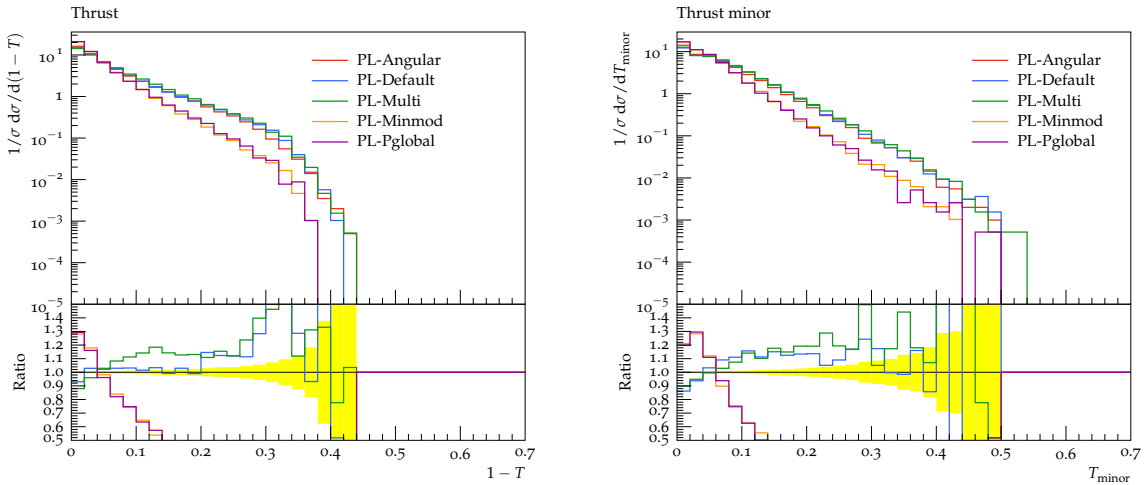

Figure 8.1.: $1 - T$ and T_{minor} for different showers from the parton-level analysis, ratio w.r.t the angular-ordered shower.

As the event simulation is set up for LEP collisions, a large number of two-jet events are expected, as is shown by the peak around zero for $1 - T$ in Fig. 8.1. The lines from the Herwig dipole and angular-ordered shower can be considered to be close to data as these are tuned to LEP data. A clear distinction can be seen in both plots between the 'Minmod' and 'Pglobal' showers and the other three showers. This is expected, because there is a clear difference in the distribution of transverse momentum for those two mappings when compared to the others, although the same branching method was used. Potentially, this indicates that there is a flaw in the implementation that could be related to the phase space or the splitting functions needing to be adjusted for these mappings. Future work will aim to investigate this discrepancy further and improve the implementation.

8.5.2. Cluster Mass

For this analysis it was necessary to go one step further with the simulation and include hadronisation. Therefore, the input-file setup for this case had just the decays switched off. This cluster-mass analysis shows the distribution of the cluster masses before and after hadronisation. This gives an indication of the mass distribution for the colour singlets coming out of the parton shower and can be used to check for pre-confinement.

Pre-confinement is derived from the basic properties of QCD and states that the mass of a colour singlet, *i.e.* cluster, is limited by a power law $\approx (M_C/Q_0)^{-4}$. Where Q_0 is the perturbative cut-off and M_C is the cluster mass. This is a result of the cluster constituents being close in momentum space and gives a peak in the cluster-mass distribution at low masses, $\mathcal{O}(1 \text{ GeV})$. As a QCD concept this was established in [34] and was discussed in the context of Herwig++ in [78]. Hard jets from different hard interactions should be colour connected when they are close in momentum space. Non-perturbative hadronisation models do not contain such correlations between jets and so a colour reconnection model has to be added to describe MPI.

The plots shown below correspond to the cluster-mass distribution before hadronisation, 'first cluster mass', and after hadronisation, 'last cluster mass'.
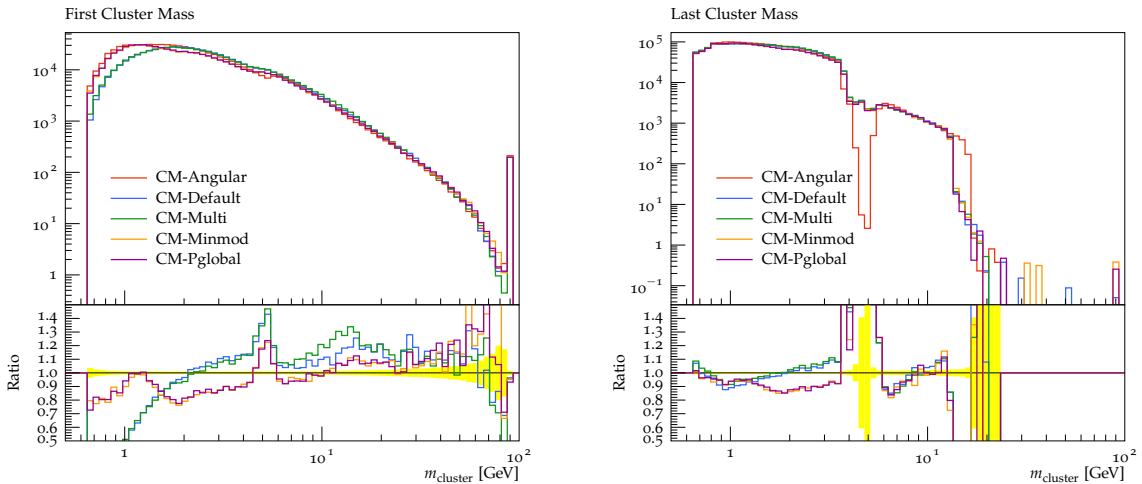

Figure 8.2.: First and last cluster-mass distributions, ratio w.r.t the angular-ordered shower.

It is already known that the initial cluster-mass spectrum should be affected by the perturbative model used in the shower and so it is expected to see a difference between the angular-ordered and dipole shower. What is interesting, in Fig. 8.2, is that the 'Minmod' and 'Pglobal' showers are closer to the behaviour of the angular ordered shower, that is usually considered to be a better description of pre-confinement. After hadronisation the mass distribution shows a higher density at lower masses, that is expected as the cluster-fission process is designed to break down heavy clusters into lighter ones. None of the dipole showers suffer from the same artefact as the angular ordered shower in the last cluster-mass distribution, which is assumed to be the result of a cut-off in the angular-ordered shower.

8.6. Conclusions from the Implementation

This Chapter has outlined three different mappings that were implemented in the Herwig dipole-shower code. This was done to compare the behaviour of these other mappings to that

of the default dipole mapping, which is based on Catani-Seymour dipole factorisation. It was also possible to compare to the angular-ordered shower to give an idea of the differences between parton-shower approaches.

The plots from the parton-level analysis show a difference between the 'Minmod' approach and the multi-emission mapping, which can largely be attributed to the different distribution of the transverse recoil. For the cluster-mass plots the 'Minmod' and 'Pglobal' mappings are in better agreement with the angular-ordered shower than the other dipole showers. This is also a better description of the cluster pre-confinement which could indicate that they result in a more physical parton evolution.

There are many possibilities to improve this implementation that will be the subject of future work. The implementation was carried out at the mapping level and uses the existing dipole-shower framework in Herwig. The first steps would be to introduce the same switch used for the different mappings into the phase-space cut-off and Jacobian. This would include the different expressions for y for each of the mappings in the shower and the corresponding Jacobian factors.

The switches for the 'Minmod' and 'Pglobal' mappings can also be used to give different expressions for the splitting functions. The mapping as given in [72], contains a dipole partitioning to conserve longitudinal momentum in the same way as an angular-ordered shower. This partitioning was not included in this implementation and could have affected the differences observed between these mappings and the others. It would be of interest to implement this in the shower as part of future work.

With the development of the CVolver code [73], which makes use of amplitude-level branching to go beyond leading colour, there is an ideal framework for the implementation of not only the multi-emission mapping but the whole formalism shown in this thesis. This would include splitting amplitudes combined with partitioning functions to give emission kernels capable of describing both soft and collinear behaviour. As was developed in previous chapters, such a formalism can be used for not only one emission but two or more emissions and so would result in a higher-order parton shower.

The NLL errors, produced by both angular-ordered and dipole showers, have been exposed in recent years and this has motivated work towards new solutions. It would also be of interest in future work to aim to describe variables shown in [68] to determine if the new mappings are NLL accurate. If such a mapping is found that is NLL accurate, then it would be of interest to include this in the Herwig dipole shower to improve the description of higher logarithmic terms. This would of course need to be fully tested and validated before being included in a future Herwig release.

Summary and Outlook

This thesis has investigated the process of IR factorisation of QCD amplitudes for more than one emission. Knowledge of IR singularities is an important component of theory predictions for the LHC and other high-energy physics experiments. The accuracy of the predictions for both signal and background effects must be improved to keep up with experimental developments. MC event generators play an important role in these predictions and the comparison of data to theory. Improved comparisons can exclude theories and give clues to guide the construction of new physics theories.

The current paradigm of MC event generators is introduced in Chapter 3, with an emphasis on the methods used in parton showers in Chapter 4. This introduces the different generator frameworks, and the differences in the parton showers and hadronisation models available. The Catani-Seymour dipole formalism is discussed in detail, because this can be used as the basis of a dipole shower, such as that in Herwig. At the end of Chapter 4, a summary is given of the logarithmic accuracy for both dipole and angular-ordered showers. The known errors for NLL accuracy are explained and some possible solutions and new methods are introduced. There are examples of ad-hoc fixes that are applied at the shower or hadronisation stage, for issues that could be better addressed by a systematic expansion within the parton shower. Such an expansion would give higher-order predictions and provide a better estimation of uncertainties.

In this thesis, a kinematic mapping and associated formalism is developed with the aim to determine an emission kernel that can describe all IR limits using one mapping. Firstly, in Chapter 5, a decomposition of the cross-section is shown and compared to the dipole formalism to illustrate which diagrams contribute to a specific kernel. The kernels are defined by a specific collinear limit, with the help of a partitioning factor, but also contain soft and soft-collinear behaviour. Then a mapping and its associated phase-space factorisation are introduced, that is based on a Sudakov decomposition and is the same as the mapping used in the Herwig dipole shower. This mapping is used to calculate the single-emission diagrams for a gluon emission from both a quark and gluon emitter. The collinear limit is taken to check the collinear behaviour of the mapping, where the splitting functions are reproduced.

Chapter 5 includes a second kinematic mapping, that introduces a Lorentz transformation to distribute the recoil from an emission across multiple final-state partons. The phase space in

this case requires detailed calculation due to the inclusion of a Lorentz transformation. This resulting expression for the factorised phase space is given, including the Jacobian factor, and is shown to be equal to the factor from the Catani-Seymour mapping in the massless limit. The behaviour of this mapping in the soft and collinear limits is discussed and it is shown that the splitting functions can again be obtained in the collinear limit.

In Chapter 6 the framework for multiple emissions is described by first extending the combinatorics from the one-emission case to the two-emission case. This is then generalised to k-emissions, that allows the possible diagrams that will contribute to the singular limits, for any number of emissions, to be identified. The decomposition of the matrix element can also be rewritten as a density-type operator, that is particularly useful for implementation in a parton-shower algorithm. To define an emission kernel for a specific collinear limit the different collinear regions need to be partitioned. The partitioning formalism is developed for an arbitrary number of emissions and checked carefully for one and two emissions, to ensure that the partitioning factors themselves do not contribute to the singular terms. To combine the partitioning with specific amplitudes it is necessary to define a kinematic mapping for k-emissions with associated phase-space factorisation. This mapping also makes use of a Lorentz transformation to distribute recoil, but introduces new parameters to describe the soft and collinear limits of each emission for multiple emitters.

To test the general mapping from Chapter 6, the two-emission case is examined in Chapter 7. First, the mapping for two emissions, both with one emitter and two emitters is defined. The one-emitter two-emissions mapping is then used to derive the two-emission splitting function for two collinear-gluon emissions from a quark. This illustrates that the mapping and partitioning formalism reproduce the correct behaviour in the collinear limit. The splitting function also contains soft and soft-collinear terms that can be extracted by taking the corresponding limits. It is of interest to compare the different terms from the splitting function to the double-soft and soft-collinear functions, that can also be determined for two gluon emissions from a quark. These different functions can be combined to determine the terms corresponding to the pure singular behaviour in each of the possible limits, and can be used to construct counter terms for NNLO subtraction.

In Chapter 8, the multi-emission mapping from Chapter 6 is implemented in Herwig 7. The Herwig dipole-shower framework is used for the implementation and a switch is included to allow the user to choose the mapping from the input file. For comparison, the analyses are run with five different shower options, the Herwig dipole and angular ordered showers, the multi-emission mapping and two versions of the minimally-modified mapping. The multi-emission and minimally-modified mappings use a Lorentz transformation to distribute recoil, that needed to be incorporated into the dipole shower code. The results of the analyses show slight variations from the standard Herwig showers, although it has to be acknowledged that the phase space has not yet been modified for the new mappings. As part of future work, the implementation could be improved to include phase-space variations and changes to the splitting kernels used.

The mapping and partitioning developed in Chapter 6 are important parts of a formalism to describe multi-emission kernels, presented in [75]. This formalism establishes a method to decompose emission amplitudes for an arbitrary number of emissions and to collect the IR singular behaviour for different collinear sectors into emission kernels. The amplitude-level approach allows access to spin and colour information, that can be used to improve the spin and colour evolution of a parton shower. The parton-branching algorithm from [70], can be readily combined with the formalism from [75] as they are both defined for emission amplitudes. Future work on the emission-kernel formalism could extend the current massless treatment to the massive case and include initial-state radiation, since the current definitions only apply to emitters and spectators in the final state.

In terms of the MC-event-generator implementation of the mapping and partitioning, shown in this thesis, there are many possible directions for future development. The current implementation in Herwig 7 can be improved by including the relevant phase-space factors and the splitting-function partitioning for the minimally-modified mapping. To include higher-order emissions in the parton shower the two-emission kernels and mapping can be implemented in the shower. This would make it possible to construct NNLO matching schemes, and give better predictions for observables that have large NNLO corrections.

It is also important to address the issues of logarithmic accuracy, shown in [66] and [67], that were discussed in Sec. 4.5. The shower presented in [72] has already been shown to be NLL accurate for some observables, but is limited by definition to leading colour. The implementation of the methods outlined in this thesis, in combination with an improved shower algorithm has the potential to give predictions at higher logarithmic accuracy and beyond leading colour. An MC code for beyond-leading-colour predictions, in the soft approximation, has been established in CVolver [73], and is still under development to include hard emissions and incoming hadrons. The combination of an amplitude-level emission-kernel formalism and the CVolver code, would allow hadron-collider observables to be simulated beyond leading colour. The resulting parton shower would be able to predict both global and non-global jet observables, with higher accuracy than currently available parton showers.

Details of Single-Emission Calculation

A.1. Single Emission, Gluon Emitter - Old Mapping

Shown here are the detailed calculations of the diagrams needed to reproduce the collinear splitting function for a gluon emission from a gluon emitter. The relevant diagrams are shown in Eq. (5.34) and Eq. (5.35). The matrix element for the gluon-exchange diagram is written down using the Feynman rules defined in Sec. 2.3.1. The exchanged gluon gives a factor of $-g_{\mu\nu}$, in a covariant gauge, from the cutting rules as explained in Sec. 2.3.3. The exchange diagram matrix-element squared can be expanded as:

$$
\begin{aligned}
|M_{g_1 g_2}^{(E)}|^2 &= (-)[-g_s f^{abc}(g^{\mu\nu}(2q_i + q)^\lambda + g^{\nu\lambda}(-q_i + q)^\mu + g^{\lambda\mu}(-q_i - 2q)^\nu)\frac{-i}{(q_i + q)^2}]_{\nu\mu} \\
&\times [\frac{i}{(q_j + q)^2}(-g_s f^{cde})(g_{\lambda\sigma}(2q + q_j)_\rho + g_{\sigma\rho}(-2q_j - q)_\lambda + g_{\rho\lambda}(q_j - q)_\sigma)]_{\rho\sigma} \\
&= \frac{-g_s^2 f^{abc} f^{cde}}{4(q_i.q)(q_j.q)}[g^{\mu\nu}(2q_i + q)^\lambda + g^{\nu\lambda}(-q_i + q)^\mu + g^{\lambda\mu}(-q_i - 2q)^\nu]_{\nu\mu} \\
&\times [g_{\lambda\sigma}(2q + q_j)_\rho + g_{\sigma\rho}(-2q_j - q)_\lambda + g_{\rho\lambda}(q_j - q)_\sigma]_{\rho\sigma} .
\end{aligned} \tag{A.1}
$$

After algebraic manipulation and implementation of the kinematic mapping, the collinear-singular terms can be extracted. Namely, those not containing any power of y because the denominator contains a factor $1/y$. The collinear-singular terms from the numerator are as follows:

$$
N_{g_1 g_2}^{(E)} = g^{\mu\nu}(p_i)_\sigma(p_i)_\rho \left(1 - z^2\right) - 2g^{\mu\nu} g_{\rho\sigma}(p_i \cdot p_j)(1 + z) . \tag{A.2}
$$

Plugging this result back into the matrix element, using the f_{abc} colour algebra given in Sec. 2.3.2 and the substitution that $q_j \cdot q = (1 - z)p_i \cdot p_j$ in the collinear limit gives:

$$
\begin{aligned}
|M_{g_1 g_2}^{(E)}|^2 &= \frac{-g_s^2(-T_i.T_j)}{4(q_i.q)(q_j.q)}[g^{\mu\nu}(p_i)_\sigma(p_i)_\rho \left(1 - z^2\right) - 2g^{\mu\nu} g_{\rho\sigma}(p_i \cdot p_j)(1 + z)] \\
&= \frac{-g_s^2(-T_i.T_j)}{4(q_i.q)} \left[g^{\mu\nu} \frac{(p_i)_\sigma(p_i)_\rho}{(p_i \cdot p_j)} \frac{(1 - z^2)}{1 - z} - 2g^{\mu\nu} g_{\rho\sigma} \frac{(1 + z)}{1 - z}\right] .
\end{aligned} \tag{A.3}
$$

In the total sum over diagrams there is a factor of two times this result, due to the conjugate diagram. The calculation of the triple-gluon vertex is dependent on the order and direction of the momentum vectors q, q_i and q_j. To account for the symmetry between the emitter and emission in this case, it is necessary to calculate the exchange diagram with q and q_i swapped, this is expected to result in the cancellation of some of the final terms found above.

$$
\begin{aligned}
|M^{(E)}_{g_2 g_1}|^2 &= (-)[-g_s f^{abc}(g^{\mu\nu}(q_i + 2q)^\lambda + g^{\nu\lambda}(q_i - q)^\mu + g^{\lambda\mu}(-2q_i - q)^\nu)\frac{-i}{(q_i + q)^2}]_{\nu\mu} \\
&\quad \times [\frac{i}{(q_j + q_i)^2}(-g_s f^{cde})(g_{\lambda\sigma}(2q_i + q_j)_\rho + g_{\sigma\rho}(-2q_j - q_i)_\lambda + g_{\rho\lambda}(q_j - q_i)_\sigma)]_{\rho\sigma} \\
&= \frac{-g_s^2 f^{abc} f^{cde}}{4(q_i.q)(q_j.q_i)}[g^{\mu\nu}(q_i + 2q)^\lambda + g^{\nu\lambda}(q_i - q)^\mu + g^{\lambda\mu}(-2q_i - q)^\nu)]_{\nu\mu} \\
&\quad \times [(g_{\lambda\sigma}(2q_i + q_j)_\rho + g_{\sigma\rho}(-2q_j - q_i)_\lambda + g_{\rho\lambda}(q_j - q_i)_\sigma)]_{\rho\sigma} \ .
\end{aligned}
\tag{A.4}
$$

After manipulating the gluon vertex terms and applying the kinematic mapping the following singular terms survive:

$$
N^{(E)}_{g_2 g_1} = g^{\mu\nu}(p_i)_\sigma (p_i)_\rho z(2 - z) + g^{\mu\nu} g_{\sigma\rho}(p_i.p_j) 2(z - 2) \ . \tag{A.5}
$$

The numerator terms in the context of the full matrix element, after using the substitution that $q_j \cdot q_i = z p_i \cdot p_j$ in the collinear limit, can be written as:

$$
\begin{aligned}
|M^{(E)}_{g_2 g_1}|^2 &= \frac{-g_s^2(-T_i.T_j)}{4(q_i.q)(q_j.q_i)}[g^{\mu\nu}(p_i)_\sigma (p_i)_\rho z(2 - z) - g^{\mu\nu} g_{\sigma\rho}(p_i.p_j) 2(2 - z)] \\
&= \frac{-g_s^2(-T_i.T_j)}{4(q_i.q)}\left[g^{\mu\nu}\frac{(p_i)_\sigma (p_i)_\rho}{(p_i \cdot p_j)}(2 - z) - 2g^{\mu\nu} g_{\sigma\rho}\frac{(2 - z)}{z}\right] \ .
\end{aligned}
\tag{A.6}
$$

The above result is the same as the q exchanged result with q and q_i swapped, that in the collinear limit is equivalent to $z \to (1 - z)$. Executing the sum over indices i and j gives a factor of C_A from colour conservation for a gluon emitter. The matrix element for the self-energy-type diagram, containing a cut gluon loop propagating clockwise, can be written down as:

$$
\begin{aligned}
|M^{(SE)}_{gg}|^2 &= [\frac{-i}{(q_i + q)^2}(-g_s f^{acg})(g^{\mu\lambda}(q_i + 2q)^\tau + g^{\lambda\tau}(q_i - q)^\mu + g^{\tau\mu}(-2q_i - q)^\lambda) \\
&\quad \times (-g_s f^{cbg})(g^{\lambda\nu}(q_i + 2q)^\tau + g^{\nu\tau}(-2q_i - q)^\lambda + g^{\tau\lambda}(q_i - q)^\nu)\frac{i}{(q_i + q)^2}]_{\nu\mu} \\
&= \frac{g_s^2 f^{cbg} f^{acg}}{4(q_i.q)^2}[(g^{\mu\lambda}(q_i + 2q)^\tau + g^{\lambda\tau}(q_i - q)^\mu + g^{\tau\mu}(-2q_i - q)^\lambda) \\
&\quad \times (g^{\lambda\nu}(q_i + 2q)^\tau + g^{\nu\tau}(-2q_i - q)^\lambda + g^{\tau\lambda}(q_i - q)^\nu)]_{\nu\mu} \ .
\end{aligned}
\tag{A.7}
$$

After simplification of the numerator algebra and using the identity, $g^{\lambda\tau} g_{\lambda\tau} = D$, where D is the number of dimensions, the numerator terms are:

$$
N^{(SE)}_{gg} = g^{\mu\nu}(8q_i \cdot q) + (D - 6)((q_i)^\nu (q_i)^\mu + (q)^\nu (q)^\mu) + (-D - 3)((q_i)^\nu (q)^\mu + (q)^\nu (q_i)^\mu)
\tag{A.8}
$$

Substituting this result back into the full amplitude gives:

$$
\begin{aligned}
|M^{(SE)}_{gg}|^2 &= \frac{g_s^2 f^{cbg} f^{acg}}{4(q_i \cdot q)^2}[g^{\mu\nu}(8q_i \cdot q) + (D - 6)((q_i)^\nu (q_i)^\mu + (q)^\nu (q)^\mu) \\
&\quad + (-D - 3)((q_i)^\nu (q)^\mu + (q)^\nu (q_i)^\mu)] \ .
\end{aligned}
\tag{A.9}
$$

At this point it is appropriate to consider the contributions from the ghost loop, which have to first be determined. The ghost-loop diagram corresponds to two separate diagrams, each with the loop propagating in a different direction, which correspond to the results for $G1$ and $G2$ shown below. Both need to be added to the gluon loop to give the correct result in a covariant gauge, such as is used here. The first ghost-loop diagram can be written as:

$$
\begin{aligned}
|M_{gg}^{(G1)}|^2 &= [\frac{i}{(q_i+q)^2}(g_s f^{bgc}(-q^\nu)(-)(g_s f^{acg} q_i^\mu)\frac{-i}{(q_i+q)^2}]_{\nu\mu} \\
&= \frac{g_s^2 f^{bgc} f^{acg}}{4(q_i.q)^2}[q^\nu q_i^\mu]_{\nu\mu} \ .
\end{aligned}
\tag{A.10}
$$

The diagram containing the ghost loop propagating in the opposite direction is given and then added to the first result to give the total contribution from the ghost loop:

$$
\begin{aligned}
|M_{gg}^{(G2)}|^2 &= \frac{g_s^2 f^{bgc} f^{acg}}{4(q_i.q)^2}[q_i^\nu q^\mu]_{\nu\mu} \ , \\
|M_{gg}^{(G)}|^2 &= |M_{gg}^{(G1)}|^2 + |M_{gg}^{(G2)}|^2 = \frac{g_s^2 f^{bgc} f^{acg}}{4(q_i.q)^2}[q^\nu q_i^\mu + q_i^\nu q^\mu]_{\nu\mu} \ .
\end{aligned}
\tag{A.11}
$$

Given that $f^{cbg} f^{acg} = -C_A \delta_{ab} = f^{bgc} f^{acg}$, it becomes clear that the pre-factors for the gluon and ghost-loop diagrams are equivalent and so the terms can be directly added. When D is considered in dimensional regularisation it can be written as $(4 - 2\epsilon)$. The total of the result from the gluon loop added to both contributions from the ghosts gives:

$$
\begin{aligned}
|M_{self}|^2 &= |M_{gg}^{(SE)}|^2 + |M_{gg}^{(G)}|^2 \\
&= \frac{-g_s^2 C_A \delta_{ab}}{4(q_i \cdot q)^2}[g^{\mu\nu}(8q_i \cdot q) + (D-6)(q_i^\nu q_i^\mu + q^\nu q^\mu) + (-D-3)(q_i^\nu q^\mu + q^\nu q_i^\mu) \\
&\quad + (q^\nu q_i^\mu + q_i^\nu q^\mu)] \\
&= \frac{g_s^2 C_A \delta_{ab}}{2(q_i.q)}[4(-g^{\mu\nu}) + (4-2D)\frac{(q_i^\nu q_i^\mu + q^\nu q^\mu)}{2(q_i.q)} + (D+2)\frac{(q_i+q)^\nu (q_i+q)^\mu}{2(q_i \cdot q)}] \\
&= \frac{16\pi\alpha_s C_A \delta_{ab}}{2(q_i.q)}[(-g^{\mu\nu}) - (1-\epsilon)\frac{(q_i^\nu q_i^\mu + q^\nu q^\mu)}{2(q_i.q)} + \frac{(3-\epsilon)}{2}\frac{(q_i+q)^\nu (q_i+q)^\mu}{2(q_i.q)}] \ .
\end{aligned}
\tag{A.12}
$$

The next step is to implement the mapping as for the exchange diagrams, where the expression can be further simplified by assuming that the momenta connected to the hard amplitude are on-shell and so any p_i^ν or p_i^μ momenta can be taken to be zero. This is a statement of transversality of the amplitude. When considering the collinear splitting function only the leading collinear-singular terms are needed *i.e.* those with a scaling of $1/\lambda^2$ in the collinear limit. In this case $(q_i+q)^\nu (q_i+q)^\mu$ term can be neglected as it maps to a term with factor y^2 and so is finite in the collinear limit. The resulting singular terms are:

$$
|M_{self}|^2 = \frac{16\pi\alpha_s C_A \delta_{ab}}{2(q_i.q)}\left((-g^{\mu\nu}) - 2(1-\epsilon)z(1-z)\frac{n_\perp^\mu n_\perp^\nu}{2(p_i.p_j)}\right) \ .
\tag{A.13}
$$

The final result shown in Eq. (5.42) is the combination of the self energy and exchange diagram results which reproduces the known collinear splitting function.

A.2. Single Emission - LT Mapping

The Lorentz transformation is designed to conserve the total momentum before and after the emissions which requires the following action:

$$
\alpha \Lambda^\mu_{\ \nu} Q^\nu = Q^\mu - y n^\mu \ ,
\tag{A.14}
$$

where α is a scaling factor. The solution which will be used here is the proper orthochronus transformation given by:

$$\Lambda^\mu{}_\nu p^\nu = \hat{p}^\mu, \qquad p^2 = \hat{p}^2 = M^2 \ ,$$

$$\Lambda^\mu{}_\nu = \eta^\mu{}_\nu - \frac{1}{M^2 + p \cdot \hat{p}}(p^\mu p_\nu + \hat{p}^\mu \hat{p}_\nu + p^\mu \hat{p}_\nu) + \frac{M^2 + 2p \cdot \hat{p}}{M^2(M^2 + p \cdot \hat{p})}\hat{p}^\mu p_\nu \ . \tag{A.15}$$

Which for $p^\nu = Q^\nu$ and $\hat{p}^\mu = (Q^\mu - yn^\mu)/\alpha$ gives:

$$\Lambda^\mu{}_\nu = \frac{yn^\mu(Q_\nu - yn_\nu) + Q^\mu(y(1+\alpha)n_\nu - (1+\alpha+\alpha^2)Q_\nu)}{\alpha(-yn \cdot Q + (1+\alpha)Q^2)}$$
$$+ \frac{(yn^\mu - Q^\mu)Q_\nu(2yn \cdot Q - (2+\alpha)Q^2)}{\alpha Q^2((1+\alpha)Q^2 - yn \cdot Q)} + \delta^\mu_\nu \ . \tag{A.16}$$

Squaring Eq. (A.14) gives in the solution $\alpha = \sqrt{1-y}$. This allows the following results to be determined in terms of p_i and Q:

$$\alpha\Lambda^\mu{}_\nu p_i^\nu = p_i^\mu \ ,$$
$$2\alpha n_\mu \Lambda^\mu{}_\nu p_i^\nu = 2p_i \cdot Q \ . \tag{A.17}$$

To investigate the mapping it is useful to determine the dot products between the momenta, where $n_{\perp,1}^2 = -2\alpha\Lambda^\mu{}_\nu p_i^\nu n_\mu$, the result above has been used to give $n_{\perp,1}^2 = -2p_i \cdot Q$. The dot products are as follows:

$$k_1 \cdot q_i = (\alpha_1 + \beta_1)yp_i \cdot Q \ ,$$

$$k_1 \cdot q_k = ((1-y)\alpha_1 - y\beta_1\frac{Q^2}{2p_i \cdot Q})p_i \cdot p_k + y\beta_1 p_k \cdot Q + \sqrt{\alpha_1\beta_1 y(1-y)}p_k \cdot n_{\perp,1} \ ,$$

$$q_i \cdot q_k = ((1-y)(1-\alpha_1) - y(1-\beta_1)\frac{Q^2}{2p_i \cdot Q})p_i \cdot p_k + y(1-\beta_1)p_k \cdot Q$$
$$- \sqrt{y(1-y)\alpha_1\beta_1} \ p_k \cdot n_{\perp,1} \ . \tag{A.18}$$

It can be shown that $\alpha_1 = 1 - \beta_1$, which is only true for the single-emission case (α_1 is comparable to $(1-z)$ in the mapping used in Sec. 5.2). This results in the following expressions:

$$k_1^\mu = (\alpha_1 - y(1-\alpha_1)\frac{Q^2}{2p_i \cdot Q})p_i^\mu + y\ (1-\alpha_1)\ Q^\mu + \sqrt{y\alpha_1(1-\alpha_1)}n_{\perp,1}^\mu \ ,$$

$$q_i^\mu = \left(1 - \alpha_1 - y\alpha_1\frac{Q^2}{2p_i \cdot Q}\right)p_i^\mu + y\alpha_1 Q^\mu - \sqrt{y\alpha_1(1-\alpha_1)}n_{\perp,1}^\mu \ ,$$

$$q_k^\mu = \alpha\Lambda^\mu{}_\nu p_k^\nu = A_1 p_i^\mu + A_2 Q^\mu + \sqrt{1-y}\ p_k^\mu \ . \tag{A.19}$$

The invariants are also redefined as:

$$k_1 \cdot q_i = yp_i \cdot Q \ ,$$

$$k_1 \cdot q_k = ((1-y)\alpha_1 - y(1-\alpha_1)\frac{Q^2}{2p_i \cdot Q})p_i \cdot p_k + y(1-\alpha_1)p_k \cdot Q$$
$$+ \sqrt{\alpha_1(1-\alpha_1)y(1-y)}p_k \cdot n_{\perp,1} \ ,$$

$$q_i \cdot q_k = ((1-y) - \alpha_1(1-y + y\frac{Q^2}{2p_i \cdot Q})p_i \cdot p_k + y\alpha_1 p_k \cdot Q$$
$$- \sqrt{\alpha_1(1-\alpha_1)y(1-y)} \ p_k \cdot n_{\perp,1} \ . \tag{A.20}$$

The collinear splitting function can be calculated using this mapping, where the calculations give results equivalent to those in Sec. 5.2.2.

A.2.1. Jacobian Calculation

Here the details are given of the calculation of the Jacobian, for the mapping used in the previous section and given in Eq. (5.45). The Jacobian is a necessary component of the phase-space factorisation. The total momentum Q is defined as $p_1 + p$, that allows Q^2 and thus n to be expressed as:

$$Q^2 = p^2 + 2p_1 \cdot p \ ,$$

$$n^\mu(p_1 + p, p_1) = p_1^\mu + p^\mu - \frac{p^2 + 2p_1 \cdot p}{2p_1 \cdot p}p_1^\mu = p^\mu - \frac{p^2}{2p_1 \cdot p}p_1^\mu \ . \tag{A.21}$$

At this stage it is useful to apply the on-shell conditions, $p^2 = \dfrac{m^2}{1-y}$ and $p_1^2 = 0$. Then q_1 and q can be written as follows:

$$q_1 = p_1 + y(p - p_1\frac{m^2}{(1-y)2p_1 \cdot p}) - k_{1,m} \ ,$$

$$q = p - y(p - p_1\frac{m^2}{(1-y)2p_1 \cdot p}) \ .$$

The emitter momentum, q_1, is set on-shell and so $q_1^2(1-y) = 0$. This can be solved to give two expressions for y, only one of which is sensible in the massless case:

$$y = -\frac{-k^2 - 2k \cdot p + 2k \cdot p_1 + \frac{m^2 k \cdot p_1}{p \cdot p_1} + 2p \cdot p_1}{4(k \cdot p - p \cdot p_1)}$$

$$-\frac{\sqrt{\left(k \cdot k + 2k \cdot p - 2k \cdot p_1 - \frac{m^2 k \cdot p_1}{p \cdot p_1} - 2p \cdot p_1\right)^2 - 8(k^2 - 2k \cdot p_1)(k \cdot p - p \cdot p_1)}}{4(k \cdot p - p \cdot p_1)} \ . \tag{A.22}$$

In the massless limit:

$$y = -\frac{k \cdot p_1}{k \cdot p - p \cdot p_1} \ . \tag{A.23}$$

The full expression for y can then be substituted into the expressions above for q_1 and q before differentiating to give the Jacobian. It is also useful to define z in terms of the dot products between the momenta:

$$z = 1 + \frac{m^2 k \cdot p_1}{2(1-y)(p \cdot p_1)^2} - \frac{k \cdot p}{p \cdot p_1} \ . \tag{A.24}$$

The above expressions for z and y can be rearranged to express the invariants as:

$$k \cdot p_1 = yz(p \cdot p_1) + \frac{k^2}{2} \ ,$$

$$k \cdot p = \frac{m^2 k^2 + 2p \cdot p_1 \left(m^2 yz + 2(1-y)(1-z)p \cdot p_1\right)}{4(1-y)p \cdot p_1} \ . \tag{A.25}$$

The phase-space limits are constrained by the term under the square root in y, that can be rewritten using the expressions for $k \cdot p_1$ and $k \cdot p$ from above:

$$\sqrt{\left(k \cdot k + 2k \cdot p - 2k \cdot p_1 - \frac{m^2 k \cdot p_1}{p \cdot p_1} - 2p \cdot p_1\right)^2 - 8(k^2 - 2k \cdot p_1)(k \cdot p - p \cdot p_1)}$$

$$= \frac{m^2 y k^2 + 2z(p \cdot p_1)\left(m^2 y^2 + 2(-1+y)^2(p \cdot p_1)\right)}{2(-1+y)(p \cdot p_1)} \ . \tag{A.26}$$

Using this expression, y can be rewritten as:

$$y = -\frac{-k^2 - 2k \cdot p + 2k \cdot p_1 + \frac{m^2 k \cdot p_1}{p \cdot p_1} + 2p \cdot p_1}{4(k \cdot p - p \cdot p_1)}$$
$$-\frac{m^2 y k^2 + 2z(p \cdot p_1)\left(m^2 y^2 + 2(-1+y)^2(p \cdot p_1)\right)}{8(-1+y)(p \cdot p_1)(k \cdot p - p \cdot p_1)} . \tag{A.27}$$

The Jacobian is defined as the determinant of the matrix of the partial derivatives of the momenta before the mapping w.r.t. the momenta after the mapping:

$$\mathcal{J} = \left| \frac{\partial(q_1, q)}{\partial(p_1, p)} \right| = \begin{vmatrix} \dfrac{\partial q_1^\mu}{\partial p_1^\nu} & \dfrac{\partial q_1^\mu}{\partial p^\nu} \\ \dfrac{\partial q^\mu}{\partial p_1^\nu} & \dfrac{\partial q^\mu}{\partial p^\nu} \end{vmatrix} .$$

As a first step in evaluating the Jacobian, the derivatives of all the dot products are defined. However, since the on-shell conditions have already been applied, the energy component can be taken out as a ratio and will be factored in later. These derivatives are w.r.t. the momentum component carrying index b:

$$\frac{\partial p \cdot p_1}{\partial p_1^b} = \frac{p^0}{p_1^0} p_{1b} - p_b ,$$
$$\frac{\partial p \cdot p_1}{\partial p^b} = \frac{p_1^0}{p^0} p_b - p_{1b} ,$$
$$\frac{\partial k \cdot p_1}{\partial p_1^b} = \frac{k^0}{p_1^0} p_{1b} - k_b ,$$
$$\frac{\partial k \cdot p}{\partial p^b} = \frac{k^0}{p^0} p_b - k_b .$$

The elements of the Jacobian are given by:

$$\frac{\partial q_1^a}{\partial p_1^b} = \delta_b^a + \frac{\partial y}{\partial p_1^b}\left(p^a - p_1^a \frac{m^2}{(1-y)2p_1 \cdot p}\right) + y\frac{\partial}{\partial p_1^b}\left(p^a - p_1^a \frac{m^2}{(1-y)2p_1 \cdot p}\right) ,$$
$$\frac{\partial q_1^a}{\partial p^b} = \frac{\partial}{\partial p^b}\left(y(p^a - p_1^a \frac{m^2}{(1-y)2p_1 \cdot p})\right) ,$$
$$\frac{\partial q^a}{\partial p_1^b} = -\frac{\partial}{\partial p_1^b}\left(y(p^a - p_1^a \frac{m^2}{(1-y)2p_1 \cdot p})\right) ,$$
$$\frac{\partial q^a}{\partial p^b} = \delta_b^a - \frac{\partial}{\partial p^b}\left(y(p^a - p_1^a \frac{m^2}{(1-y)2p_1 \cdot p})\right) .$$

To evaluate the Jacobian it is useful to work in a frame where p and p_1 are back-to-back and both have a zero transverse component:

$$p_1^\mu = \left(\frac{Q^2 - \frac{m^2}{1-y}}{2Q}, \vec{0}_\perp, \frac{Q^2 - \frac{m^2}{1-y}}{2Q}\right) ,$$
$$p^\mu = \left(\frac{Q^2 + \frac{m^2}{1-y}}{2Q}, \vec{0}_\perp, \frac{\frac{m^2}{1-y} - Q^2}{2Q}\right) . \tag{A.28}$$

In this frame the longitudinal component is denoted by the superscript l e.g. $p^l = \dfrac{Q^2 - \frac{m^2}{1-y}}{2Q}$, the following expressions can be written as:

$$2p_1 \cdot p = Q^2 - \frac{m^2}{(1-y)} \ ,$$

$$p^\mu - p_1^\mu \frac{m^2}{(1-y)Q^2 - m^2} = \left(\frac{Q}{2}, \vec{0}_\perp, \frac{-Q}{2} \right) \ ,$$

$$k \cdot p = k^0 p^0 - k^l p^l = k^0 \frac{(1-y)Q^2 + m^2}{2Q(1-y)} - k^l \frac{(1-y)Q^2 - m^2}{2Q(1-y)}$$

$$= \frac{Q}{2}(k^0 - k^l) + \frac{m^2}{2Q(1-y)}(k^0 + k^l) \ ,$$

$$k \cdot p_1 = k^0 p_1^0 - k^l p_1^l = k^0 \frac{(1-y)Q^2 - m^2}{2Q(1-y)} + k^l \frac{(1-y)Q^2 - m^2}{2Q(1-y)}$$

$$= \frac{Q}{2}(k^0 + k^l) - \frac{m^2}{2Q(1-y)}(k^0 + k^l) \ .$$

$$(\text{A.29})$$

The expressions for the dot products are then substituted into those for y and z to give frame specific definitions in terms of y, z, m^2, Q^2, k^2 and k^0 and k^l. These are then solved to give expressions for k^0 and k^l. In the massless limit of $m^2 \to 0$ and $k^2 \to 0$ these are:

$$k^0 = \frac{Q}{2}(1 - z + yz) \ ,$$

$$k^l = \frac{Q}{2}(-1 + z + yz) \ .$$

$$(\text{A.30})$$

This allows the derivatives to be written in terms of z, y, m^2, Q^2 and k^2 when considering this specific frame.

The resulting terms present in the Lagrangian all contain p^a, p_1^a or δ_b^a. This gives a zero column in the transverse-z block which allows the determinant to be reduced and the only transverse-transverse terms contributing are from δ_b^a. Expanding along the zero columns gives:

$$\mathcal{J} = \frac{p^0 p_1^0}{q^0 q_1^0}(z_{11} z_{22} - z_{21} z_{12}) \begin{vmatrix} \dfrac{m^2(1+y) - Q^2(1-y)}{m^2 - Q^2(1-y)} \mathbb{1}_\perp, & y \, \mathbb{1}_\perp \\[2mm] y \dfrac{m^2}{Q^2(1-y) - m^2} \mathbb{1}_\perp, & (1-y) \, \mathbb{1}_\perp \end{vmatrix}$$

$$= \frac{p^0 p_1^0}{q^0 q_1^0}(z_{11} z_{22} - z_{21} z_{12}) \left(\frac{m^2 - Q^2(-1+y)^2}{m^2 + Q^2(-1+y)} \right)^{d-2} \ ,$$

where the z terms are the $z - z$ components of each of the partial derivatives determined above. To determine the z terms only the longitudinal component of the momentum vectors needs to be considered e.g. $p^a \to p^l$, $\delta_b^a \to 1$. The resulting terms are multiplied and subtracted to evaluate $(z_{11} z_{22} - z_{21} z_{12})$.

In the massless limit the energies and the longitudinal terms should agree with the Catani-Seymour case and give a factor of $\dfrac{1}{z(1-y)}$. Using Mathematica the expression was evaluated and the massless limit checked:

$$(z_{11} z_{22} - z_{21} z_{12}) \overset{m \to 0}{=} 1 + y \left(-1 + \frac{1}{z} \right) \ . \tag{A.31}$$

Multiplied by the external factors also in the massless limit, this gives:

$$\frac{p^0 p_1^0}{q^0 q_1^0}(z_{11}z_{22} - z_{21}z_{12}) \overset{m \to 0}{=} \frac{1}{z - yz} \,, \tag{A.32}$$

which agrees with the expected result. For the full Jacobian this needs to be multiplied with the transverse result to give:

$$\begin{aligned}
\mathcal{J} &= \frac{p^0 p_1^0}{q^0 q_1^0}(z_{11}z_{22} - z_{21}z_{12}) \left(\frac{m^2 - Q^2(-1+y)^2}{m^2 + Q^2(-1+y)}\right)^{d-2} \\
&\overset{m,k^2 \to 0}{=} \frac{(1-y)^{d-3}}{z} \,.
\end{aligned} \tag{A.33}$$

Combinatorics

B.1. Two-Emission Combinatorics

The two-emission case results in cross-section contributions that are proportional to the second order in α_s. From squaring Eq. (6.3), there are three terms proportional to g_s^4. Each combination will be discussed in this section and the possible matching of the indices for each shown.

The first $\mathcal{O}(\alpha_s^2)$ term is the triplet with triplet combination:

$$
\langle n|\mathcal{M}^{\text{Triplet}}(n)\rangle^2 = g_s^4 \sum_{i<j<k}^{n} \sum_{\beta} \langle i,j,k|\text{Sp}(i,j,k,i+j+k)\langle [n]_{\overline{ijk}}|\mathcal{M}([n]_{\overline{ijk}},(i+j+k))\rangle
$$

$$
\times \sum_{l<m<r}^{n} \sum_{\beta'} \langle \mathcal{M}([n]_{\overline{lmr}},(l+m+r))|[n]_{\overline{lmr}}\rangle \text{Sp}(l,m,r,l+m+r)|l,m,r\rangle \Delta_{ijk}^{lmr}
$$

$$
|\mathcal{M}^T(n)|^2 = \sum_{i<j<k} \sum_{l<m<r} \mathcal{M}(i,j,k)\mathcal{M}^*(l,m,r)\Delta_{ijk}^{lmr}
$$

(B.1)

The possible index pairings are:

$$
\Delta_{ijk}^{lmr} = (\delta_{il}\delta_{jm}\delta_{kr} + \delta_{il}\delta_{jm}\bar{\bar{\delta}}_{kr} + \delta_{il}\delta_{jr}\bar{\bar{\delta}}_{km} + \delta_{im}\delta_{jr}\bar{\delta}_{kl} + \delta_{il}\delta_{km}\bar{\bar{\delta}}_{jr}
$$
$$
+ \delta_{il}\delta_{kr}\bar{\bar{\delta}}_{jm} + \delta_{im}\delta_{kr}\bar{\delta}_{jl} + \delta_{jm}\delta_{kr}\bar{\delta}_{il} + \delta_{jl}\delta_{kr}\bar{\delta}_{im} + \delta_{jl}\delta_{km}\bar{\delta}_{ir}) \ .
$$

(B.2)

Which after relabelling indices in the case of an ordered sum gives the following final terms:

$$
|\mathcal{M}^T(n)|^2 = \sum_{i<j<k} \mathcal{M}(i,j,k)\mathcal{M}^*(i,j,k) + \sum_{i<j<k<l} 2\text{Re}\{\mathcal{M}(i,j,k)\mathcal{M}^*(i,j,l)
$$
$$
+ \mathcal{M}(i,j,k)\mathcal{M}^*(i,k,l) + \mathcal{M}(i,j,l)\mathcal{M}^*(i,k,l) + \mathcal{M}(i,j,l)\mathcal{M}^*(j,k,l)
$$
$$
+ \mathcal{M}(j,k,l)\mathcal{M}^*(i,j,k) + \mathcal{M}(j,k,l)\mathcal{M}^*(i,k,l)\} \ .
$$

(B.3)

The above expression contains a self-energy term and six exchange amplitudes between ordered triplets. This result can also be seen by considering all possible ordered triplets from

four indices, (ijk, ijl, ikl, jkl). Taking pairs between the triplets gives a total of six combinations.

The second term for the double emission case is that of two pairs with two pairs. This contains a self-energy diagram, and double-exchange diagrams with one and two spectators :

$$
\begin{aligned}
\langle n|\mathcal{M}^{Pairs}(n)\rangle^2 =& g_s^4 \sum_{i<j}^n \sum_{k<l}^n \sum_\beta \sum_\gamma \langle i,j|\mathbf{Sp}(i,j,i+j)\langle i,j|\mathbf{Sp}(k,l,k+l)\langle [n]_{\overline{ijkl}}|\mathcal{M}([n]_{\overline{ijkl}},(i+j),(k+l))\rangle \\
& \times \sum_{m<r}^n \sum_{s<t}^n \sum_{\beta^*} \sum_{\gamma^*} \langle \mathcal{M}([n]_{\overline{mrst}},(m+r),(s+t))|[n]_{\overline{mrst}}\rangle \mathbf{Sp}(s,t,s+t)|s,t\rangle \\
& \times \mathbf{Sp}(m,r,m+r)|m,r\rangle \Delta_{ijkl}^{mrst}\ , \\
|\mathcal{M}^P(n)|^2 =& \sum_{i<j} \sum_{k<l} \sum_{m<r} \sum_{s<t} \mathcal{M}(i,j,k,l)\mathcal{M}^*(m,r,s,t)\Delta_{ijkl}^{mrst}\ .
\end{aligned}
$$

$$(\text{B.4})$$

For this term the possible scenarios are:

$$
\begin{aligned}
\Delta_{ijkl}^{mrst} =& \delta_{im}\delta_{jr}\delta_{ks}\delta_{lt} + \delta_{is}\delta_{jt}\delta_{km}\delta_{lr} + \delta_{im}\delta_{js}\delta_{kr}\delta_{lt} + \delta_{im}\delta_{js}\delta_{kt}\delta_{lr} + \delta_{is}\delta_{jm}\delta_{kt}\delta_{lr} \\
& + \delta_{is}\delta_{jm}\delta_{kr}\delta_{lt} + \delta_{im}\delta_{js}\delta_{kr}\bar{\delta}_{lt} + \bar{\delta}_{im}\delta_{js}\delta_{kr}\delta_{lt} + \delta_{im}\delta_{js}\bar{\delta}_{kt}\delta_{lr} + \bar{\delta}_{im}\delta_{js}\delta_{kt}\delta_{lr} \\
& + \delta_{is}\delta_{jm}\bar{\delta}_{kt}\delta_{lr} + \delta_{is}\bar{\delta}_{jm}\delta_{kt}\delta_{lr} + \delta_{is}\delta_{jm}\delta_{kr}\bar{\delta}_{lt} + \delta_{is}\bar{\delta}_{jm}\delta_{kr}\delta_{lt}\ ,
\end{aligned}
$$

$$(\text{B.5})$$

where the first two terms are self-energy diagrams, equivalent to twice the single-emission self-energy diagram. The other terms with four deltas are exchange diagrams with one spectator. The terms with three deltas and one delta-bar correspond to exchange diagrams with two spectators. After applying these functions and relabelling indices for an ordered sum over all indices, the final terms are:

$$
\begin{aligned}
|\mathcal{M}^P(n)|^2 =& \sum_{i<j<k<l} \Bigg(\mathcal{M}(i,j,k,l)\mathcal{M}^*(i,j,k,l) + \mathcal{M}(i,k,j,l)\mathcal{M}^*(i,k,j,l) + \mathcal{M}(j,k,i,l)\mathcal{M}^*(j,k,i,l) \\
& + 2\mathrm{Re}\{\mathcal{M}(i,j,k,l)\mathcal{M}^*(i,k,j,l) + \mathcal{M}(i,j,k,l)\mathcal{M}^*(j,k,i,l) + \mathcal{M}(i,k,j,l)\mathcal{M}^*(j,k,i,l)\}\Bigg) \\
& + \sum_{i<j<k<l,m} \Bigg(2\mathrm{Re}\{\mathcal{M}(i,j,k,l)\mathcal{M}^*(i,k,j,m) + \mathcal{M}(i,j,k,l)\mathcal{M}^*(j,k,i,m) \\
& + \mathcal{M}(i,k,j,l)\mathcal{M}^*(j,k,i,m)\}\Bigg)\ .
\end{aligned}
$$

$$(\text{B.6})$$

The third term to be considered is the cross term between the triplet and two pairs, that when squaring the expanded terms will carry a factor of two in the final expression. This does not contain a self-energy diagram, although it does contribute to the one and two-spectator double-exchange cases:

$$
\begin{aligned}
\langle \mathcal{M}^{Triplet}(n)|n\rangle\langle n|\mathcal{M}^{Pairs}(n)\rangle =& g_s^4 \sum_{i<j<k}^n \sum_{\beta,\beta^*,\gamma^*} \langle i,j,k|\mathbf{Sp}(i,j,k,i+j+k)\langle [n]_{\overline{ijk}}|\mathcal{M}([n]_{\overline{ijk}},(i+j+k))\rangle \\
& \times \sum_{m<r}^n \sum_{s<t}^n \langle \mathcal{M}([n]_{\overline{mrst}},(m+r),(s+t))|[n]_{\overline{mrst}}\rangle \\
& \times \mathbf{Sp}(s,t,s+t)|s,t\rangle \mathbf{Sp}(m,r,m+r)|m,r\rangle \Delta_{ijk}^{mrst}\ .
\end{aligned}
$$

$$(\text{B.7})$$

For this term the possible scenarios are:

$$
\begin{aligned}
\Delta_{ijk}^{mrst} = {} & \delta_{im}\delta_{jr}(\delta_{ks} + \delta_{kt}) + \delta_{im}\delta_{js}(\delta_{kr} + \delta_{kt}) + \delta_{im}\delta_{jt}\delta_{kr} \\
& + \delta_{is}\delta_{jt}(\delta_{km} + \delta_{kr}) + \delta_{is}\delta_{jm}(\delta_{kt} + \delta_{kr}) + \delta_{is}\delta_{jr}\delta_{kt} \\
& + \delta_{ir}\delta_{js}\delta_{kt} + \delta_{it}\delta_{jm}\delta_{kr} + \Big(\delta_{it}\delta_{jr}(\bar{\delta}_{ks} + \bar{\delta}_{km}) \\
& + \delta_{im}\delta_{jr}(\bar{\delta}_{ks} + \bar{\delta}_{kt}) + \delta_{im}\delta_{js}(\bar{\delta}_{kr} + \bar{\delta}_{kt}) + \delta_{im}\delta_{jt}\bar{\delta}_{kr} \\
& + \delta_{is}\delta_{jt}(\bar{\delta}_{km} + \bar{\delta}_{kr}) + \delta_{is}\delta_{jm}(\bar{\delta}_{kt} + \bar{\delta}_{kr}) + \delta_{is}\delta_{jr}\bar{\delta}_{kt} \\
& + \delta_{ir}\delta_{jt}(\bar{\delta}_{ks} + \bar{\delta}_{km}) + \delta_{ir}\delta_{js}\bar{\delta}_{kt} + \delta_{it}\delta_{jm}\bar{\delta}_{kr} \Big) \\
& + \Big(\bar{\delta}_{it}\delta_{jr}(\delta_{ks} + \delta_{km}) + ... \Big) + \Big(\delta_{it}\bar{\delta}_{jr}(\delta_{ks} + \delta_{km}) + ... \Big) .
\end{aligned}
\tag{B.8}
$$

The dots in the last line refer to the same terms repeated, as in the terms with $\bar{\delta}$ for k, with the $\bar{\delta}$ containing the i or j index respectively. Any possible combination not shown in the delta expressions is either against the ordering of indices or not allowed by the observable, *i.e.* singular emissions connecting to the hard amplitude.

$$
\begin{aligned}
|\mathcal{M}^{TP}(n)|^2 = {} & \sum_{i<j<k<l} \Big(\mathcal{M}(i,j,k)\mathcal{M}^*(i,j,k,l) + \mathcal{M}(i,j,k)\mathcal{M}^*(i,k,j,l) + \mathcal{M}(i,j,k)\mathcal{M}^*(j,k,i,l) \Big) \\
& + \sum_{i<j<k<l,m} \Big(\mathcal{M}(i,j,k)\mathcal{M}^*(j,l,k,m) + \mathcal{M}(i,j,k)\mathcal{M}^*(k,l,j,m) \\
& + \mathcal{M}(i,j,k)\mathcal{M}^*(i,l,k,m) + \mathcal{M}(i,j,k)\mathcal{M}^*(k,l,i,m) \\
& + \mathcal{M}(i,j,k)\mathcal{M}^*(i,l,j,m) + \mathcal{M}(i,j,k)\mathcal{M}^*(j,l,i,m) \Big) .
\end{aligned}
\tag{B.9}
$$

Shown above are the terms which correspond to the topologies for two exchanged partons for both one and two spectators. This formalism can be extended to the k-emissions case which is discussed in Sec. 6.2.

B.2. Two-Emission Diagrams

Using the combinatorics from the previous section, all of the two-emission diagrams can be illustrated. Distinctions can be made between self-energy-type diagrams and exchange diagrams. Within these there are both triplet-triplet and pairs-pairs combinations. The triplet-pairs combinations are only relevant to the exchange diagrams, that includes the one and two-spectator exchange diagrams. The following diagrams are completely general *i.e.* the lines can represent any partons. Some of these will only appear in the non-abelian case as they require one or more triple gluon vertices.

Firstly the self-energy type diagrams are shown, where both the emissions connect to the emitter line on both sides of the diagram.
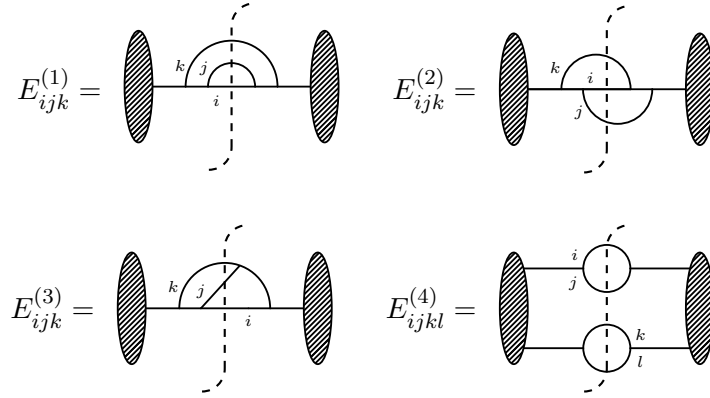
$$E_{ijk}^{(1)} = \quad\quad\quad\quad E_{ijk}^{(2)} =$$

$$E_{ijk}^{(3)} = \quad\quad\quad\quad E_{ijkl}^{(4)} =$$

Figure B.1.: Self energy diagrams

B.2.1. Exchange Diagrams with One Spectator

The following diagrams are the topologies relevant for two emissions exchanged between an emitter and a spectator. These first five diagrams are labelled triplet-triplet where both the emissions are exchanged from the emitter to spectator:
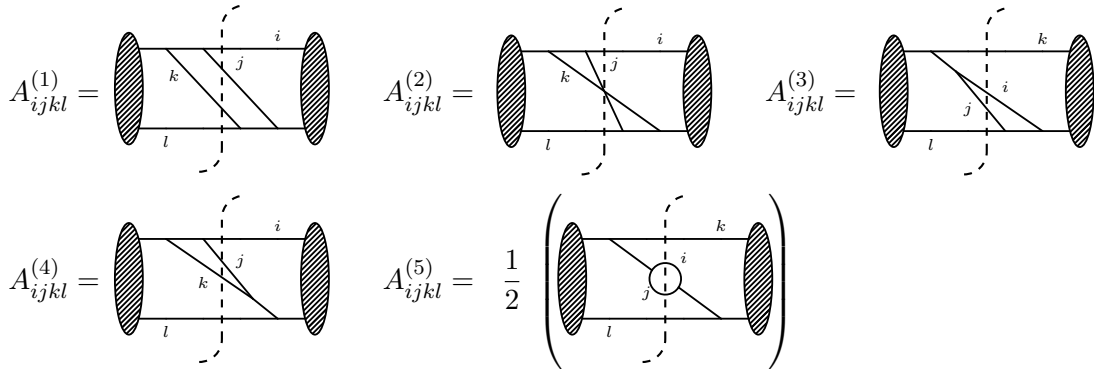
$$A_{ijkl}^{(1)} = \quad\quad A_{ijkl}^{(2)} = \quad\quad A_{ijkl}^{(3)} =$$

$$A_{ijkl}^{(4)} = \quad\quad A_{ijkl}^{(5)} = \frac{1}{2}\left(\quad\quad\right)$$

Figure B.2.: Triplet-triplet exchange diagrams

The next group of diagrams are the triplet-pairs combinations which involve only one of the emissions being exchanged from the emitter to the spectator:
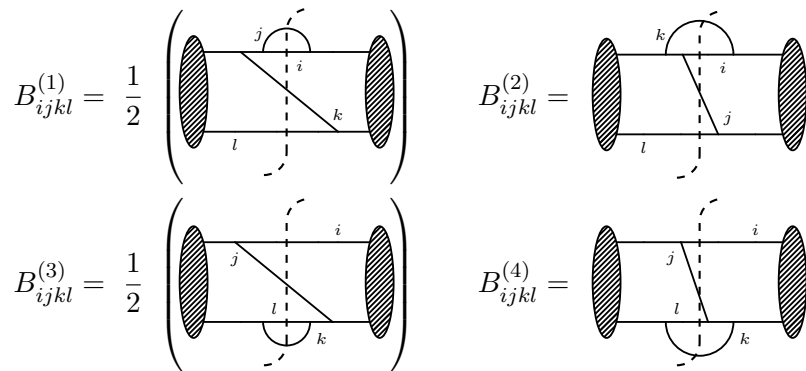
$$B_{ijkl}^{(1)} = \frac{1}{2}\left(\quad\quad\right) \quad\quad B_{ijkl}^{(2)} =$$

$$B_{ijkl}^{(3)} = \frac{1}{2}\left(\quad\quad\right) \quad\quad B_{ijkl}^{(4)} =$$

Figure B.3.: Triplet-pairs exchange diagrams.

The last exchange diagram with one spectator, *i.e.* with a total of four momenta involved, is the so called X-diagram which is the combination of two pairs-splitting amplitudes and is symmetric in $(i \leftrightarrow l)$ and $(j \leftrightarrow k)$:
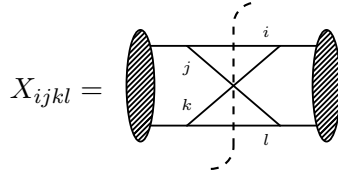
$$X_{ijkl} = \quad$$

Figure B.4.: Pairs-pairs exchange diagram

B.2.2. Exchange Diagrams with Two Spectators

This set of topologies show the possible cases for two emissions exchanged between an emitter and two spectators. The nine diagrams below show the resulting combinations from the triplet-pairs case where only two indices are matched:
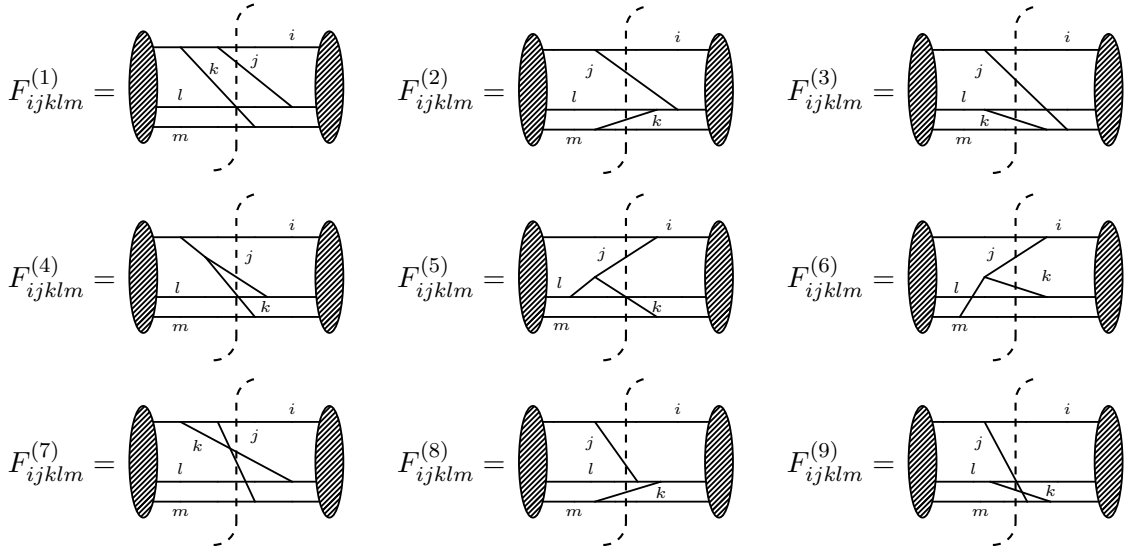
$$F_{ijklm}^{(1)} = \qquad F_{ijklm}^{(2)} = \qquad F_{ijklm}^{(3)} =$$

$$F_{ijklm}^{(4)} = \qquad F_{ijklm}^{(5)} = \qquad F_{ijklm}^{(6)} =$$

$$F_{ijklm}^{(7)} = \qquad F_{ijklm}^{(8)} = \qquad F_{ijklm}^{(9)} =$$

Figure B.5.: Two spectator triplet-pairs diagrams

The final three two spectator topologies come from the pairs-pairs combinations with four indices on each side but only three of them matched resulting in five momenta:
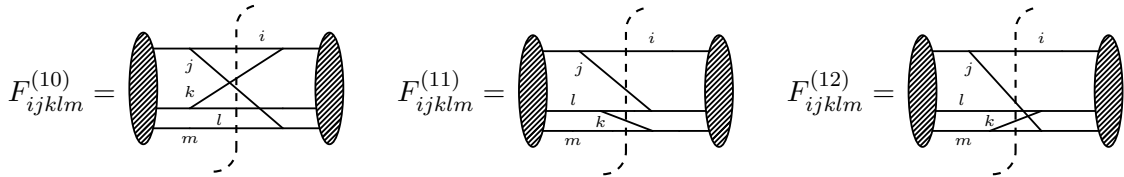
$$F_{ijklm}^{(10)} = \qquad F_{ijklm}^{(11)} = \qquad F_{ijklm}^{(12)} =$$

Figure B.6.: Two spectator pairs-pairs diagrams

Partitioning

C.1. Partitioning Example for Two Emissions

Here the partitioning will be illustrated for the two emission exchange diagram B_2, making use of the formalism outlined in Sec. 6.3.
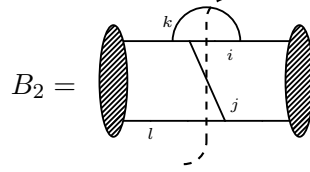

$$B_2 =$$

Figure C.1.: Diagram B_2, a two-emission triplet-pairs exchange diagram.

The denominator for this diagram contains the following factors:

$$\mathcal{D}(B_2) = \frac{1}{S_{ij}S_{ijk}S_{ik}S_{jl}} \ . \tag{C.1}$$

The set of singular configurations for this diagram, $\mathbf{C}^{B_2}$, corresponds to the first column in the Table C.1. The numerator terms for the partitioning factors, as defined in Eq. (6.15), which cancel the non-singular terms, for this diagram are:

$$
\begin{aligned}
F^{(B_2)}_{(ijk)} &= (S_{ij}S_{ik}S_{ijk}\mathcal{D}(B_2))^{-1} = \varsigma^2\,S_{jl} \ , \\
F^{(B_2)}_{(ijl)} &= (S_{ij}S_{jl}\mathcal{D}(B_2))^{-1} = \varsigma\,S_{ijk}S_{ik} \ , \\
F^{(B_2)}_{(ij)(kl)} &= (S_{ij}\mathcal{D}(B_2))^{-1} = S_{ijk}S_{ik}S_{jl} \ .
\end{aligned}
\tag{C.2}
$$

These terms are the non-vanishing terms given in table C.1. All of these factors can then be applied to the full denominator to give a sum of the contributions to different collinear limits:

$$
\begin{aligned}
\sum_{c \in \mathbf{C}_{B_2}} \mathbb{P}^{(B_2)}_c \mathcal{D}(B_2) =& \frac{1}{\varsigma^2 S_{jl} + \varsigma(S_{ijk}S_{ik} + S_{ij}S_{ijk}) + S_{ij}S_{ijk}S_{jl} + S_{ij}S_{ijk}S_{ik} + S_{ijk}S_{ik}S_{jl}} \\
&\times \left(\frac{\varsigma^2}{S_{ij}S_{ik}S_{ijk}} + \frac{\varsigma}{S_{ij}S_{jl}} + \frac{\varsigma}{S_{ik}S_{jl}} + \frac{1}{S_{ik}} + \frac{1}{S_{jl}} + \frac{1}{S_{ij}} \right) .
\end{aligned}
$$

$$\tag{C.3}$$

configuration	vanishing	non-vanishing
$(i \parallel j \parallel k)$	$S_{ij}S_{ik}S_{ijk}$	S_{jl}
$(i \parallel j \parallel l)$	$S_{ij}S_{jl}$	$S_{ijk}S_{ik}$
$(i \parallel k \parallel l)$	S_{ik}	$S_{ij}S_{ijk}S_{jl}$
$(j \parallel k \parallel l)$	S_{jl}	$S_{ij}S_{ijk}S_{ik}$
$(i \parallel j),(k \parallel l)$	S_{ij}	$S_{ijk}S_{ik}S_{jl}$
$(i \parallel k),(j \parallel l)$	$S_{ik}S_{jl}$	$S_{ij}S_{ijk}$

Table C.1.: Singular configurations and the contributing denominator factors for the two emission diagram B_2.

Only the first three terms in Eq. (C.3) give leading contributions in the collinear limit to the corresponding splitting kernels $\mathbb{U}_{(ijk)}$, $\mathbb{U}_{(ijl)}$ and $\mathbb{U}_{(ik)(jl)}$. The other three terms give sub-leading contributions to the kernels $\mathbb{U}_{(ikl)}$, $\mathbb{U}_{(jkl)}$ and $\mathbb{U}_{(ij)(kl)}$.

The full set of collinear combinations, for all two-emission diagrams with one spectator, includes four possible triplets and three sets of pairs given by:

$$\mathbf{C} = \{(ijk),(ijl),(ikl),(jkl),(ij)(kl),(ik)(jl),(il)(jk)\} \ . \tag{C.4}$$

C.2. Collinear Contributions for All Topologies

The tables below show the different double-collinear limits and the denominator terms from each diagram that are singular in each of the limits. The two-emission topologies for both one and two spectators are shown in App. B.2. There are three classes of exchange topologies, triplet-triplet (A), triplet-pairs (B) and pairs-pairs (X) and all two-spectator topologies are labelled F.

	$A_{ijkl}^{(1)}$	$A_{ijkl}^{(2)}$	$A_{ijkl}^{(3)}$	$A_{ijkl}^{(4)}$	$A_{ijkl}^{(5)}$
	$S_{ij}S_{kl}S_{ijk}S_{jkl}$	$S_{ij}S_{jl}S_{ijk}S_{jkl}$	$S_{ij}S_{jl}S_{ijk}S_{ijl}$	$S_{ij}S_{jk}S_{ijk}S_{jkl}$	$S_{ij}^2 S_{ijk}S_{ijl}$
$i \parallel j \parallel k$	$S_{ij}S_{ijk}$	$S_{ij}S_{ijk}$	$S_{ij}S_{ijk}$	$S_{ij}S_{jk}S_{ijk}$	$S_{ij}^2 S_{ijk}$
$i \parallel j \parallel l$	S_{ij}	$S_{ij}S_{jl}$	$S_{ij}S_{jl}S_{ijl}$	S_{ij}	$S_{ij}^2 S_{ijl}$
$i \parallel k \parallel l$	S_{kl}	$\times$	$\times$	$\times$	$\times$
$j \parallel k \parallel l$	$S_{kl}S_{jkl}$	$S_{jl}S_{jkl}$	S_{jl}	$S_{jk}S_{jkl}$	$\times$
$(i \parallel j),(k \parallel l)$	$S_{ij}S_{kl}$	S_{ij}	S_{ij}	S_{ij}	S_{ij}^2
$(i \parallel k),(j \parallel l)$	$\times$	S_{jl}	S_{jl}	$\times$	$\times$
$(i \parallel l),(j \parallel k)$	$\times$	$\times$	$\times$	S_{jk}	$\times$

Table C.2.: Collection of S-invariants giving rise to singularities w.r.t. the set of collinearity structures for two-emission triplet-triplet diagrams.

	$B^{(1)}_{ijkl}$	$B^{(2)}_{ijkl}$	$B^{(3)}_{ijkl}$	$B^{(4)}_{ijkl}$	X_{ijkl}
	$S_{ij}^2 S_{kl} S_{ijk}$	$S_{ij}S_{ik}S_{jl}S_{ijk}$	$S_{ij}S_{kl}^2 S_{jkl}$	$S_{ij}S_{kl}S_{jl}S_{jkl}$	$S_{ij}S_{ik}S_{jl}S_{kl}$
$i \parallel j \parallel k$	$S_{ij}^2 S_{ijk}$	$S_{ij}S_{ik}S_{ijk}$	S_{ij}	S_{ij}	$S_{ij}S_{ik}$
$i \parallel j \parallel l$	S_{ij}^2	$S_{ij}S_{jl}$	S_{ij}	$S_{ij}S_{jl}$	$S_{ij}S_{jl}$
$i \parallel k \parallel l$	S_{kl}	S_{ik}	S_{kl}^2	S_{kl}	$S_{ik}S_{kl}$
$j \parallel k \parallel l$	S_{kl}	S_{jl}	$S_{kl}^2 S_{jkl}$	$S_{kl}S_{jl}S_{jkl}$	$S_{jl}S_{kl}$
$(i \parallel j), (k \parallel l)$	$S_{ij}^2 S_{kl}$	S_{ij}	$S_{ij}S_{kl}^2$	$S_{ij}S_{kl}$	$S_{ij}S_{kl}$
$(i \parallel k), (j \parallel l)$	$\times$	$S_{ik}S_{jl}$	$\times$	S_{jl}	$S_{ik}S_{jl}$
$(i \parallel l), (j \parallel k)$	$\times$	$\times$	$\times$	$\times$	$\times$

Table C.3.: Collection of S-invariants giving rise to singularities w.r.t. the set of collinearity structures for two-emission triplet-pairs and pairs-pairs diagrams.

	$E^{(1)}_{ijk}$	$E^{(2)}_{ijk}$	$E^{(3)}_{ijk}$	$E^{(4)}_{ijkl}$
	$S_{ij}^2 S_{ijk}^2$	$S_{ij}S_{ik}S_{ijk}^2$	$S_{ij}S_{jk}S_{ijk}^2$	$S_{ij}^2 S_{kl}^2$
$i \parallel j \parallel k$	$S_{ij}^2 S_{ijk}^2$	$S_{ij}S_{ik}S_{ijk}^2$	$S_{ij}S_{jk}S_{ijk}^2$	S_{ij}^2
$i \parallel j \parallel l$	S_{ij}^2	S_{ij}	S_{ij}	S_{ij}^2
$i \parallel k \parallel l$	$\times$	S_{ik}	$\times$	S_{kl}^2
$j \parallel k \parallel l$	$\times$	$\times$	S_{jk}	S_{kl}^2
$(i \parallel j), (k \parallel l)$	S_{ij}^2	S_{ij}	S_{ij}	$S_{ij}^2 S_{kl}^2$
$(i \parallel k), (j \parallel l)$	$\times$	S_{ik}	$\times$	$\times$
$(i \parallel l), (j \parallel k)$	$\times$	$\times$	S_{jk}	$\times$

Table C.4.: Collection of S-invariants giving rise to singularities w.r.t. the set of collinearity structures for two-emission self-energy diagrams.

	$F_{ijklm}^{(1)}$ $S_{ij}S_{jl}S_{km}S_{ijk}$	$F_{ijklm}^{(2)}$ $S_{ij}S_{km}S_{kl}S_{jkl}$	$F_{ijklm}^{(3)}$ $S_{ij}S_{kl}S_{jm}S_{jkm}$	$F_{ijkl}^{(4)}$ $S_{jl}S_{km}S_{jk}S_{ijk}$	$F_{ijklm}^{(5)}$ $S_{ij}S_{km}S_{jk}S_{jkl}$	$F_{ijklm}^{(6)}$ $S_{ij}S_{kl}S_{jk}S_{jkm}$
$i\|j\|k$	$S_{ij}S_{ijk}$	S_{ij}	S_{ij}	$S_{jk}S_{ijk}$	$S_{ij}S_{jk}$	$S_{ij}S_{jk}$
$i\|j\|l$	$S_{ij}S_{jl}$	S_{ij}	S_{ij}	S_{jl}	S_{ij}	S_{ij}
$i\|j\|m$	S_{ij}	S_{ij}	$S_{ij}S_{jm}$	✗	S_{ij}	S_{ij}
$i\|k\|l$	✗	S_{kl}	S_{kl}	✗	✗	S_{kl}
$i\|k\|m$	S_{km}	S_{km}	✗	S_{km}	S_{km}	✗
$i\|l\|m$	✗	✗	✗	✗	✗	✗
$j\|k\|l$	S_{jl}	$S_{kl}S_{jkl}$	S_{kl}	$S_{jk}S_{jl}$	$S_{jk}S_{jkl}$	$S_{jk}S_{kl}$
$j\|k\|m$	S_{km}	S_{km}	$S_{jm}S_{jkm}$	$S_{jk}S_{km}$	$S_{jk}S_{km}$	$S_{jk}S_{jkm}$
$j\|l\|m$	S_{jl}	✗	S_{jm}	S_{jl}	✗	✗
$k\|l\|m$	S_{km}	$S_{kl}S_{km}$	S_{kl}	S_{km}	S_{km}	S_{kl}
$(i\|j),(k\|l)$	S_{ij}	$S_{ij}S_{kl}$	$S_{ij}S_{kl}$	✗	S_{ij}	$S_{ij}S_{kl}$
$(i\|j),(k\|m)$	$S_{ij}S_{km}$	$S_{ij}S_{km}$	S_{ij}	S_{km}	$S_{ij}S_{km}$	S_{ij}
$(i\|j),(l\|m)$	S_{ij}	S_{ij}	S_{ij}	✗	S_{ij}	S_{ij}
$(i\|k),(j\|l)$	S_{jl}	✗	✗	S_{jl}	✗	✗
$(i\|k),(j\|m)$	✗	✗	S_{jm}	✗	✗	✗
$(i\|k),(l\|m)$	✗	✗	✗	✗	✗	✗
$(i\|l),(j\|k)$	✗	✗	✗	S_{jk}	S_{jk}	S_{jk}
$(i\|l),(j\|m)$	✗	✗	S_{jm}	✗	✗	✗
$(i\|l),(k\|m)$	S_{km}	S_{km}	✗	S_{km}	S_{km}	✗
$(i\|m),(j\|k)$	✗	✗	✗	S_{jk}	S_{jk}	S_{jk}
$(i\|m),(j\|l)$	S_{jl}	✗	✗	S_{jl}	✗	✗
$(i\|m),(k\|l)$	✗	S_{kl}	S_{kl}	✗	✗	S_{kl}
$(l\|m),(j\|k)$	✗	✗	✗	S_{jk}	S_{jk}	S_{jk}
$(k\|m),(j\|l)$	$S_{km}S_{jl}$	S_{km}	✗	$S_{jl}S_{km}$	S_{km}	✗
$(k\|l),(j\|m)$	✗	S_{kl}	$S_{kl}S_{jm}$	✗	✗	S_{kl}

Table C.5.: Collection of S-invariants giving rise to singularities w.r.t. the set of collinearity structures for two-emission diagrams with two spectators.

Soft and Collinear functions

The tables below show the different infrared singular functions in different limits and can be used as a reference to construct subtraction terms. $\langle\hat{P}_{ggq}\rangle$ is the collinear splitting function, $E_{23}(p_1)P_{q_3g_2}$ is the soft-collinear function and E^2 is the double-eikonal double-soft function. The limits applied are:

- S_1S_2 = double soft limit, where partons 1 and 2 are soft

- S_1C_{23} = soft-collinear limit where parton 1 is soft and partons 2 and 3 are collinear

- S_2C_{13} = soft-collinear limit where parton 2 is soft and partons 1 and 3 are collinear

- C_1C_2 = triple-collinear limit where partons 1 and 2 are collinear to parton 3

These expressions are referred to in Sec. 7.3.3.

	S_1S_2
$\langle\hat{P}_{ggq}\rangle$	$\dfrac{4C_F^2(n\cdot p_3)^2}{n\cdot p_1 n\cdot p_2 s_{13}s_{23}} + C_FC_A\ P_{ggq}^{(nab)}\Big|_{SS}$
$E_{23}(p_1)P_{q_3g_2}$	$\dfrac{2C_Fn\cdot p_3(C_A(n\cdot p_2 s_{13} - n\cdot p_3 s_{12}) + 4C_Fn\cdot p_3 s_{12})}{n\cdot p_1 n\cdot p_2 s_{12}s_{13}s_{23}}$
E^2	$\dfrac{4C_F^2(p_j\cdot p_3)(p_l\cdot p_3)}{p_j\cdot p_1 p_l\cdot p_2 s_{13}s_{23}} + C_FC_A\displaystyle\sum_{i,j}\mathcal{S}_{ij}(q_1,q_2)$

	S_1C_{23}
$\langle\hat{P}_{ggq}\rangle$	$\dfrac{\left(np_2^2(1-\epsilon) + 2np_3^2 + 2np_2np_3\right)}{2s_{12}s_{13}s_{23}np_1np_2(np_2 + np_3)(s_{12} + s_{13})}\big[-C_FC_A(s_{12} + s_{13})(np_3 s_{12} - np_2 s_{13})$ $+2C_F^2 s_{12}(np_2 s_{13} + np_3(s_{12} + 2s_{13}))\big]$
$E_{23}(p_1)P_{q_3g_2}$	$\dfrac{\left(np_2^2(1-\epsilon) + 2np_3^2 + 2np_2np_3\right)}{s_{12}s_{13}s_{23}np_1np_2(np_2 + np_3)(s_{12} + s_{13})}\big[-C_FC_A(s_{12} + s_{13})(np_3 s_{12} - np_2 s_{13})$ $+2C_F^2 s_{12}(np_2 s_{13} + np_3(s_{12} + 2s_{13}))\big]$
E^2	$\dfrac{2C_Fn\cdot p_3((2C_F - C_A)n\cdot p_3 s_{12} + C_An\cdot p_2 s_{13})}{n\cdot p_1 n\cdot p_2 s_{12}s_{13}s_{23}}$

	$S_2 C_{13}$
$\langle \hat{P}_{ggq} \rangle$	$P_{ggq}\vert_{S_1 C_2} (1 \leftrightarrow 2)$
$E_{23}(p_1) P_{q_3 g_2}$	$\dfrac{2C_F (2C_F - C_A)(n \cdot p_3)^2}{n \cdot p_1 n \cdot p_2 s_{13} s_{23}}$
E^2	$\dfrac{2C_F n \cdot p_3 ((2C_F - C_A) n \cdot p_3 s_{12} + C_A n \cdot p_1 s_{23})}{n \cdot p_1 n \cdot p_2 s_{12} s_{13} s_{23}}$

	$C_1 C_2$
$\langle \hat{P}_{ggq} \rangle$	$\langle \hat{P}_{ggq} \rangle$
$E_{23}(p_1) P_{q_3 g_2}$	$\dfrac{(np_2^2(1-\epsilon) + 2np_3^2 + 2np_2 np_3)}{s_{12}s_{13}s_{23} np_1 np_2 (np_2 + np_3)(s_{12} + s_{13})} \big[-C_F C_A (s_{12} + s_{13})(np_3 s_{12} - np_2 s_{13})$
	$+ 2C_F^2 s_{12}(np_2 s_{13} + np_3(s_{12} + 2s_{13}))\big]$
E^2	$\dfrac{4C_F^2 (n \cdot p_3)^2}{n \cdot p_1 n \cdot p_2 s_{13} s_{23}} + C_F C_A \sum_{i,j} \mathcal{S}_{ij}(q_1, q_2)$

The full expressions for the abelian and non-abelian parts of the splitting function for two gluon emissions from a quark are given by:

$$\langle \hat{P}_{ggq}^{(\text{ab})} \rangle = \left\{ \frac{S_{i12}^2}{2 S_{i2} S_{i1}} (1 - \alpha_{i1} - \alpha_{i2}) \left(-\frac{\epsilon (\alpha_{i2}^2 + \alpha_{i1}^2)}{\alpha_{i1} \alpha_{i2}} + \frac{(1 - \alpha_{i1} - \alpha_{i2})^2 + 1}{\alpha_{i1} \alpha_{i2}} - \epsilon(\epsilon + 1) \right) \right.$$
$$+ \frac{S_{i12}}{S_{i2}} \left(\frac{(1 - \alpha_{i2})(1 - \alpha_{i1} - \alpha_{i2}) + (1 - \alpha_{i1})^3}{\alpha_{i1} \alpha_{i2}} - \frac{(1 - \alpha_{i1})}{\alpha_{i1} \alpha_{i2}} \epsilon (\alpha_{i2}^2 + \alpha_{i2} \alpha_{i1} + \alpha_{i1}^2) \right.$$
$$\left. + (2 - \alpha_{i1} - \alpha_{i2}) \epsilon^2 \right) + (1 - \epsilon) \left(\epsilon - \frac{S_{i1}(1 - \epsilon)}{S_{i2}} \right) \bigg\} + (1 \leftrightarrow 2)$$

$$\text{(D.1)}$$

$$\langle \hat{P}_{ggq}^{(\text{nab})} \rangle = \left\{ (1 - \epsilon) \left(\frac{t_{123}^2}{4 S_{12}^2} - \frac{\epsilon}{2} + \frac{1}{4} \right) + \frac{S_{i12}}{2 S_{12}} \left(\frac{(1 - \epsilon)(\alpha_{i2}(\alpha_{i2}^2 - 2\alpha_{i2} + 2) - \alpha_{i1}(\alpha_{i1}^2 - 6\alpha_{i1} + 6))}{\alpha_{i1}(\alpha_{i1} + \alpha_{i2})} \right. \right.$$
$$+ \frac{2\epsilon((1 - \alpha_{i1} - \alpha_{i2})(\alpha_{i2} - 2\alpha_{i1}) - \alpha_{i1})}{\alpha_{i1}(\alpha_{i1} + \alpha_{i2})} \bigg) + \frac{S_{i12}}{2 S_{i2}} \bigg[(1 - \alpha_{i1}) \epsilon \left(\frac{\alpha_{i2}^2 + \alpha_{i1}^2}{\alpha_{i1} \alpha_{i2}} - \epsilon \right)$$
$$- \frac{(1 - \alpha_{i2})(1 - \alpha_{i1} - \alpha_{i2}) + (1 - \alpha_{i1})^3}{\alpha_{i1} \alpha_{i2}} + \frac{(1 - \epsilon)((1 - \alpha_{i1})^3 - \alpha_{i1} + (1 - \alpha_{i1} - \alpha_{i2})^2)}{\alpha_{i1}(\alpha_{i1} + \alpha_{i2})}$$
$$- \epsilon \left(-\alpha_{i2} + \frac{2(1 - \alpha_{i1})(\alpha_{i1} - (1 - \alpha_{i1} - \alpha_{i2}))}{\alpha_{i1}(\alpha_{i1} + \alpha_{i2})} + \alpha_{i1} \right) \bigg]$$
$$+ \frac{S_{i12}^2}{2 S_{12} S_{i2}} \left(\frac{\alpha_{i1}^2(1 - \epsilon) + 2(1 - \alpha_{i1})}{\alpha_{i1} + \alpha_{i2}} + \frac{(\alpha_{i1} + \alpha_{i2})^2 (1 - \epsilon) + 2(1 - \alpha_{i1} - \alpha_{i2})}{\alpha_{i1}} \right)$$
$$\left. - \frac{S_{i12}^2}{4 S_{i2} S_{i1}} (1 - \alpha_{i1} - \alpha_{i2}) \left(\frac{(\alpha_{i1} + \alpha_{i2})^2 (1 - \epsilon) + 2(1 - \alpha_{i1} - \alpha_{i2})}{\alpha_{i1} \alpha_{i2}} + (1 - \epsilon)\epsilon \right) \right\}$$
$$+ (1 \leftrightarrow 2) \,.$$

$$\text{(D.2)}$$

Acknowledgements

Firstly, I would like to thank PD Dr. Stefan Gieseke for supervising me during the last three years and for the opportunity to extend my knowledge in this field. I am thankful to him for allowing me to come to Karlsruhe and to be part of MCnet, that has provided me with a community across Europe and many helpful discussions. The financial support of MCnet has allowed me to work in Karlsruhe and travel to many other countries to attend schools, workshops and meetings.

I would like to thank Prof. Dr Dieter Zeppenfeld for his guidance, and for agreeing to review this thesis. Dieter and all my ITP colleagues have provided a friendly atmosphere at the institute and many interesting lunchtime discussions.

Throughout my PhD I have been lucky to be able to work in Vienna on several occasions. This is thanks to the collaborative work carried out with Simon Plätzer, who has always welcomed me at the institute in Vienna. Simon has also been the driving force behind the work that I have carried out during my PhD and has spent many hours discussing with me both in person and via video call. For almost the last two years Max Löschner has been part of the many discussions with Simon and I and has made important contributions to our collaborative work, some of which are included in this thesis. I would also like to thank Simon and Max for reading this thesis and their helpful comments.

For the proofreading of this thesis, Alice Shipley, Emma Butcher, Hannah Jolly and Cody Duncan also deserve a mention and I would like to thank them all for their constructive comments.

A special thanks goes to Steffen Gay, who also helped with the proofreading effort and has supported me throughout my PhD. I am very grateful for the support of my family throughout my studies, both in London and in Karlsruhe, that has made this work possible.

References

[1] **FCC** Collaboration, A. Abada *et al.*, "FCC Physics Opportunities: Future Circular Collider Conceptual Design Report Volume 1," *Eur. Phys. J. C* **79** no. 6, (2019) 474.

[2] A. Accardi *et al.*, "Electron Ion Collider: The Next QCD Frontier: Understanding the glue that binds us all," *Eur. Phys. J. A* **52** no. 9, (2016) 268, `arXiv:1212.1701 [nucl-ex]`.

[3] T. Sjöstrand, S. Ask, J. R. Christiansen, R. Corke, N. Desai, P. Ilten, S. Mrenna, S. Prestel, C. O. Rasmussen, and P. Z. Skands, "An Introduction to PYTHIA 8.2," *Comput. Phys. Commun.* **191** (2015) 159–177, `arXiv:1410.3012 [hep-ph]`.

[4] M. Bähr *et al.*, "Herwig++ Physics and Manual," *Eur. Phys. J.* **C58** (2008) 639–707, `arXiv:0803.0883 [hep-ph]`.

[5] J. Bellm *et al.*, "Herwig 7.0/Herwig++ 3.0 release note," *Eur. Phys. J.* **C76** no. 4, (2016) 196, `arXiv:1512.01178 [hep-ph]`.

[6] T. Gleisberg, S. Höche, F. Krauss, M. Schönherr, S. Schumann, F. Siegert, and J. Winter, "Event generation with SHERPA 1.1," *JHEP* **02** (2009) 007, `arXiv:0811.4622 [hep-ph]`.

[7] **Sherpa** Collaboration, E. Bothmann *et al.*, "Event Generation with Sherpa 2.2," *SciPost Phys.* **7** no. 3, (2019) 034, `arXiv:1905.09127 [hep-ph]`.

[8] G. Dissertori, I. G. Knowles, and M. Schmelling, *Quantum Chromodynamics - High Energy Experiments and Theory*. Oxford University Press, New York, 2003.

[9] R. Ellis, W. Stirling, and B. Webber, *QCD and collider physics*, vol. 8. Cambridge University Press, 2, 2011.

[10] F. Bloch and A. Nordsieck, "Note on the Radiation Field of the electron," *Phys. Rev.* **52** (1937) 54–59.

[11] T. Kinoshita, "Mass singularities of Feynman amplitudes," *J. Math. Phys.* **3** (1962) 650–677.

[12] T. Lee and M. Nauenberg, "Degenerate Systems and Mass Singularities," *Phys. Rev.* **133** (1964) B1549–B1562.

[13] G. F. Sterman, *An Introduction to quantum field theory*. Cambridge University Press, 8, 1993.

[14] T. Becher, A. Broggio, and A. Ferroglia, *Introduction to Soft-Collinear Effective Theory*, vol. 896. Springer, 2015. `arXiv:1410.1892 [hep-ph]`.

[15] S. Catani and M. H. Seymour, "A General algorithm for calculating jet cross-sections in NLO QCD," *Nucl. Phys.* **B485** (1997) 291–419, `arXiv:hep-ph/9605323 [hep-ph]`. [Erratum: Nucl. Phys.B510,503(1998)].

[16] S. Frixione, Z. Kunszt, and A. Signer, "Three-jet cross sections to next-to-leading order," *Nuclear Physics B* **467** no. 3, (May, 1996) 399–442. http://dx.doi.org/10.1016/0550-3213(96)00110-1.

[17] W. Giele, E. Glover, and D. A. Kosower, "Higher-order corrections to jet cross sections in hadron colliders," *Nuclear Physics B* **403** no. 3, (Aug, 1993) 633–667. http://dx.doi.org/10.1016/0550-3213(93)90365-V.

[18] R. Cutkosky, "Singularities and discontinuities of Feynman amplitudes," *J. Math. Phys.* **1** (1960) 429–433.

[19] M. D. Schwartz, *Quantum Field Theory and the Standard Model.* Cambridge University Press, 3, 2014.

[20] N. Metropolis and S. Ulam, "The Monte Carlo Method," *Journal of the American Statistical Association* **44** no. 247, (1949) 335–341. PMID: 18139350.

[21] R. E. Caflisch, "Monte carlo and quasi-monte carlo methods," *Acta Numerica* **7** (1998) 1–49.

[22] S. Weinzierl, "Introduction to Monte Carlo methods," `arXiv:hep-ph/0006269 [hep-ph]`.

[23] G. P. Lepage, "VEGAS - an adaptive multi-dimensional integration program," Tech. Rep. CLNS-447, Cornell Univ. Lab. Nucl. Stud., Ithaca, NY, Mar, 1980. http://cds.cern.ch/record/123074.

[24] A. Buckley *et al.*, "General-purpose event generators for LHC physics," *Phys. Rept.* **504** (2011) 145–233, `arXiv:1101.2599 [hep-ph]`.

[25] T. Stelzer and W. Long, "Automatic generation of tree level helicity amplitudes," *Computer Physics Communications* **81** no. 3, (Jul, 1994) 357–371. http://dx.doi.org/10.1016/0010-4655(94)90084-1.

[26] M. R. Whalley, D. Bourilkov, and R. C. Group, "The Les Houches Accord PDFs (LHAPDF) and Lhaglue," `arXiv:hep-ph/0508110 [hep-ph]`.

[27] T. Sjostrand, "A Model for Initial State Parton Showers," *Phys. Lett. B* **157** (1985) 321–325.

[28] G. Marchesini and B. Webber, "Monte Carlo Simulation of General Hard Processes with Coherent QCD Radiation," *Nucl. Phys. B* **310** (1988) 461–526.

[29] S. Höche, "Introduction to parton-shower event generators," in *Theoretical Advanced Study Institute in Elementary Particle Physics: Journeys Through the Precision Frontier: Amplitudes for Colliders*, pp. 235–295. 2015. `arXiv:1411.4085 [hep-ph]`.

[30] S. Frixione and B. R. Webber, "Matching NLO QCD computations and parton shower simulations," *JHEP* **06** (2002) 029, `arXiv:hep-ph/0204244`.

[31] P. Nason, "A New method for combining NLO QCD with shower Monte Carlo algorithms," *JHEP* **11** (2004) 040, `arXiv:hep-ph/0409146`.

[32] S. Catani, F. Krauss, R. Kuhn, and B. Webber, "QCD matrix elements + parton showers," *JHEP* **11** (2001) 063, `arXiv:hep-ph/0109231`.

[33] G. P. Salam, "Towards Jetography," *Eur. Phys. J. C* **67** (2010) 637–686, `arXiv:0906.1833 [hep-ph]`.

[34] D. Amati and G. Veneziano, "Preconfinement as a Property of Perturbative QCD," *Phys. Lett. B* **83** (1979) 87–92.

[35] B. Webber, "A QCD Model for Jet Fragmentation Including Soft Gluon Interference," *Nucl. Phys. B* **238** (1984) 492–528.

[36] J.-C. Winter, F. Krauss, and G. Soff, "A modified cluster-hadronization model," *Eur. Phys. J. C* **36** (2004) 381–395, `arXiv:hep-ph/0311085`.

[37] B. Andersson, G. Gustafson, G. Ingelman, and T. Sjöstrand, "Parton fragmentation and string dynamics," *Physics Reports* **97** no. 2, (1983) 31 – 145. `http://www.sciencedirect.com/science/article/pii/0370157383900807`.

[38] B. Andersson, *The Lund model*, vol. 7. Cambridge University Press, 7, 2005.

[39] D. Lange, "The EvtGen particle decay simulation package," *Nucl. Instrum. Meth. A* **462** (2001) 152–155.

[40] P. Golonka, B. Kersevan, T. Pierzchala, E. Richter-Was, Z. Was, and M. Worek, "The Tauola photos F environment for the TAUOLA and PHOTOS packages: Release. 2.," *Comput. Phys. Commun.* **174** (2006) 818–835, `arXiv:hep-ph/0312240`.

[41] T. Sjöstrand and M. van Zijl, "A Multiple Interaction Model for the Event Structure in Hadron Collisions," *Phys. Rev.* **D36** (1987) 2019.

[42] G. Altarelli and G. Parisi, "Asymptotic Freedom in Parton Language," *Nucl. Phys. B* **126** (1977) 298–318.

[43] M. Seymour, "Soft isolated photon production as a probe of the parton shower mechanism," *Z. Phys. C* **64** (1994) 445–452.

[44] Y. L. Dokshitzer, "Calculation of the Structure Functions for Deep Inelastic Scattering and e+ e- Annihilation by Perturbation Theory in Quantum Chromodynamics.," *Sov. Phys. JETP* **46** (1977) 641–653.

[45] L. Lipatov, "The parton model and perturbation theory," *Sov. J. Nucl. Phys.* **20** (1975) 94–102.

[46] V. Gribov and L. Lipatov, "Deep inelastic e-p scattering in perturbation theory," *Sov. J. Nucl. Phys.* **15** (1972) 438–450.

[47] R. Ellis, D. Ross, and A. Terrano, "The Perturbative Calculation of Jet Structure in e^+e^- Annihilation," *Nucl. Phys. B* **178** (1981) 421–456.

[48] Z. Kunszt, P. Nason, G. Marchesini, and B. Webber, "QCD AT LEP," in *LEP Physics Workshop*, pp. 373–453. 8, 1989.

[49] Z. Kunszt and D. E. Soper, "Calculation of jet cross-sections in hadron collisions at order α_s^3," *Phys. Rev. D* **46** (1992) 192–221.

[50] S. Ellis, Z. Kunszt, and D. Soper, "The one jet inclusive cross-section at order α_s^3: Gluons only," in *3rd Les Rencontres de Physique de la Vallee d'Aoste: Results and Perspectives in Particle Physics*, pp. 251–262. 1989.

[51] Z. Nagy and Z. Trocsanyi, "Calculation of QCD jet cross-sections at next-to-leading order," *Nucl. Phys. B* **486** (1997) 189–226, `arXiv:hep-ph/9610498`.

[52] V. Sudakov, "Vertex parts at very high-energies in quantum electrodynamics," *Sov. Phys. JETP* **3** (1956) 65–71.

[53] S. Catani, S. Dittmaier, M. H. Seymour, and Z. Trocsanyi, "The Dipole formalism for next-to-leading order QCD calculations with massive partons," *Nucl. Phys. B* **627** (2002) 189–265, `arXiv:hep-ph/0201036`.

[54] W. T. Giele, D. A. Kosower, and P. Z. Skands, "A simple shower and matching algorithm," *Phys. Rev. D* **78** (2008) 014026, `arXiv:0707.3652 [hep-ph]`.

[55] N. Fischer, S. Prestel, M. Ritzmann, and P. Skands, "Vincia for Hadron Colliders," *Eur. Phys. J. C* **76** no. 11, (2016) 589, `arXiv:1605.06142 [hep-ph]`.

[56] Z. Nagy and D. E. Soper, "A parton shower based on factorization of the quantum density matrix," *JHEP* **06** (2014) 097, `arXiv:1401.6364 [hep-ph]`.

[57] L. Lonnblad, "ARIADNE version 4: A Program for simulation of QCD cascades implementing the color dipole model," *Comput. Phys. Commun.* **71** (1992) 15–31.

[58] G. Gustafson and U. Pettersson, "Dipole Formulation of QCD Cascades," *Nucl. Phys. B* **306** (1988) 746–758.

[59] T. Sjostrand and P. Z. Skands, "Transverse-momentum-ordered showers and interleaved multiple interactions," *Eur. Phys. J. C* **39** (2005) 129–154, `arXiv:hep-ph/0408302`.

[60] S. Platzer and S. Gieseke, "Coherent Parton Showers with Local Recoils," *JHEP* **01** (2011) 024, `arXiv:0909.5593 [hep-ph]`.

[61] S. Schumann and F. Krauss, "A Parton shower algorithm based on Catani-Seymour dipole factorisation," *JHEP* **03** (2008) 038, `arXiv:0709.1027 [hep-ph]`.

[62] S. Catani and M. Grazzini, "Infrared factorization of tree level QCD amplitudes at the next-to-next-to-leading order and beyond," *Nucl. Phys.* **B570** (2000) 287–325, `arXiv:hep-ph/9908523 [hep-ph]`.

[63] H. T. Li and P. Skands, "A framework for second-order parton showers," *Phys. Lett. B* **771** (2017) 59–66, `arXiv:1611.00013 [hep-ph]`.

[64] S. Höche and S. Prestel, "Triple collinear emissions in parton showers," *Phys. Rev. D* **96** no. 7, (2017) 074017, `arXiv:1705.00742 [hep-ph]`.

[65] S. Gieseke, P. Kirchgaeßer, S. Plätzer, and A. Siodmok, "Colour Reconnection from Soft Gluon Evolution," *JHEP* **11** (2018) 149, `arXiv:1808.06770 [hep-ph]`.

[66] M. Dasgupta, F. A. Dreyer, K. Hamilton, P. F. Monni, and G. P. Salam, "Logarithmic accuracy of parton showers: a fixed-order study," *JHEP* **09** (2018) 033, `arXiv:1805.09327 [hep-ph]`. [Erratum: JHEP 03, 083 (2020)].

[67] G. Bewick, S. Ferrario Ravasio, P. Richardson, and M. H. Seymour, "Logarithmic accuracy of angular-ordered parton showers," *JHEP* **04** (2020) 019, `arXiv:1904.11866 [hep-ph]`.

[68] M. Dasgupta, F. A. Dreyer, K. Hamilton, P. F. Monni, G. P. Salam, and G. Soyez, "Parton showers beyond leading logarithmic accuracy," `arXiv:2002.11114 [hep-ph]`.

[69] A. Banfi, G. P. Salam, and G. Zanderighi, "Principles of general final-state resummation and automated implementation," *JHEP* **03** (2005) 073, `arXiv:hep-ph/0407286`.

[70] J. R. Forshaw, J. Holguin, and S. Plätzer, "Parton branching at amplitude level," *JHEP* **08** (2019) 145, `arXiv:1905.08686 [hep-ph]`.

[71] R. A. Martinez, M. De Angelis, J. R. Forshaw, S. Plätzer, and M. H. Seymour, "Soft gluon evolution and non-global logarithms," `arXiv:1802.08531 [hep-ph]`.

[72] J. R. Forshaw, J. Holguin, and S. Plätzer, "Building a consistent parton shower," *JHEP* **09** (2020) 014, `arXiv:2003.06400 [hep-ph]`.

[73] M. D. Angelis, J. R. Forshaw, and S. Plätzer, "Resummation and simulation of soft gluon effects beyond leading colour," `arXiv:2007.09648 [hep-ph]`.

[74] S. Plätzer, "Summing Large-N Towers in Colour Flow Evolution," *Eur. Phys. J.* **C74** no. 6, (2014) 2907, `arXiv:1312.2448 [hep-ph]`.

[75] M. Löschner, S. Plätzer, and E. Simpson Dore, "Multi-Emission Kernels for Parton Evolution," *to appear* (2020) .

[76] A. Buckley, J. Butterworth, L. Lonnblad, D. Grellscheid, H. Hoeth, J. Monk, H. Schulz, and F. Siegert, "Rivet user manual," *Comput. Phys. Commun.* **184** (2013) 2803–2819, `arXiv:1003.0694 [hep-ph]`.

[77] E. Farhi, "A QCD Test for Jets," *Phys. Rev. Lett.* **39** (1977) 1587–1588.

[78] S. Gieseke, C. Röhr, and A. Siódmok, "Colour reconnections in Herwig++," *Eur. Phys. J.* **C72** (2012) 2225, `arXiv:1206.0041 [hep-ph]`.